Identification and characterization of regulators of GLUT4 trafficking

By

Daniel Richard Gulbranson

B. S., Saint Cloud State, 2008

A thesis submitted to the

Faculty of the Graduate School of the

University of Colorado in partial fulfillment

of the requirement for the degree of

Doctor of Philosophy

Department of Molecular, Cellular and Developmental Biology

2017

This thesis entitled:

Identification and characterization of regulators of GLUT4 trafficking

written by Daniel Richard Gulbranson

has been approved for the Department of Molecular, Cellular and Developmental Biology

_____

Jingshi Shen

_____

Michael Stowell

Date_____

The final copy of this thesis has been examined by the signatories, and we find that both the content and the form meet acceptable presentation standards of scholarly work in the above mentioned discipline.

Gulbranson, Daniel Richard (Ph.D. Molecular, Cellular and Developmental Biology)

Identification and characterization of regulators of GLUT4 trafficking

Thesis directed by Associate Professor Jingshi Shen

Cargo proteins moving between organelles are transported by membrane-enclosed vesicles. Identifying the factors regulating vesicle-mediated transport remains a major challenge in mammalian cells. Here, we performed unbiased genome-wide CRISPR-Cas9 genetic screens to systematically dissect insulin-dependent translocation of glucose transporters (GLUTs), a classic vesicle transport pathway crucial to mammalian physiology. These screens identified known regulators of the pathway as well as a large number of unknown regulatory factors that we validated in secondary screens. The identified genes encode established or predicted factors involved in vesicle budding or fusion, cargo sorting, signal transduction, cell motility, and cellular metabolism, as well as proteins lacking annotated functions. Mechanistic analysis demonstrated that Rab-interacting factor (RABIF), a putative guanine nucleotide exchange factor (GEF), positively regulates GLUT translocation by stabilizing Rab GTPases, a new function independent of its GEF catalytic activity. Alpha- and gamma-adaptin binding protein (AAGAB), identified as a negative regulator of GLUT translocation, acts as a key regulator of AP2 adaptor formation in clathrin-mediated endocytosis. Mass spectrometry-based proteomic analysis showed that both AAGAB and RABIF regulate diverse cargo proteins, suggesting that the factors identified in our screens play broad roles in vesicle transport regulation. Our findings reveal new facets of vesicle-mediated cargo transport and suggest a general strategy for genetically dissecting complex membrane processes in mammalian cells.

ACKNOWLEDGEMENTS

I thank current and former members of the Shen laboratory for their support and discussions throughout this work. The MCDB department has been an excellent training environment, and I have benefitted greatly from discussions with researchers with a wide array of expertise. My thesis committee has provided critical guidance and support throughout graduate school. Jingshi has been a great mentor, taught me a lot, and provided the necessary support at critical junctures. Finally, I would like to thank Brittany for her unwavering support. It's been so much fun to go through graduate school with you!

TABLE OF CONTENTS:

FIGURES:

Chapter 1

GLUT4 vesicle trafficking screens

Introduction

A universal feature of eukaryotic cells is a compartmentalized cytoplasm filled with functionally specialized membrane-bound organelles (Palade, 1975). Maintenance and propagation of the organelles require constant inter-organelle transport of cargo proteins via membrane-enclosed vesicles (Schekman and Novick, 2004; Sudhof and Rothman, 2009). Vesicle-mediated cargo transport was first genetically dissected in yeasts, leading to the identification of vesicle transport mediators conserved in all eukaryotes (Schekman and Novick, 2004). Vesicle transport is substantially more complex in mammalian cells and is often tightly regulated by extracellular and intracellular stimuli such that the speed and direction of cargo flow can be adjusted according to physiological demands (Bonifacino and Glick, 2004; Bryant et al., 2002). Mammalian vesicle transport, however, has not been systematically characterized using genetic screens due to a lack of robust genetic tools. The recent advent of Clustered Regularly Interspaced Short Palindromic Repeats (CRISPR)-Cas9 system has revolutionized mammalian cell genetics by enabling efficient and complete ablation of target genes (Cong et al., 2013; Doudna and Charpentier, 2014; Gilbert et al., 2014; Mali et al., 2013). Pooled CRISPR libraries introduced into cultured cells generate mutant populations that can be subsequently selected

based on cellular phenotypes (Gilbert et al., 2014; Koike-Yusa et al., 2014; Shalem et al., 2014; Wang et al., 2014; Zhou et al., 2014).

One widespread regulated vesicle transport pathway is the insulin-dependent translocation of glucose transporters (GLUTs), which controls nutrient homeostasis in cell types ranging from adipocytes to neurons and tumors (Bryant et al., 2002; Huang and Czech, 2007; Simpson et al., 2008). Upon binding to its receptor, the anabolic hormone insulin facilitates glucose uptake by acutely relocating GLUTs (e.g., GLUT4) from intracellular organelles to the cell surface (Antonescu et al., 2014; Bryant et al., 2002; Saltiel and Kahn, 2001). To dissect insulin-dependent GLUT translocation, we took advantage of the newly introduced Clustered Regularly Interspaced Short Palindromic Repeats (CRISPR)-Cas9 genetic screens (Gilbert et al., 2014; Koike-Yusa et al., 2014; Shalem et al., 2014; Wang et al., 2014; Zhou et al., 2014).

Live cell vesicle trafficking reporter

Insulin-dependent GLUT translocation was monitored using a dual-tag GLUT reporter in which GFP was fused to a cytosolic domain of GLUT4 and a hemagglutinin (HA) epitope was inserted into an exoplasmic loop (Fig. 1.1a) (Muretta et al., 2008). Surface levels of the reporter were tracked by staining the HA tag using anti-HA antibodies and allophycocyanin (APC)-conjugated secondary antibodies. The total reporter levels were reflected by GFP fluorescence. The ratio of APC and GFP fluorescence was measured by flow cytometry to quantify the relative surface levels of the reporter in live cells (Fig. 1.1).

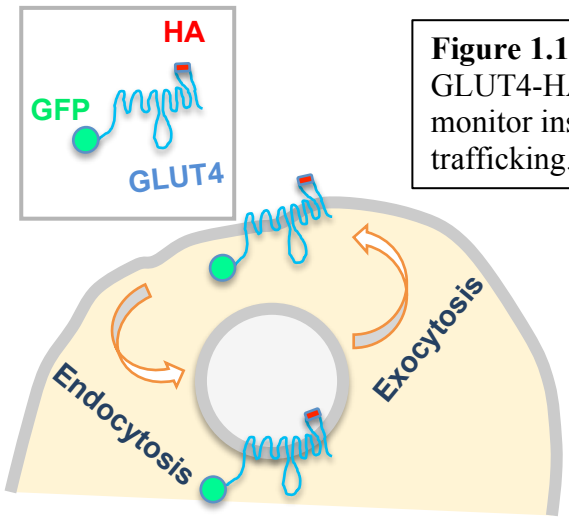

Figure 1.1: Diagram of the GFP-GLUT4-HA reporter used to monitor insulin-dependent GLUT trafficking.

Insulin stimulation markedly increased the surface levels of the GLUT reporter in HeLa cells (Fig. 1.2a), consistent with the previously reported insulin responsiveness of these cells (Trefely et al., 2015). Insulin-triggered GLUT reporter translocation was abolished by wortmannin, a phosphoinositide-3 kinase inhibitor that interferes with insulin signaling (Fig. 1.2a). Knockout (KO) of *RAB10,* which encodes a known positive regulator (Sano et al., 2007), abrogated insulin-triggered GLUT reporter translocation (Fig. 1.2). KO of *TBC1D4*, which encodes a known negative regulator (Eguez et al., 2005), resulted in constitutive surface translocation of the reporter (Fig. 1.2a). These data are reminiscent of the observations in other insulin-responsive tissues such as adipocytes (Fig. 1.2b) (Eguez et al., 2005; Sano et al., 2007), suggesting that the GLUT translocation pathway is governed by a conserved mechanism. Therefore, we chose to perform genome-wide CRISPR screens in the readily expandable HeLa cells and then extended the findings to other cell types and pathways.

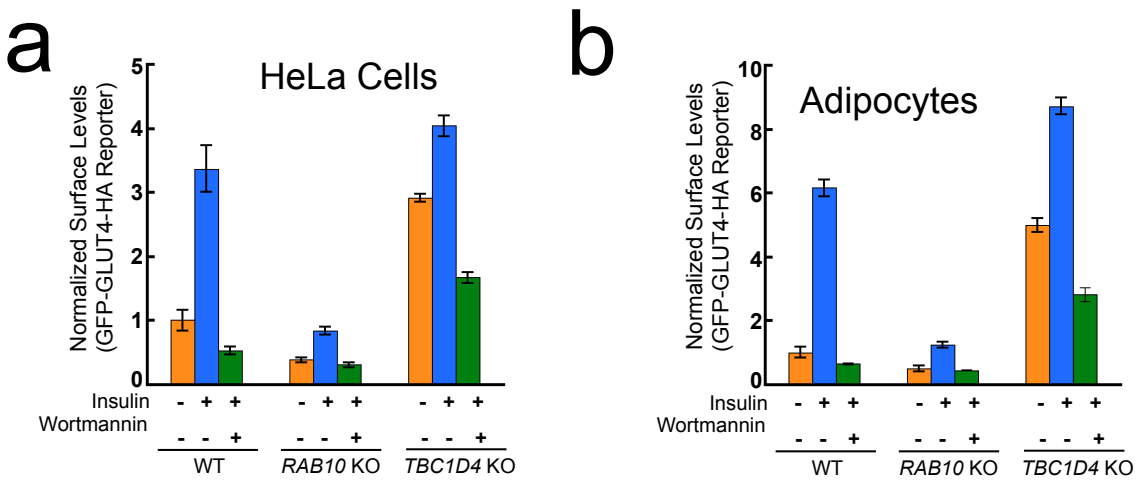

Figure 1.2: **GLUT4 regulation is conserved between HeLa cells and adipocytes.** HeLa cells (**a**) or adipocytes (**b**) expressing the GFP-GLUT4-HA reporter were either untreated or treated with 100 nM insulin for 30 min before the surface reporters were stained with anti-HA antibodies and APC-conjugated secondary antibodies. To inhibit insulin signaling, the cells were incubated with 100 nM wortmannin for 10 minutes prior to insulin stimulation. The ratio of APC and GFP fluorescence was measured by flow cytometry and the mean fluorescence was normalized to that of untreated WT cells. Error bars indicate standard deviation. *RAB10* and *TBC1D4* KO cell lines were generated using CRISPR-Cas9 genome editing.

Genetic library creation

We first selected for HeLa cells with a large dynamic range in insulin response. Using a population of HeLa cells stably expressing the GLUT reporter we treated the cells with insulin and used cell sorting to enrich for cells with the largest fraction of GLUT reporter on the surface. Subsequently, after expanding the sorted population, we selected for cells with the lowest level of GLUT reporter on the surface in the absence of insulin. Finally, a third enrichment step was performed, again enriching for cells with the highest level of GLUT reporter on the surface after

insulin treatment. These highly responsive HeLa cells were subsequently cloned prior to building the mutant library. This clonal cell line was then mutagenized by a pooled lentiviral CRISPR library containing 123,411 independent single guide RNAs (sgRNAs) targeting 19,050 protein-coding genes and 1,864 miRNAs (Sanjana et al., 2014). Using this mutant collection, we performed two complementary genome-wide genetic screens (Figure 1.3).

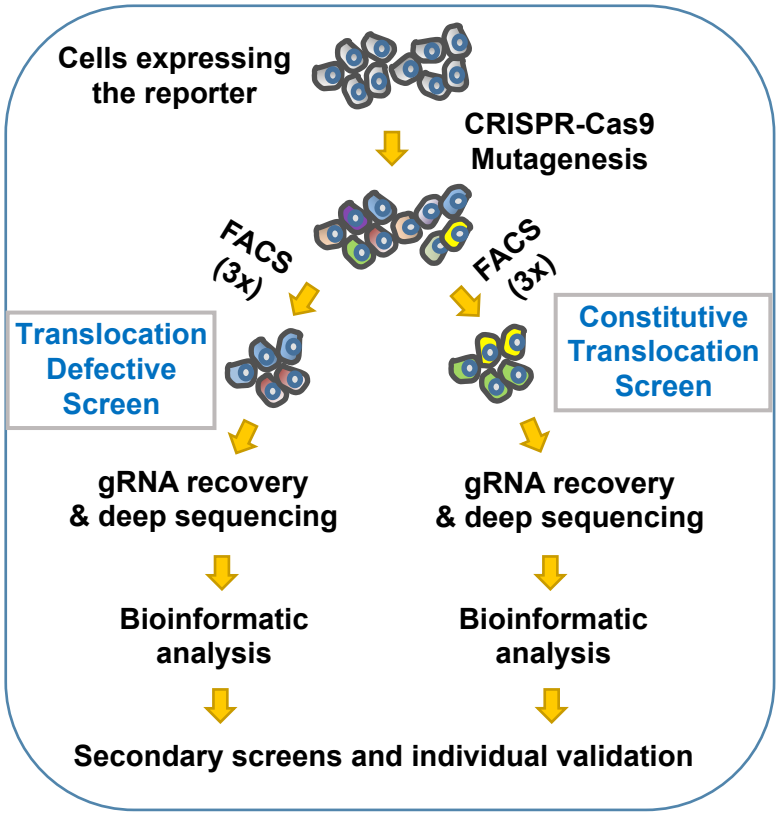

Figure 1.3: Illustration of the genome-wide genetic screens of insulin-dependent GLUT translocation.

Fluorescence activated cell sorting can be used for phenotypic selection

In the translocation defective screen (Fig. 1.4a), which was designed to identify positive regulators of GLUT translocation, flow cytometry was used to isolate mutant cells exhibiting reduced insulin-triggered GLUT translocation. In the constitutive translocation screen (Fig. 1.4b)

we collected mutant cells with high surface GLUT reporter levels in the absence of insulin stimulation, aiming to identify negative regulators of GLUT translocation.

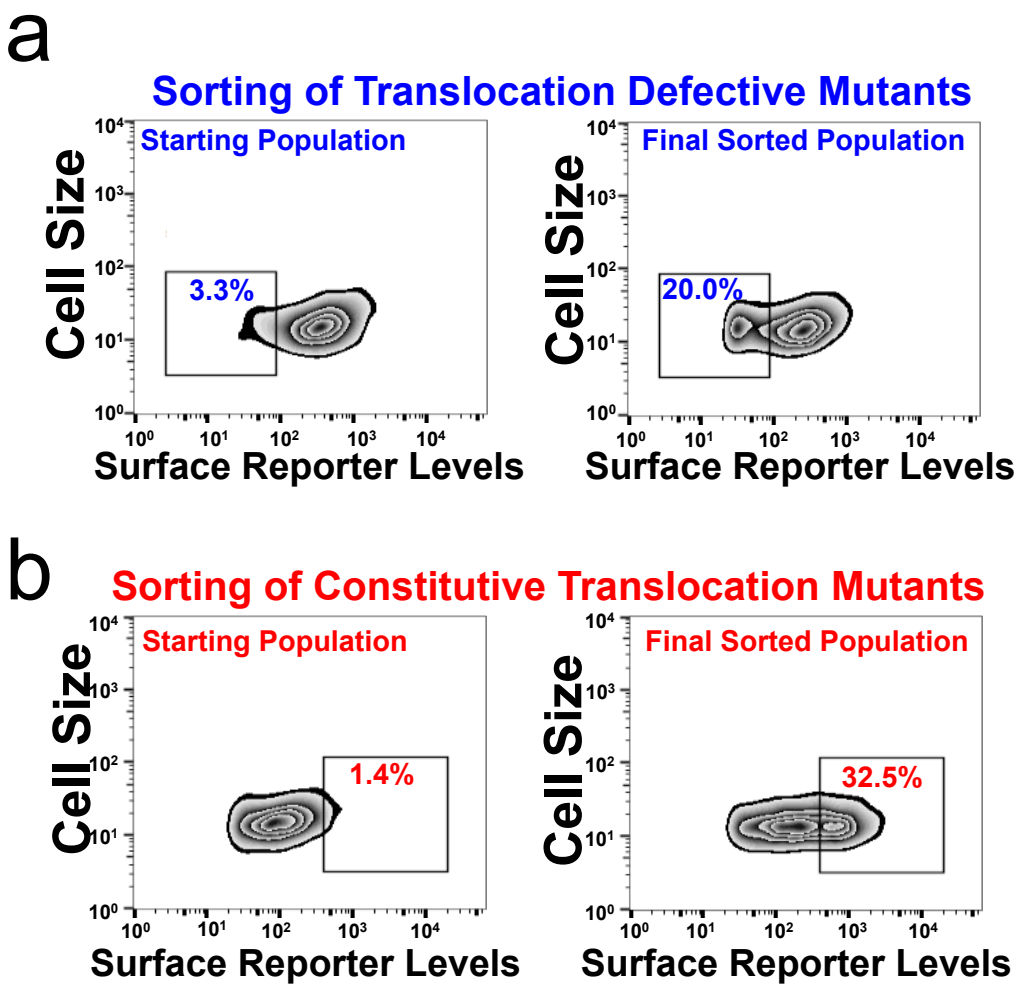

Figure 1.4: Flow cytometry selection for GLUT4 translocation mutants in genome-wide screen. **a,** Flow cytometry analysis of starting mutant population and final sorted population (after three rounds of sorting) in the genome-wide translocation defective screen. Cells were treated with 100 nM insulin for 30 minutes before the cells were stained and analyzed by flow cytometry. **b,** Flow cytometry analysis of starting mutant population and final sorted population (after three rounds of sorting) in the genome-wide constitutive translocation screen. Cells were stained and analyzed without insulin stimulation.

To effectively enrich true positives, the mutagenized cells were successively sorted for three rounds (Fig. 1.3) before sgRNAs were recovered and analyzed by deep sequencing. The abundance of many sgRNAs in the sorted populations was substantially increased compared to the unsorted control population grown under the same condition. Among them, sgRNAs targeting *SLC2A4, RABIF*, *AP2S1* and *AAGAB* were highly enriched (Fig. 1.5 a,b). By contrast, non-targeting control sgRNAs overall exhibited little enrichment (Fig. 1.5 a,b). Genes were ranked based on the enrichment of their targeting sgRNAs using the MAGeCK algorithm (Li et al., 2014).

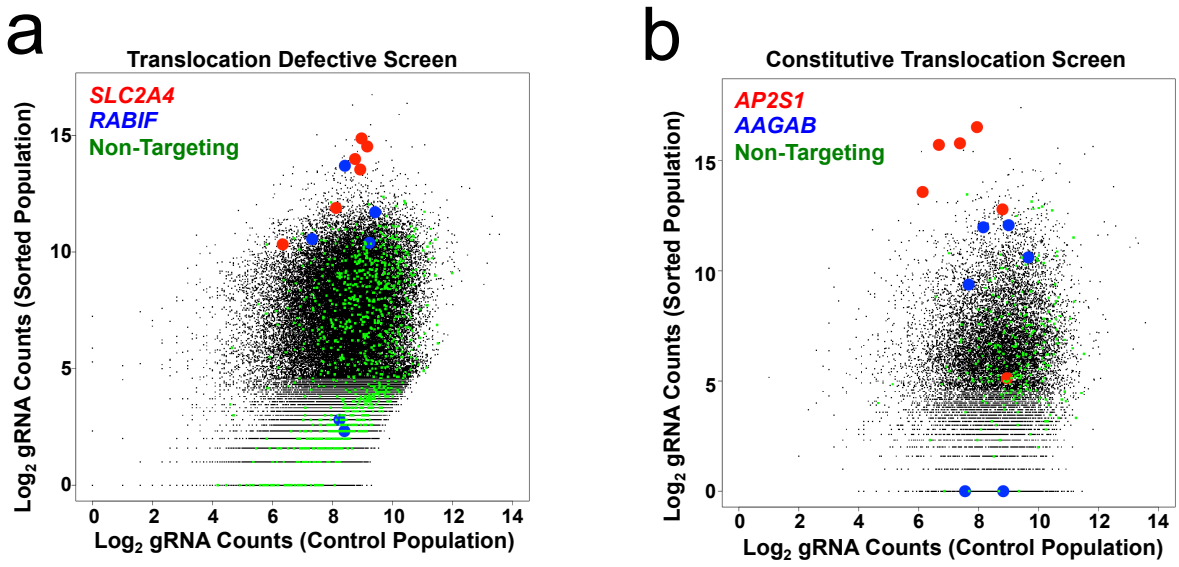

Fig 1.5: Enrichment of sgRNA in selected populations.
a, Relative abundance of sgRNAs in the genome-wide translocation defective screen. **b**, Relative abundance of sgRNAs in the genome-wide constitutive translocation screen. Data in a and b are shown as $\log_2$ of sgRNA abundance.

Secondary screens validate the candidate list

To identify true regulators, we performed deeper secondary screens by building a pooled CRISPR library targeting the top 1,170 candidate genes from the two genome-wide screens with 10 new sgRNAs for each gene. HeLa cells expressing the GLUT reporter were mutagenized by the secondary CRISPR library and sorted by flow cytometry (Fig. 1.6). Enrichment of sgRNAs in the sorted populations was then determined. A gene is considered significant only if its corresponding sgRNAs were enriched in both the primary and secondary screens. Altogether, 329 significant genes were identified in the translocation defective screens and 235 in the constitutive translocation screens (Fig 1.7).

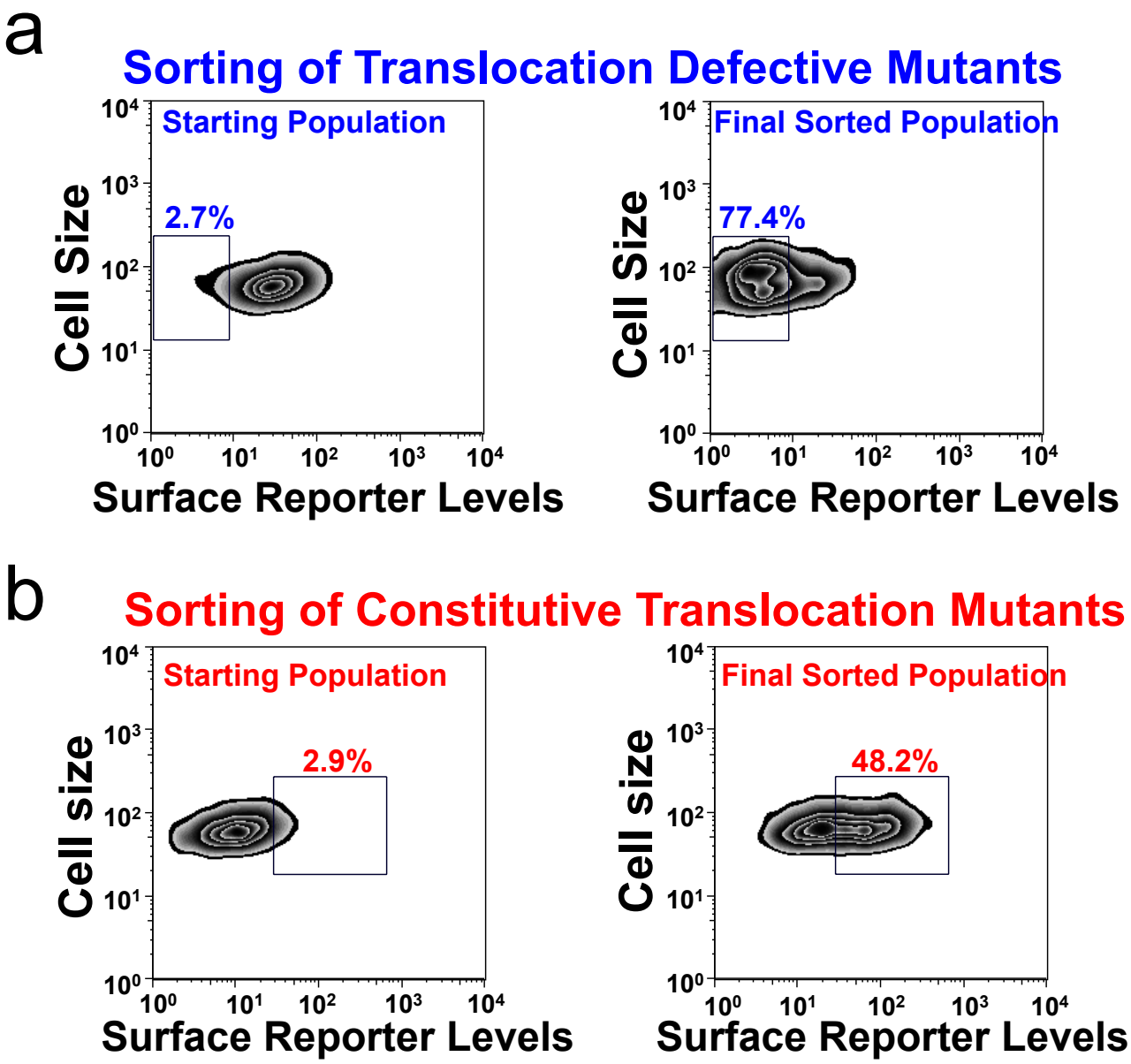

Figure 1.6: Flow cytometry selection for GLUT4 translocation mutants in secondary screen. **a,** Flow cytometry analysis of starting mutant population and final sorted population (after two rounds of sorting) in the secondary translocation defective screen. Cells were treated with 100 nM insulin for 30 minutes before the cells were stained and analyzed by flow cytometry. **b,** Flow cytometry analysis of starting mutant population and final sorted population (after three rounds of sorting) in the secondary constitutive translocation screen. Cells were stained and analyzed without insulin stimulation.

Translocation Defective Screen

LIAS	CRTC3	NEO1	NDUFAF7	INSR	KCTD9
RAB10	MRPS35	CDIP1	TRMT10B	MTMR9	PXK
DLD	COQ2	CGGBP1	MFAP3	G3BP2	TBCEL
SDHD	IRF1	GRSF1	COX16	SAFB	ZNF292
EXOC7	EXOC1	LRRC20	STK17A	TFDP2	USP31
LIPT1	MDH2	FH	MRPS16	PIK3R4	NDUFA11
NDUFB2	NDUFA3	UBL3	ENPP2	SIKE1	STX3
FOXRED1	PYROXD1	TMED2	NDUFS1	C21orf2	MPP5
EXOC8	NDUFB10	ZNF251	LNPEP	GTPBP1	HMOX1
MRPS18A	TARBP1	NDUFS7	HAUS7	BZW2	C6orf62
NDUFB9	HLA-DPB1	MRPS31	CRLF3	SUMF2	PPIL3
NDUFA2	PNKD	AIF1L	NDUFAF4	C5orf28	KIAA2018
NDUFC1	AP4S1	PDXDC1	ING2	FKBP9	AES
ASPH	ZNF254	NDUFA1	MORN4	PKP4	TTC12
NDUFAF1	MSRB1	SERINC5	PACRGL	TMEM135	FLI1
NDUFB3	IFT81	RAB4A	TTC4	SUMO1	ANKZF1
NDUFAF3	C8orf82	PIK3CB	NGFRAP1	MAFB	HGS
ZNF263	PLEKHG1	ABR	SORT1	GRB2	SNAP29
DNAAF2	PEX12	MMADHC	ITCH	APOL1	C6orf136
PDHA1	CDH13	ATP1B3	PAAF1	COQ7	HDHD1
RPRD1A	VPS35	PHLDB2	NDUFB4	ALG3	PSEN1
CS	IFNAR2	NDUFS2	IRAK4	BTG1	AAED1
CCSER2	KIF3A	EZH1	ZBTB14	GGA1	PELI1
CAMTA1	RABIF	COQ4	ALS2	MTERF	DNAJB2
TRUB1	PLEKHF2	IRS2	TUBA1A	SLC25A36	ENG
					USP38

MUC4	VN1R2	CYP2J2	PNMT	CST9L	ZNF138
CLVS2	TAS2R39	SLC2A4	PF4	FAM217A	ZNF737
ARPP21	DEFB125	MTNR1A	CABP1	MAGEB2	C9orf172
GPC2	FAM78B	SLCO4C1	PGM2L1	SLCO6A1	ZNF221
MEP1A	SOD3	EVA1A	ASB3	SLC22A14	ZNF708
HEPACAM2	RTBDN	NPNT	GABRG2	ODF3	ZNF845
ACY1	AOX1	ST8SIA6	SYN1	ZCWPW1	PDSS1
C15orf62	C19orf38	TMEM125	IL1RAPL1	TSKS	PREX2
GPR157	FAM46A	PRX	GABRB1	PRR23C	ZNF234
RSPH9	NUSAP1	TCF7	NIM1	PIAS2	ZNF709
MAK	ARHGDIG	TESPA1	TMEM132D	VCX3B	WNT2B
CCDC147	LAMP5	CD84	C8orf46	PDZD9	CD300C
APOBEC4	BEST3	GREB1	ACTL6B	ZNF683	FKBP1B
MDH1B	GOLGA7B	DIO3	GRIN2A	SSMEM1	TMEM261
FHL2	GALNTL6	AREG	FGFBP1	RAD9B	NOSTRIN
DCUN1D2	PCSK1	CLEC12B	NPPB	MAGEA6	PUS7L
ACSM2B	KIAA2022	OCA2	ANKRD1	LEMD1	ZNF879
UGT2B7	RASGEF1A	IGSF6	INHBC	USP26	XYLT1
CLCNKB	STAC2	BACE2	ANGPTL3	TRIML1	PTCHD4
SLC5A12	SSTR2	SALL4	GCKR	ZNF816	HYKK
SOX14	RHBDL3	CEP19	APOA2	FGF13	PLEKHA8
VSIG8	GRIA3	DDX3Y	SLC34A2	ZBTB12	CACHD1
PDILT	SMIM22	ZNF732	PRH2	APBB1IP	EML4
MRGPRG	FOLR1	UTS2B	ACHE	LIPT2	GRAMD1C
CST9	NPHP1	DDHD1	LCE2A	RANBP17	DACT3
KRTAP19-2	PLCH1	SENP8	POU3F1	CENPH	DNAJC17
SIX6	HOXB5	ZNF19	COL17A1	DMXL2	PPIC
DEFB116	CXorf64	CLDN11	TMEM45A	C1orf210	FCER1A
KRT38	LIF	FAM53A	PRKACG	TNIK	ARHGEF19
ASCL5	OGN	FABP4	KIF4B		

Constitutive Translocation Screen

AP2S1	TTC7B	TMUB2	DCUN1D5	GOT1	ANGEL2
AAGAB	SLC35A2	IL16	DPCD	ACSS1	RALGAPA2
B3GNT2	CCDC91	GTF2A1	SESN1	RNF14	TGS1
FAM3A	SCAF8	ADNP	FAM122B	LAPTM5	OGT
ANKRD13D	C19orf66	HLA-DRA	RNF5	PARP6	DNAJB14
AP2M1	RBM43	VWA9	RNF7	COG3	COG6
HSD17B11	STIM1	AAED1	JMJD4	NFIX	ELMSAN1
COG2	LARP4	MLH3	SERBP1	PACS2	NUMBL
CBX7	TBC1D4	C12orf43	SLC39A9	ROCK2	GALE
CIC	FARP1	RND3	DPY19L1	CNOT7	SIN3B
UBTD2	RECK	HNRNPA3	MSL1	TAX1BP3	UBE3C
MGAT1	SLAIN1	LTBR	GOLIM4	COG7	RAB24
OSBPL8	ABHD12	HERC3	GALK1	FCHO2	IMPDH1
NDUFAF6	VHL	NCKAP5L	SIAH1	PEBP1	NCF4
SDCBP	LGALS3	MLLT3	SERINC1	ATXN2L	C16orf13
ZNF362	ZNF222	CDKN2AIPNL	ACCS	CNN3	ZNF202

MCF2L2	MYB	CRIP3	SALL4	ALPP	NTPCR
BRINP2	S100P	TRPV4	FAM53A	CHAT	NUAK2
POU3F3	KIF21B	ABCA4	KATNAL2	LGALS13	CYP4X1
KCTD4	UNC5D	SLCO4C1	CAPRIN2	PRR4	PRTFDC1
DDX25	FAM169A	A1CF	SDK2	CCL28	DLGAP5
MOGAT3	GNAZ	DNAJC25	GLB1L	KLHL33	PCDHB10
ATOH1	RORB	CYP4B1	SALL1	KCNJ12	TMED8
PCK2	FAM171B	CETP	NTRK1	IL37	CDC14B
TMEM40	SORCS3	KLRG1	NETO1	TFF2	C8orf44
GLTP	MAP1B	VIT	PTPN5	TCP10	TLR1
C14orf105	CDR1	MCC	BRSK1	LIPJ	ATXN7L2
IGF2BP1	TRABD2A	ADAMTSL4	MAS1	PTCHD3	ARHGAP29
TGM7	B3GNT7	SLC15A2	TMEM235	SPANXN3	CYSLTR1
IFNA5	HKDC1	GCNT2	DYNAP	FOXR2	ZFP14
HOXB1	LMX1A	SPDEF	MOGAT1	DCAF8L1	VASN
C9orf170	RSPO1	CAPN9	CAPN12	RFPL4B	FLT3LG
ERVW-1	DUOXA1	KCNN4	TNNI3	HSPB9	SAPCD2
PTX3	C2orf54	KLHL30	ANKRD1	OTOS	BAIAP2L1
KCNA4	FBXL13	ESPN	UMOD	MGAT2	TMEM194B
CNGB1	TTC26	NXPH4	SLC17A1	KIAA1462	GLIPR1
SULT2A1	CFTR	DPYSL3	TMEM27	CHKB	EFS
SIGLEC10	LIF	KLRD1	CLDN16	IRAK2	GDAP2
EMR3	RBM24	FAM177B	CDH16	OSBPL10	DDO
					SLC5A7

Figure 1.7: List of the genes identified in the genetic screens. These genes were identified in the genome-wide genetic screens and validated in the secondary screens. Genes with ubiquitous expression are highlighted in blue whereas genes with tissue-specific expression are highlighted in red. The tissue distribution of a gene is based on RNA expression data in Human Protein Atlas (www.proteinatlas.org). Genes associated with human diseases are indicated with boxes. A gene is included if its disease connections are shown in both MalaCards (www.malacards.org) and UniProtKB (www.uniprot.org).

The screens identified known and novel regulators of GLUT4 localization

The top-ranking gene in the translocation defective screen is *SLC2A4,* which encodes GLUT4 itself (the GFP-GLUT4-HA reporter is also targeted by *SLC2A4* sgRNAs), highlighting the quantitative nature of the screens. The screens identified known regulators of insulin-dependent GLUT translocation including RAB10, TBC1D4, sortilin-1, AP2 adaptor, and insulin signaling molecules (Fig 1.8). Recovery of these known regulators indicates that the screens were sensitive and specific. The vast majority of the identified genes, however, have not previously been linked to the GLUT translocation pathway, including 92 genes lacking annotated functions (Fig. 1.9 a,b). These findings highlight that we are still at the early stage of understanding the regulatory networks of GLUT translocation.

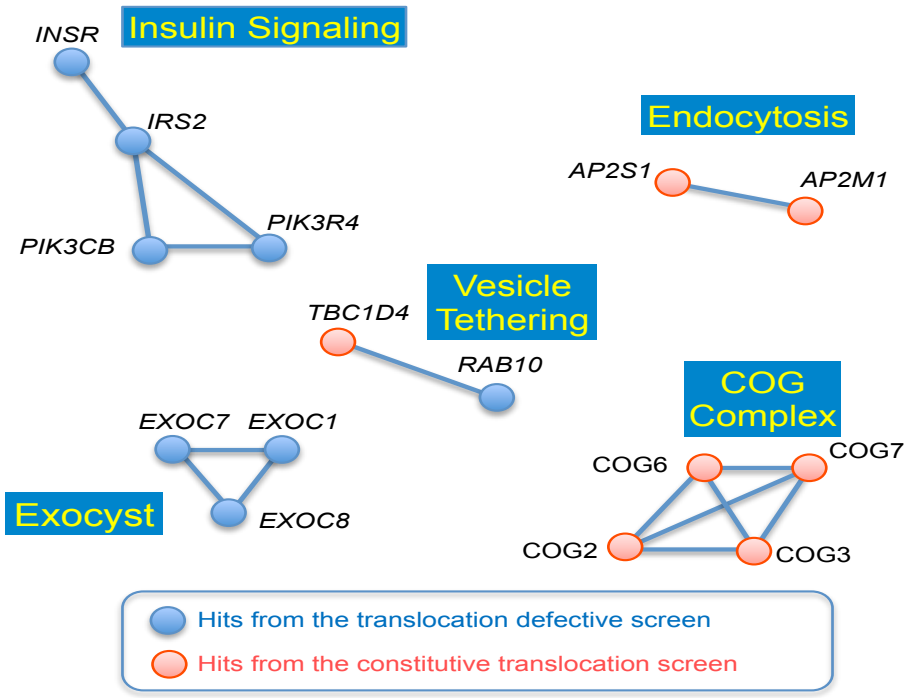

Figure 1.8: Regulatory factors identified in the CRISPR screens form protein complexes or functional modules. Only selected complexes or modules related to insulin signaling or vesicle transport are shown. The genes are colored according to the screen in which they were identified.

Translocation Defective Screen

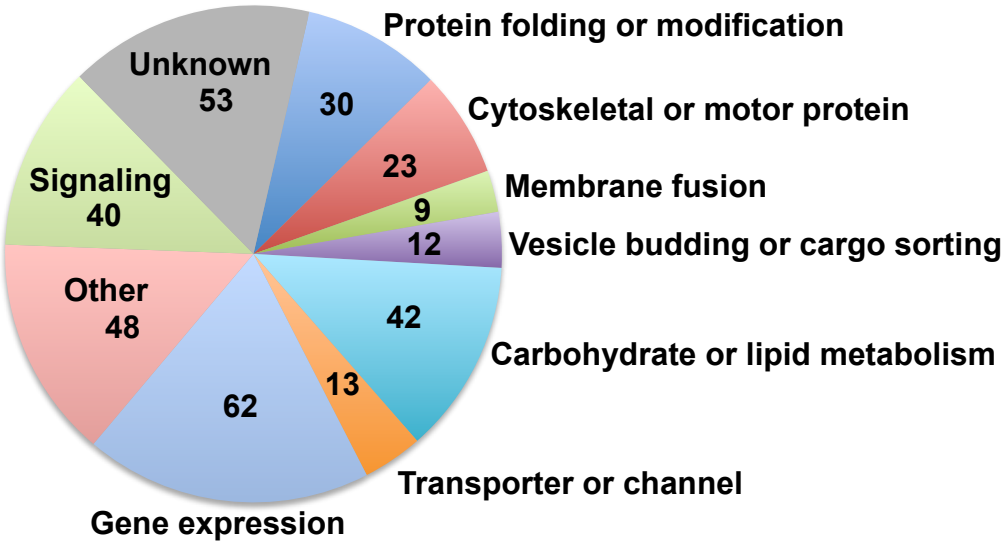

Constitutive Translocation Screen

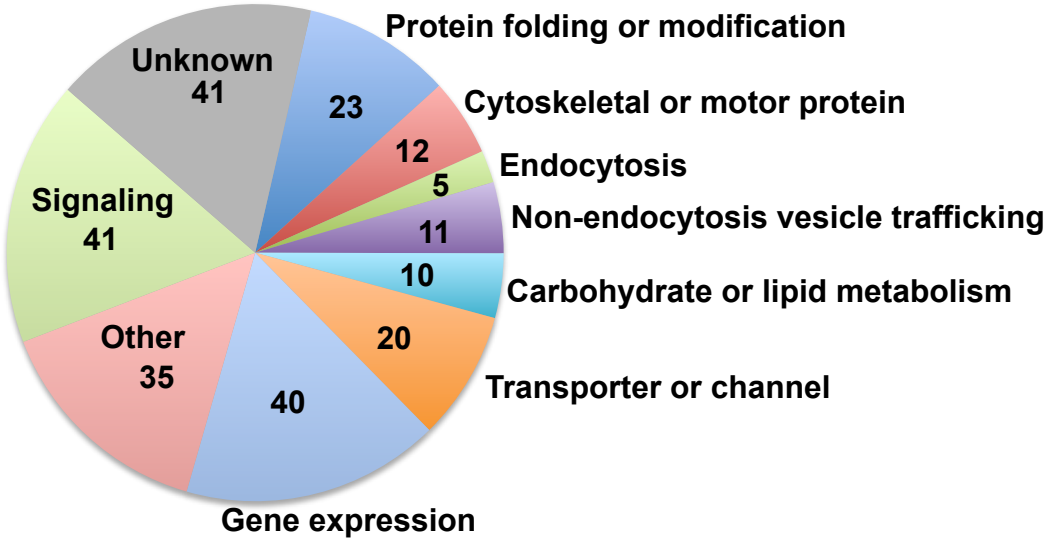

Figure 1.9: Summary of genes validated by the secondary screens. a, Translocation defective screen. **b,** Constitutive translocation screen.

The genes were classified as either positive or negative regulators of GLUT translocation according to the screen in which they were identified (Fig 1.9). From these two functional groups, genes were further characterized according to their known or predicted biological function (Fig 1.9 a,b). Approximately half of the identified genes have been implicated in various aspects of vesicle transport regulation such as vesicle budding/fusion, cargo sorting, cell motility, and signal transduction (Fig. 1.9 a,b). Other genes encode enzymes involved in lipid/carbohydrate metabolism, mediators of gene expression, and solute transporters (Fig 1.9). A significant portion of the identified genes may indirectly impact GLUT translocation by controlling the expression or localization of a direct regulator. Nevertheless, these genes constitute critical components of the regulatory networks because their deficiency leads to dysregulation of GLUT translocation. Identification of these diverse genes indicates that the GLUT translocation pathway is considerably more complex than previously thought, and its exploitation of cellular processes is extensive.

Many identified factors form protein complexes or functional modules such as exocyst, conserved oligomeric Golgi complex, AP2 adaptor, and insulin signaling (Fig 1.8). Recovery of these functionally linked genes suggests that the screens were exhaustive. Missing components of a complex or module are likely due to functional redundancy, rather than incompleteness of the mutant library, because their corresponding sgRNAs were present in the control mutant population (Supplementary Table 1). For example, the translocation defective screen identified the entire insulin signaling pathway except AKT (Fig 1.8). The absence of AKT is readily explained by the known redundancy of AKT isoforms (Dummler et al., 2006). The constitutive translocation screen isolated the μ2 and σ2 subunits of the tetrameric AP2 adaptor involved in

endocytosis (Fig 1.8) (Brodsky, 2012). The α and β2 subunits of the A2P adaptor, however, were not recovered. This finding is in full agreement with the known redundancy of the genes encoding the α subunit (*AP2A1* and *AP2A2*) or the β2 subunit (*AP2B1* and *AP1B1*) (Traub and Bonifacino, 2013). We anticipate that our screens will facilitate the identification of previously unrecognized gene redundancy.

A large fraction of the regulatory factors exhibit ubiquitous tissue distributions and/or disease connections (Fig 1.7), underscoring their importance in physiology. We next examined whether the new genes identified in the screens also regulate GLUT translocation in other insulin-responsive cell types. Deletion of *VPS35*, which encodes a subunit of the retromer complex, abrogated insulin-triggered GLUT translocation in adipocytes (Fig 1.10a,). Similarly, deletion of *RABIF*, a putative Rab GEF, diminished GLUT translocation in adipocytes (Fig 1.10a). Deletion of *AAGAB*, which was identified in the constitutive translocation screen, dramatically increased the basal surface levels of GLUT reporter in adipocytes (Fig 1.10b). To examine the dynamic range of the genes; we also tested lower-ranking (still above the cutoff) genes from the screens. KO of *OSBPL8* or *OSBPL10*, which encode putative lipid transfer proteins, resulted in about twofold increases in the basal surface levels of GLUT reporter in adipocytes (Fig 1.10b). Similarly, KO of *ANKRD13D*, a poorly characterized ubiquitin-binding factor, doubled the basal surface levels of GLUT reporter in adipocytes (Fig 1.10b). These results suggest that the findings of our HeLa screens are applicable to other cell types (Fig 1.11, Fig 1.12, Table 1.1).

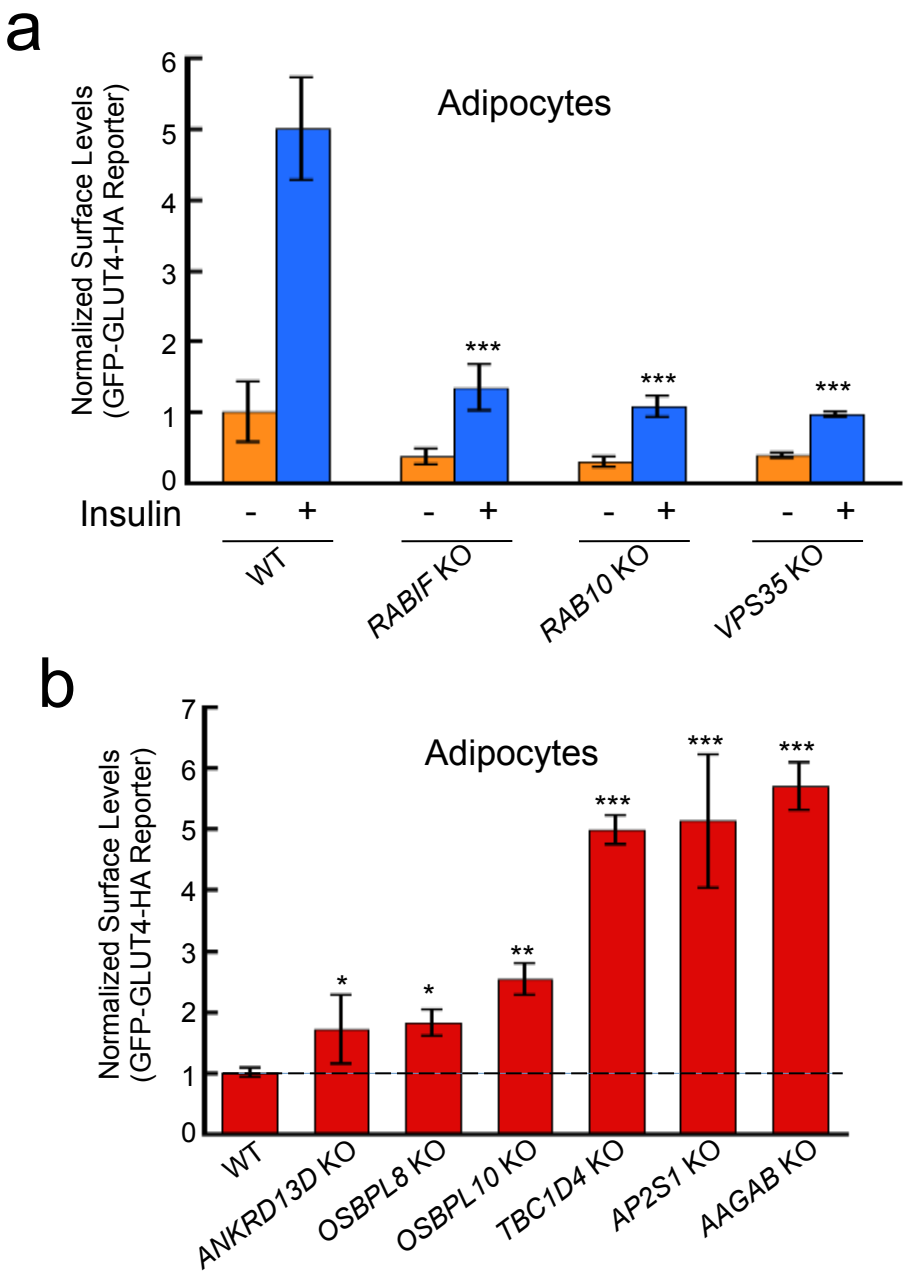

Figure 1.10: Genes identified in the HeLa cell screen could be validated in adipocytes. **a,** Selected genes from the translocation defective screen were individually mutated in mouse adipocytes using CRISPR-Cas9. Effects of the mutations on insulin-dependent GLUT translocation were measured by flow cytometry. **b**, Selected genes from the constitutive translocation screen were individually mutated in mouse adipocytes using CRISPR-Cas9. Effects of the mutations on surface reporter levels were measured by flow cytometry (without insulin treatment). The dashed line indicates the surface GLUT reporter level in WT cells without insulin stimulation. Error bars in e and f indicate standard deviation. **P*<0.05; ***P*<0.01; ****P*<0.001.

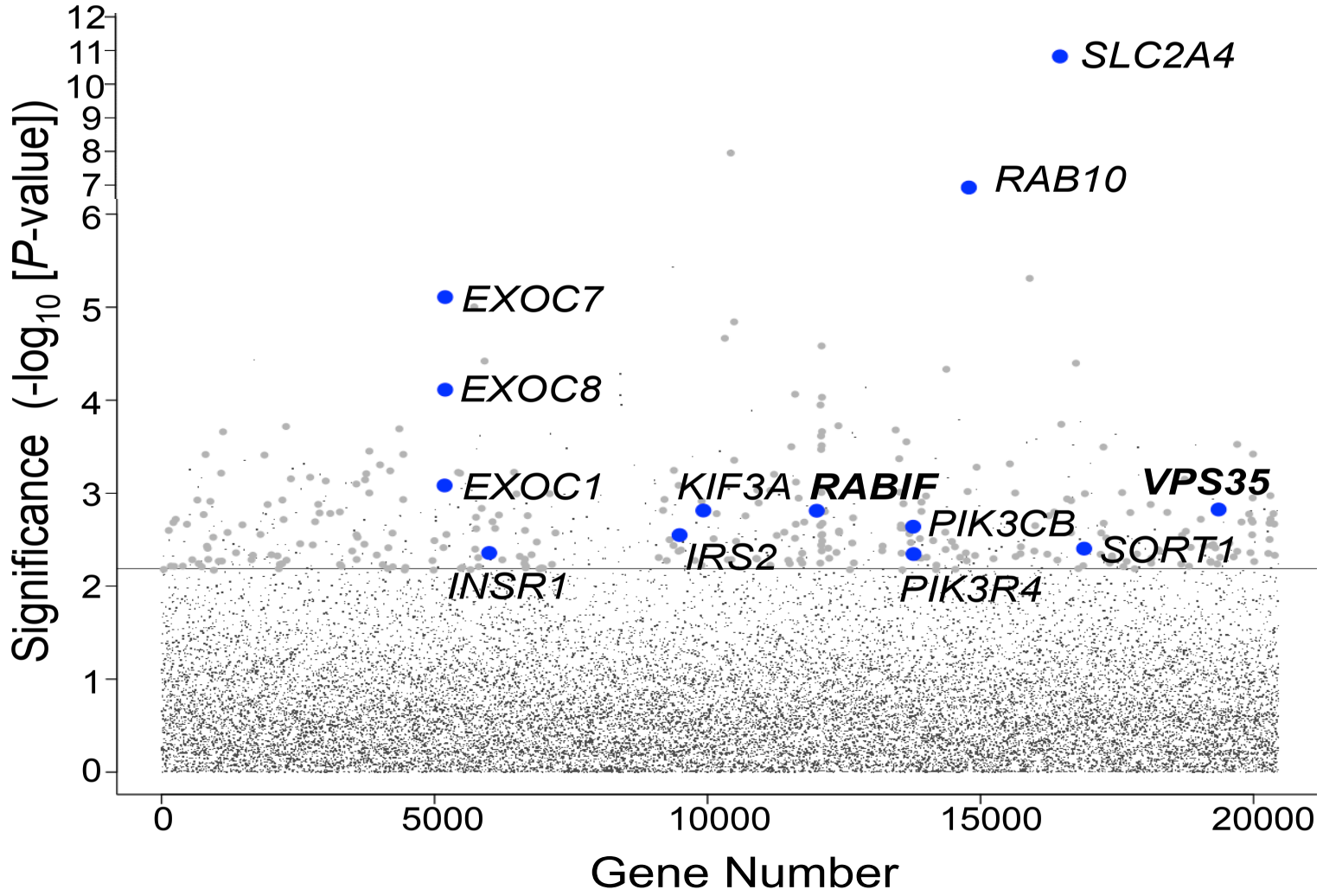

Figure 1.11: Ranking of genes in the translocation defective screen based on p-value. Each dot represents a gene. Genes above the horizontal line were tested in the secondary screen. A gene is shown as a large dot if it was validated in the secondary screen. Genes regulating GLUT trafficking in both HeLa and adipocytes are shown in blue, and genes validated in figure 1.10 are shown in bold

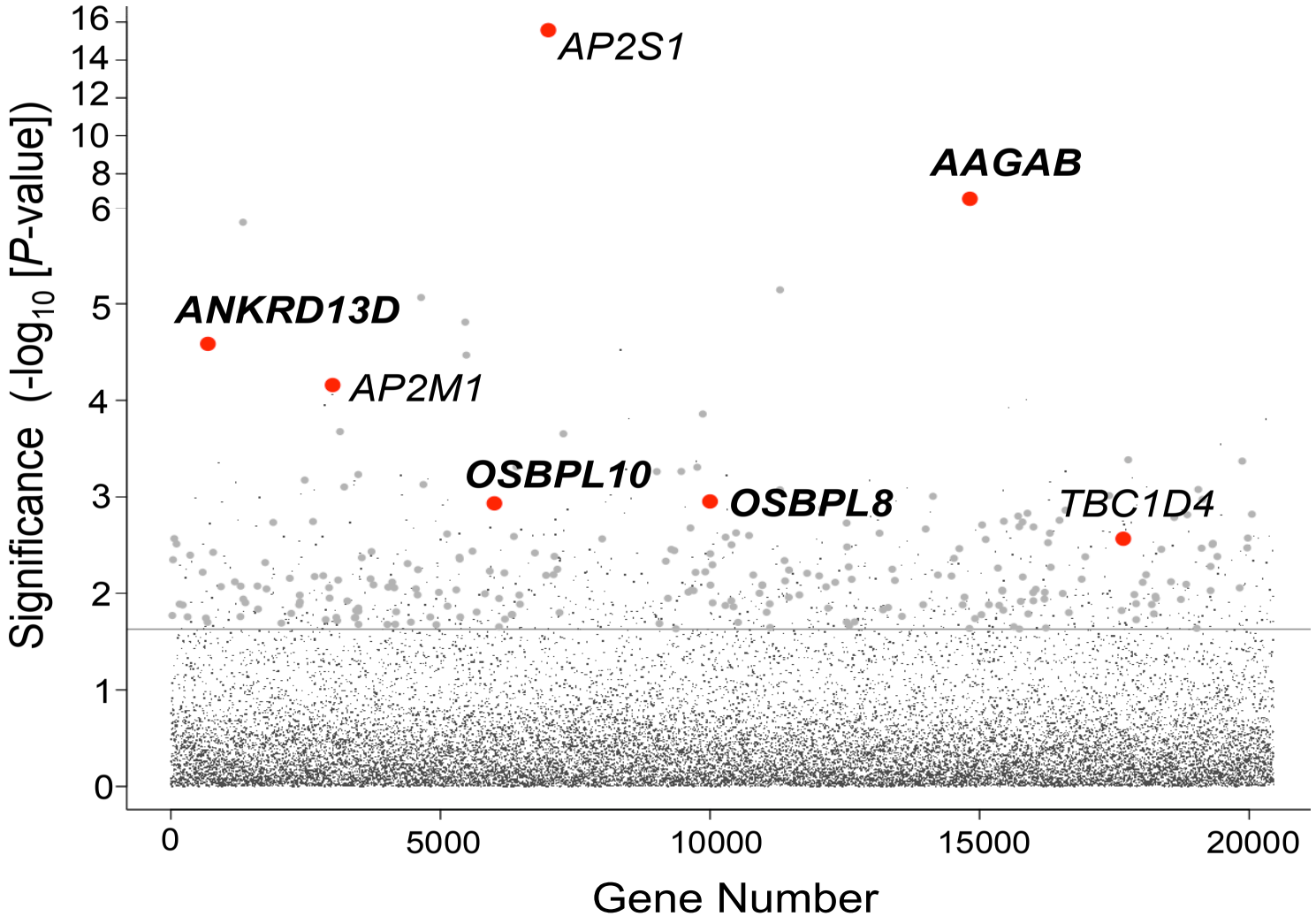

Figure 1.12: Ranking of genes in the constitutive translocation screen based on p-value. Each dot represents a gene. Genes above the horizontal line were tested in the secondary screen. A gene is shown as a large dot if it was validated in the secondary screen. Genes regulating GLUT trafficking in both HeLa and adipocytes are shown in red, and genes validated in figure 1.10 are shown in bold

Table 1.1: Summary of top ranking genes in either the translocation defective screens or the constitutive translocation screens. (Genes enriched in both primary and secondary screens are highlighted)

Ranking of genes enriched in the genome-wide translocation defective screen				Ranking of genes enriched in the genome-wide constitutive translocation screen			
Rank in primary screen	**Gene ID**	***p*-value**	**Rank in secondary screen**	**Rank in primary screen**	**Gene ID**	***p*-value**	**Rank in secondary screen**
1	*SLC2A4*	1.50E-11	33	1	*AP2S1*	2.66E-16	2
2	*LIAS*	1.12E-08	46	2	*AAGAB*	2.11E-07	12
3	*RAB10*	1.19E-07	13	3	*B3GNT2*	1.43E-06	17
4	*DLD*	6.02E-07	34	4	*MGAT2*	7.17E-06	3
5	*IMPA1*	3.71E-06	632	5	*DUOXA1*	8.61E-06	260
6	*SDHD*	4.90E-06	275	6	*FAM3A*	1.55E-05	7
7	*EXOC7*	7.79E-06	3	7	*ANKRD13D*	2.60E-05	428
8	*FGF13*	9.90E-06	384	8	*FAM53A*	3.40E-05	293
9	*LIPT1*	1.44E-05	318	9	*AP2M1*	6.95E-05	4
10	*LCE2A*	2.16E-05	478	10	*CELSR1*	8.72E-05	911
11	*NDUFB2*	2.61E-05	11	11	*SCPEP1*	9.87E-05	838
12	*C10orf68*	3.68E-05	639	12	*CDC42EP5*	0.00011191	636
13	*FOXRED1*	3.80E-05	5	13	*RPRML*	0.00011878	644
14	*SMIM22*	4.00E-05	497	14	*KIAA1462*	0.00013866	487
15	*PRKACG*	4.65E-05	431	15	*ZNF74*	0.00015641	NA
16	*OR4F5*	7.29E-05	NA	16	*CHKB*	0.00021099	54
17	*EXOC8*	7.72E-05	301	17	*HS3ST6*	0.00022209	548
18	*MRPS18A*	8.63E-05	524	18	*WDR52*	0.00028559	789
19	*NDUFB9*	9.30E-05	21	19	*TCP10*	0.00041319	344
20	*NDUFA2*	0.00011274	12	20	*ZIK1*	0.00042649	555
21	*LUC7L3*	0.00012981	1062	21	*KCNU1*	0.00043059	682
22	*CEP19*	0.00014179	220	22	*ARAP1*	0.00044134	912
23	*PSRC1*	0.00016294	629	23	*GNAZ*	0.00049154	117
24	*SNRPE*	0.0001698	1110	24	*KCTD4*	0.00049325	512
25	*SLC34A2*	0.00018174	78	25	*SLC5A5*	0.00054254	1054
26	*NPHP1*	0.00018849	515	26	*IRAK2*	0.00054516	524
27	*CABP1*	0.00019187	402	27	*HSD17B11*	0.00054716	74
28	*DIO3*	0.00020332	310	28	*COG2*	0.00058712	5
29	*PCSK1*	0.00020921	38	29	*DENR*	0.00059706	667
30	*NDUFC1*	0.00021771	19	30	*LCA5L*	0.00059897	595
31	*ASPH*	0.00021875	62	31	*TEX13B*	0.00063693	731
32	*OCLM*	0.00022501	NA	32	*EED*	0.00064897	699
33	*HLTF*	0.00022967	737	33	*CBX7*	0.00067059	249
34	*SYNCRIP*	0.00023366	781	34	*OR52M1*	0.00067435	NA

35	*FLYWCH1*	0.00024217	1134	35	*CNGA2*	0.00068602	729
36	*NDUFAF1*	0.00024262	24	36	*SLC16A14*	0.00070087	1053
37	*OPA1*	0.00024917	1107	37	*ATP1A4*	0.00070686	NA
38	*SERPINB2*	0.00026364	890	38	*DYNAP*	0.00074515	484
39	*KIF4B*	0.00028006	50	39	*CMTM7*	0.00075277	585
40	*PGM2L1*	0.00028027	313	40	*CIC*	0.0007896	472
41	*SCN2B*	0.00028557	590	41	*TMEM105*	0.00079329	1039
42	*ZBTB12*	0.00029872	492	42	*PHAX*	0.00080467	1020
43	*SMARCA2*	0.00030094	720	43	*UBTD2*	0.00083834	101
44	*TXNDC5*	0.000301	1049	44	*MGAT1*	0.00084451	11
45	*NDUFB3*	0.000308	23	45	*CCL21*	0.000846	NA
46	*MRGPRG*	0.00031648	414	46	*ROBO1*	0.00085656	740
47	*ST8SIA6*	0.00031923	453	47	*CARD17*	0.00092906	629
48	*TGFBI*	0.00032308	668	48	*DFNB31*	0.00095528	831
49	*FHOD3*	0.00033378	925	49	*SULT2A1*	0.00097053	400
50	*NDUFAF3*	0.00033878	17	50	*POU3F3*	0.00098695	129
51	*CST9L*	0.00035348	403	51	*BTF3L4*	0.0010122	1094
52	*KRTAP9-6*	0.00035507	867	52	*AHDC1*	0.0010202	NA
53	*ZNF263*	0.00037987	178	53	*UNC5D*	0.0010641	392
54	*DNAAF2*	0.00038258	405	54	*ESR1*	0.0010782	687
55	*APBB1IP*	0.00038388	181	55	*SLC12A4*	0.0010818	728
56	*C19orf38*	0.0003894	381	56	*PCTP*	0.0010969	908
57	*KCNK9*	0.0004035	909	57	*OSBPL8*	0.001116	540
58	*PPIAL4F*	0.00042404	NA	58	*ARHGEF11*	0.0011371	1086
59	*PDHA1*	0.00042611	199	59	*OSBPL10*	0.0011679	221
60	*BLM*	0.00044131	704	60	*EPHA8*	0.0012093	793
61	*LIPT2*	0.00044234	14	61	*THAP9*	0.0012198	NA
62	*SPCS2*	0.00047995	1065	62	*ITGB2*	0.0012716	781
63	*CCDC64B*	0.00048354	1019	63	*NDUFAF6*	0.0013235	18
64	*RPRD1A*	0.0004843	585	64	*LCE2B*	0.0013455	NA
65	*CYP2J2*	0.0004956	156	65	*SLC5A7*	0.0013754	108
66	*RANBP17*	0.00052583	212	66	*TSHR*	0.0013764	619
67	*CAPZA1*	0.00054513	821	67	*POLR3B*	0.001441	965
68	*AKR1C2*	0.00055808	736	68	*SDCBP*	0.0014791	495
69	*INHBC*	0.00056875	260	69	*NCF1*	0.0014972	645
70	*DDX3Y*	0.0005755	359	70	*ZNF362*	0.0015136	198
71	*GOLGA7B*	0.00059573	58	71	*TTC7B*	0.001531	353
72	*FAM217A*	0.00059703	556	72	*WDR5B*	0.0015478	NA
73	*ASB3*	0.00060926	352	73	*S100P*	0.0015829	209
74	*FAM46A*	0.00061011	158	74	*OR5B2*	0.0016039	NA
75	*CS*	0.00061706	29	75	*TRIM15*	0.0016347	543
76	*CDK19*	0.00062547	1021	76	*HMGA1*	0.0017154	NA
77	*MEP1A*	0.00062703	378	77	*OSBPL7*	0.0017286	950

78	*TGIF1*	0.00063634	943	78	*DIXDC1*	0.0017384	NA
79	*MRPL33*	0.00064893	670	79	*ATP6AP1*	0.0017419	1134
80	*SLC7A11*	0.00066712	870	80	*SLC35A2*	0.0017485	15
81	*CCSER2*	0.00067477	338	81	*ELFN2*	0.0017805	883
82	*ANKS3*	0.0006846	621	82	*TBC1D25*	0.0017903	NA
83	*PRM1*	0.00068685	970	83	*RORB*	0.0017915	476
84	*CAMTA1*	0.00070083	420	84	*CCDC91*	0.0018025	51
85	*TRUB1*	0.00070721	436	85	*SCAF8*	0.0018249	91
86	*CRTC3*	0.00071792	297	86	*C19orf66*	0.0018415	328
87	*HSD3B2*	0.00072561	624	87	*CLIC4*	0.0018421	NA
88	*CENPH*	0.0007398	429	88	*TENM3*	0.0018455	NA
89	*MRPS35*	0.00076023	60	89	*NTPCR*	0.0018666	292
90	*COCH*	0.00077358	745	90	*ANKRD61*	0.001894	NA
91	*CLUAP1*	0.00077604	1100	91	*TBKBP1*	0.0019458	876
92	*ZCCHC12*	0.00078031	1032	92	*RBM43*	0.0019518	107
93	*HSPA12A*	0.00078842	747	93	*BRAT1*	0.0019977	1041
94	*FAS*	0.00078868	916	94	*SALL1*	0.0020359	431
95	*COQ2*	0.00079675	30	95	*STIM1*	0.0020495	373
96	*FABP4*	0.00081272	274	96	*FRAT1*	0.0020816	704
97	*IRF1*	0.00082423	204	97	*KATNAL2*	0.0021014	135
98	*EXOC1*	0.0008265	16	98	*FLOT1*	0.0021092	894
99	*PARP3*	0.00082913	1042	99	*TNNI3*	0.0021532	210
100	*ANKLE2*	0.00085652	1139	100	*TCEAL1*	0.0021907	1100
101	*FAM64A*	0.000893	818	101	*GPATCH4*	0.0021926	783
102	*CCDC167*	0.00089819	801	102	*RAMP1*	0.0022124	NA
103	*LEPROTL1*	0.00090017	835	103	*SLC23A1*	0.0022569	854
104	*RALYL*	0.00090841	885	104	*STBD1*	0.0022574	NA
105	*MAGEB2*	0.00092676	417	105	*TTLL7*	0.0022788	NA
106	*FCRL3*	0.00093184	698	106	*RPL29*	0.002281	974
107	*MDH2*	0.00093674	489	107	*SUN1*	0.0023087	648
108	*NDUFA3*	0.00095939	8	108	*LIPJ*	0.0023606	53
109	*PYROXD1*	0.0009603	574	109	*SLC15A2*	0.0023795	339
110	*PDILT*	0.00097467	159	110	*OTOS*	0.0023801	531
111	*NDUFB10*	0.00098271	27	111	*KRT84*	0.0023888	792
112	*TARBP1*	0.00098584	262	112	*FAM168B*	0.0024124	630
113	*CST9*	0.00099485	512	113	*ERVW-1*	0.0024215	112
114	*RSPH9*	0.00099498	397	114	*HDAC9*	0.0024497	NA
115	*SPHAR*	0.00099963	NA	115	*HMGB1*	0.0024642	1143
116	*SOX14*	0.0010122	147	116	*GSDMB*	0.0025093	NA
117	*HLA-DPB1*	0.0010138	123	117	*LRRC46*	0.002516	570
118	*GPC2*	0.0010198	145	118	*ZNF83*	0.0025394	NA
119	*OR5V1*	0.0010213	NA	119	*ZNF425*	0.0025552	NA
120	*MGRN1*	0.0010363	982	120	*GLTP*	0.0025734	36

121	*ZNF732*	0.0010641	474	121	*C4B_2*	0.0025799	NA
122	*PNKD*	0.0010727	163	122	*CD86*	0.0025918	1030
123	*AGAP9*	0.0010816	949	123	*LARP4*	0.0026197	177
124	*AP4S1*	0.0011012	68	124	*RPS4Y1*	0.0026626	NA
125	*SMAD5*	0.0011159	NA	125	*ZNF234*	0.0026715	556
126	*ZNF254*	0.0011249	567	126	*ZNF559*	0.0026827	NA
127	*MSRB1*	0.0011305	566	127	*ABCA4*	0.0027061	532
128	*SLC5A12*	0.0011532	66	128	*TBC1D4*	0.0027162	13
129	*UTS2*	0.0011639	1082	129	*FARP1*	0.0027233	273
130	*IFT81*	0.0011678	105	130	*NAT6*	0.0027534	787
131	*DMXL2*	0.0011713	406	131	*RECK*	0.0027619	231
132	*ANGPTL3*	0.0011852	110	132	*ENPP7*	0.0027746	904
133	*C8orf82*	0.0011853	333	133	*PGRMC2*	0.0028787	653
134	*SLCO6A1*	0.0012037	191	134	*CAPN1*	0.002886	NA
135	*FHL3*	0.0012079	810	135	*ERO1L*	0.0029305	NA
136	*CEBPD*	0.0012107	719	136	*TMEM219*	0.0029534	873
137	*KIAA2022*	0.0012197	82	137	*NDUFAB1*	0.0029815	1109
138	*AREG*	0.0012259	155	138	*SLAIN1*	0.0029823	197
139	*PLEKHG1*	0.0012492	299	139	*VIT*	0.0030341	258
140	*MAK*	0.0012734	466	140	*ABHD12*	0.0030748	417
141	*GRINA*	0.0012838	966	141	*ALX1*	0.0030859	NA
142	*PEX12*	0.0012987	271	142	*KPNA3*	0.003094	1011
143	*OGT*	0.0013023	964	143	*VHL*	0.003116	31
144	*CDH13*	0.0013194	129	144	*CCNDBP1*	0.0031377	932
145	*TMEM125*	0.0013235	311	145	*LGALS3*	0.0031384	61
146	*FAM115A*	0.0013243	843	146	*OPALIN*	0.0031436	NA
147	*C1orf210*	0.0013245	95	147	*ZNF281*	0.0031658	NA
148	*INPP5K*	0.0013301	625	148	*TRAPPC4*	0.0031895	1059
149	*RASGRP3*	0.0013602	753	149	*METTL25*	0.0032413	986
150	*MYF6*	0.0013753	649	150	*SPNS3*	0.0032844	842
151	*ARHGAP28*	0.0013939	608	151	*NYAP2*	0.0032931	1106
152	*HMGCS2*	0.0014041	884	152	*NUAK2*	0.0033028	465
153	*PRKCB*	0.0014105	832	153	*PDGFRA*	0.0033385	NA
154	*FAM21A*	0.001421	752	154	*SNRPN*	0.0033399	NA
155	*CMPK1*	0.0014284	647	155	*ZNF222*	0.0033739	281
156	*FOLR1*	0.0014569	578	156	*STRADB*	0.0033967	589
157	*NEXN*	0.0014595	861	157	*UMOD*	0.0034022	303
158	*GOLGA6L4*	0.0014705	NA	158	*PTCHD3*	0.0034373	477
159	*ZNF581*	0.0014938	944	159	*TMUB2*	0.003494	442
160	*VPS35*	0.0014987	18	160	*IL16*	0.0035003	499
161	*EOGT*	0.0015046	994	161	*MED10*	0.0035021	NA
162	*IFNAR2*	0.0015309	165	162	*GAR1*	0.003552	NA
163	*KIF3A*	0.0015369	569	163	*DIO2*	0.0035843	NA

164	*HSPA4*	0.0015423	782	164	*ZSCAN4*	0.0035994	NA
165	*ZSCAN32*	0.0015434	968	165	*IL37*	0.0036038	140
166	*RABIF*	0.0015451	6	166	*HS3ST4*	0.0036266	NA
167	*ZNF213*	0.0015527	859	167	*ZFP57*	0.0036438	613
168	*PLEKHF2*	0.0015698	81	168	*IL18BP*	0.0036476	NA
169	*NEO1*	0.0015777	303	169	*FBXL13*	0.0036556	421
170	*CLCNKB*	0.0015931	467	170	*CRYL1*	0.0036716	NA
171	*SLC22A14*	0.0015938	72	171	*CRP*	0.0036907	546
172	*TNIK*	0.00161	114	172	*RIOK3*	0.0037074	1046
173	*CBLB*	0.001617	749	173	*CYP4X1*	0.0037591	539
174	*TCF7*	0.001618	264	174	*LHFPL5*	0.0037925	866
175	*EDA2R*	0.0016261	597	175	*GTF2A1*	0.0038109	436
176	*CDIP1*	0.0016346	457	176	*COL4A2*	0.0038123	NA
177	*C17orf75*	0.0016456	598	177	*TMEM44*	0.0038627	1006
178	*CGGBP1*	0.0016528	339	178	*KIF2A*	0.0038824	NA
179	*ZNF816-ZNF321P*	0.0016606	473	179	*KLHL30*	0.0038847	376
180	*KRTAP19-2*	0.0016615	251	180	*DDX60*	0.0039144	726
181	*ZNF138*	0.0016774	150	181	*NSUN5*	0.00392	958
182	*C1orf100*	0.0016796	911	182	*RRP15*	0.0039662	771
183	*AKT1S1*	0.0016865	869	183	*PLAA*	0.0039845	NA
184	*AOX1*	0.0016992	401	184	*ADNP*	0.0040179	277
185	*IMMT*	0.0017015	651	185	*ZNF185*	0.0040428	NA
186	*GCKR*	0.0017166	83	186	*TLX1NB*	0.0040541	NA
187	*SMARCE1*	0.0017288	724	187	*CRMP1*	0.0040697	574
188	*GRSF1*	0.0017454	1	188	*ARIH2*	0.0041146	832
189	*DISC1*	0.0017471	653	189	*HLA-DRA*	0.0041327	190
190	*SIX6*	0.0017509	336	190	*VWA9*	0.0041479	62
191	*LRRC20*	0.0017537	361	191	*SPANXN3*	0.0041757	269
192	*DLEC1*	0.0017902	945	192	*SEL1L3*	0.0041857	NA
193	*EPB42*	0.0017968	773	193	*KCNH5*	0.0041906	935
194	*FH*	0.0018158	558	194	*KCND3*	0.0041989	NA
195	*NMNAT2*	0.0018301	858	195	*CASK*	0.0042023	NA
196	*ODF3*	0.0018421	184	196	*LAMA1*	0.0042223	991
197	*LONP2*	0.0018656	735	197	*FAM169A*	0.004225	535
198	*ZNF737*	0.001902	64	198	*COMMD6*	0.0042642	559
199	*UBL3*	0.0019083	75	199	*HOMEZ*	0.0042767	819
200	*ACY1*	0.00191	426	200	*L1TD1*	0.0042934	582
201	*C9orf172*	0.0019217	291	201	*CTH*	0.0043284	678
202	*C8orf31*	0.0019223	677	202	*PRTFDC1*	0.0043334	208
203	*C2orf91*	0.0019254	951	203	*SAP30L*	0.0043504	NA
204	*TMED2*	0.0019311	579	204	*HOXC6*	0.0043802	1061
205	*ZNF221*	0.0019446	560	205	*NDFIP2*	0.0043896	NA

206	*CRISP3*	0.0019457	839	206	*FAM171B*	0.0044085	352
207	*SLC9A3R2*	0.0019483	589	207	*KLF9*	0.0044102	NA
208	*EPAS1*	0.0019867	874	208	*AAED1*	0.0044837	475
209	*ASB8*	0.0019976	1023	209	*PRPF40B*	0.0045261	NA
210	*C16orf58*	0.0020199	850	210	*YTHDC2*	0.0045354	656
211	*RASGEF1A*	0.0020238	107	211	*MLH3*	0.0045743	67
212	*GABRG2*	0.002028	136	212	*ZNF418*	0.004583	803
213	*CD84*	0.0020282	316	213	*HOXC10*	0.0045871	937
214	*ZCWPW1*	0.0020426	463	214	*IFNA5*	0.0046389	518
215	*MUC4*	0.0020455	419	215	*TMEM199*	0.0046906	872
216	*ZNF251*	0.0020475	309	216	*AFAP1*	0.0047048	981
217	*WDR12*	0.0020612	1105	217	*PRMT3*	0.0047399	NA
218	*ACSM2B*	0.0020689	121	218	*SEC63*	0.0047423	1105
219	*KHDC1L*	0.0020782	626	219	*UBE2L6*	0.004743	NA
220	*ZNF708*	0.0021013	84	220	*MSS51*	0.0047529	NA
221	*STAC2*	0.0021034	465	221	*C12orf43*	0.0047941	259
222	*NDUFS7*	0.0021065	26	222	*ZNF765*	0.0048209	NA
223	*RNF151*	0.0021307	930	223	*EMB*	0.0048342	NA
224	*FCHO2*	0.0021448	772	224	*ARL8A*	0.0048361	1095
225	*ZNF845*	0.0021455	131	225	*GPS1*	0.0048458	895
226	*C2CD4A*	0.0021531	1090	226	*OR2Z1*	0.0048597	NA
227	*MRPS31*	0.0021574	35	227	*PIP5KL1*	0.0048975	948
228	*AIF1L*	0.002158	221	228	*DLGAP5*	0.0049112	510
229	*OIP5*	0.0021787	1033	229	*PSPH*	0.004946	823
230	*BEST3*	0.00219	85	230	*DCSTAMP*	0.0049492	893
231	*FBXW11*	0.0021908	929	231	*CAP2*	0.004957	NA
232	*PDXDC1*	0.0022004	428	232	*METRN*	0.0049607	NA
233	*DCAF17*	0.0022103	760	233	*PRRC2A*	0.004971	NA
234	*SREBF2*	0.002229	703	234	*RAB31*	0.0049845	717
235	*NDUFA1*	0.0022313	9	235	*KLRD1*	0.0050526	299
236	*SERINC5*	0.0022364	528	236	*ACER3*	0.0051022	NA
237	*ARHGEF15*	0.0022568	928	237	*SLFNL1*	0.0051044	694
238	*SYN1*	0.0022646	450	238	*PEA15*	0.0051113	NA
239	*RAB4A*	0.0022806	519	239	*SIRPB2*	0.0051561	1073
240	*PIK3CB*	0.0022922	194	240	*EMC7*	0.0052078	1083
241	*SMIM18*	0.0023031	825	241	*OR11G2*	0.0052166	NA
242	*KLHL6*	0.0023085	657	242	*OR2W1*	0.0052199	NA
243	*STATH*	0.0023086	853	243	*USP17L8*	0.0052534	NA
244	*ROCK2*	0.0023144	710	244	*VASP*	0.0052595	565
245	*HMOX2*	0.0023163	793	245	*FRMD7*	0.005295	761
246	*SLC22A13*	0.002317	955	246	*NUDT7*	0.0053112	541
247	*PKD1L3*	0.0023273	NA	247	*SLC17A1*	0.0053629	201
248	*RGS9BP*	0.0023604	1063	248	*WBSCR27*	0.0054146	706

249	*PDSS1*	0.0023707	15	249	*ASCC2*	0.0054254	874
250	*PF4*	0.0023778	265	250	*RND3*	0.0054663	193
251	*KRTAP3-2*	0.0023778	617	251	*DUSP7*	0.0054959	661
252	*SPATA19*	0.0023844	738	252	*SOX9*	0.005518	665
253	*C2orf54*	0.0023845	671	253	*C19orf60*	0.0055242	NA
254	*GALNTL6*	0.0023942	371	254	*COLEC12*	0.0055697	580
255	*FHL2*	0.0024123	185	255	*PCDHB10*	0.0056191	283
256	*TMEM192*	0.002448	721	256	*HNRNPA3*	0.0056213	286
257	*C12orf39*	0.0024641	691	257	*ADAM28*	0.0056286	1043
258	*NPAS3*	0.0024678	917	258	*DPYSL3*	0.005673	294
259	*DBC1*	0.0024735	NA	259	*MOGAT3*	0.0057247	379
260	*COLGALT2*	0.0025106	891	260	*POSTN*	0.0057764	NA
261	*GREB1*	0.0025154	341	261	*NPFFR2*	0.0058281	700
262	*ABR*	0.0025159	304	262	*MPZ*	0.0058305	NA
263	*SH3GL2*	0.0025366	812	263	*R3HCC1*	0.0058645	786
264	*FEM1C*	0.0025421	823	264	*FOXR2*	0.0058798	361
265	*NPNT*	0.0025525	176	265	*C9orf64*	0.0058839	NA
266	*AQP11*	0.0025566	705	266	*KIF21B*	0.0059831	467
267	*MAB21L3*	0.0025665	638	267	*ALPP*	0.0060348	78
268	*TSKS*	0.0025686	461	268	*KCNN4*	0.0060555	155
269	*ZNF670*	0.0025829	838	269	*ALMS1*	0.0060653	767
270	*MMADHC*	0.0026312	160	270	*GCNT2*	0.0061346	10
271	*PREX2*	0.0026334	146	271	*MYB*	0.0061898	297
272	*ATP1B3*	0.0026456	261	272	*PPP2R5A*	0.0061993	NA
273	*NPPB*	0.0026553	186	273	*RBM15*	0.0062043	1102
274	*SLCO4C1*	0.002669	236	274	*MXD3*	0.0062414	1098
275	*OR5K1*	0.0026714	NA	275	*WASF3*	0.0062543	884
276	*HOXB5*	0.0026742	273	276	*MRGPRD*	0.0062744	1007
277	*SSTR2*	0.002678	477	277	*CLU*	0.0062931	862
278	*C1orf226*	0.002679	926	278	*PMP22*	0.0063398	615
279	*DEFB116*	0.0026868	112	279	*FAM161A*	0.0063448	914
280	*GPATCH2L*	0.002704	622	280	*C1orf105*	0.0063723	NA
281	*PRKCDBP*	0.002716	711	281	*HKDC1*	0.0063964	313
282	*LOC200726*	0.0027232	NA	282	*TMED8*	0.0064105	164
283	*PHLDB2*	0.0027271	501	283	*DBNDD1*	0.0064207	NA
284	*FAM84A*	0.0027521	972	284	*WNT10B*	0.0064308	NA
285	*NDUFS2*	0.0027743	25	285	*LTBR*	0.0064481	68
286	*C15orf62*	0.0027809	79	286	*PPP1R15B*	0.0064511	558
287	*EZH1*	0.0027815	37	287	*HERC3*	0.0064997	203
288	*MTUS2*	0.002801	688	288	*CDC14B*	0.0065583	199
289	*ZNF234*	0.0028042	98	289	*NCKAP5L*	0.0065839	278
290	*COQ4*	0.0028145	32	290	*PRR4*	0.006603	336
291	*IRS2*	0.0028219	45	291	*FPR3*	0.0066547	NA

292	*ZNF207*	0.0028282	989	292	*GOPC*	0.0066818	978
293	*NDUFAF7*	0.002835	10	293	*CCL28*	0.0066869	183
294	*TRMT10B*	0.0028398	399	294	*STK39*	0.0067063	848
295	*MFAP3*	0.0028488	209	295	*COL1A2*	0.0067283	NA
296	*NR4A1*	0.0028868	1031	296	*SCAMP3*	0.0067579	542
297	*TBX5*	0.0029172	750	297	*EMC1*	0.0068096	916
298	*CLVS2*	0.0029204	324	298	*OR52I2*	0.0068585	NA
299	*LPHN2*	0.0029304	715	299	*ADAM11*	0.0069057	889
300	*ARHGDIG*	0.0029784	202	300	*FUT11*	0.0069128	820
301	*COX16*	0.0029822	334	301	*C18orf8*	0.0069645	1144
302	*NAGPA*	0.0029824	1037	302	*C8orf44*	0.0069696	409
303	*STK17A*	0.003034	380	303	*OR8H1*	0.0070161	NA
304	*MRPS16*	0.0030556	59	304	*ZNF664*	0.007064	NA
305	*PLCH1*	0.0030839	485	305	*CRIP3*	0.0070677	306
306	*TDP1*	0.0030858	1127	306	*COL4A5*	0.0070956	754
307	*ARHGAP8*	0.003088	658	307	*SORCS3*	0.0071194	137
308	*KRT38*	0.0030894	494	308	*PIGK*	0.0071331	606
309	*MACROD2*	0.0031376	829	309	*NXPH4*	0.0071417	75
310	*SNRPB2*	0.0031411	787	310	*SHKBP1*	0.0072508	684
311	*ZNF709*	0.0031455	269	311	*EXD2*	0.0072723	909
312	*PRKG2*	0.0031631	789	312	*CHAT*	0.0072742	147
313	*IL1RAPL1*	0.003167	223	313	*PCK2*	0.0073423	44
314	*MIS18BP1*	0.0031888	809	314	*ROS1*	0.0074127	749
315	*ASTN2*	0.0031956	674	315	*MLLT3*	0.0074291	405
316	*SBSPON*	0.0031999	672	316	*KCNK5*	0.0074807	899
317	*ACAD10*	0.0032055	739	317	*TOX2*	0.0075543	892
318	*ENPP2*	0.0032401	292	318	*TRABD2A*	0.0075839	138
319	*POU3F1*	0.0032425	263	319	*ATOH1*	0.0075982	142
320	*STK16*	0.0032453	764	320	*DCAF8L1*	0.0076477	323
321	*NDUFS1*	0.0032757	7	321	*CDRT15*	0.0076532	1128
322	*DNAJC16*	0.0032929	1007	322	*ECSIT*	0.0076697	NA
323	*LNPEP*	0.0032934	472	323	*NMUR1*	0.0076862	545
324	*PRR23C*	0.0033085	189	324	*TLR1*	0.0076871	139
325	*AGER*	0.0033085	599	325	*MRPS31*	0.0077387	816
326	*NUP160*	0.0033138	1050	326	*IRX1*	0.0077903	961
327	*RYR1*	0.0033311	947	327	*HIST1H2BG*	0.0078419	602
328	*CENPQ*	0.0033328	636	328	*GNA15*	0.007945	907
329	*ZNF322*	0.0033447	813	329	*ZNF154*	0.0079813	660
330	*HAUS7*	0.0033503	247	330	*TRIM77*	0.0079966	NA
331	*PION*	0.0033537	NA	331	*LSR*	0.0079981	647
332	*ITIH4*	0.0033731	805	332	*ITGB1BP2*	0.0080206	NA
333	*LCP2*	0.0033959	729	333	*TTC26*	0.0080482	272
334	*PIAS2*	0.0033965	374	334	*HDGF*	0.0080998	810

335	*TAF12*	0.0034128	918	335	*CSF1R*	0.0081514	561
336	*TGOLN2*	0.0034257	718	336	*MAP1B*	0.0081562	506
337	*OCA2*	0.0034348	138	337	*KIAA0907*	0.0081676	878
338	*ULK2*	0.0034457	697	338	*KLHL33*	0.008203	178
339	*WNT2B*	0.0034483	464	339	*ZNF106*	0.0082545	877
340	*GPR116*	0.0034634	799	340	*MSX1*	0.0082643	861
341	*KCNH5*	0.0034798	896	341	*MAP1LC3A*	0.008266	549
342	*CCDC147*	0.0035001	141	342	*KCNE2*	0.0083061	NA
343	*AXIN1*	0.0035075	615	343	*APOE*	0.0083215	857
344	*CRLF3*	0.0035387	479	344	*SIGLEC11*	0.0083846	NA
345	*CKM*	0.0035433	1001	345	*BRINP2*	0.0083931	104
346	*CAAP1*	0.0035473	830	346	*ATXN7L2*	0.0084092	184
347	*C5orf34*	0.0035518	732	347	*ZNF513*	0.0084608	922
348	*UTS2B*	0.0035658	231	348	*ARHGAP29*	0.0085124	501
349	*PIGX*	0.0035883	855	349	*HLX*	0.0085288	742
350	*HSPB9*	0.0035898	893	350	*NETO1*	0.008552	38
351	*CD300C*	0.0036036	400	351	*CYSLTR1*	0.0086155	37
352	*PLEKHO2*	0.0036062	1113	352	*CDON*	0.0086858	603
353	*NDUFAF4*	0.0036231	20	353	*NCBP2*	0.0087151	NA
354	*ING2*	0.0036535	80	354	*CDKN2AIPNL*	0.0087186	144
355	*USP38*	0.0036554	452	355	*DCUN1D5*	0.0087443	102
356	*FAM107A*	0.0036796	713	356	*ZFP14*	0.0087702	186
357	*PACRGL*	0.0037057	281	357	*GBF1*	0.0087913	649
358	*UGT2B7*	0.0037072	164	358	*MMP16*	0.0088089	929
359	*APOA2*	0.0037192	149	359	*TMEM205*	0.0088217	597
360	*FKBP1B*	0.0037213	104	360	*DNAJC2*	0.0088265	1021
361	*MPG*	0.0037331	806	361	*TTLL4*	0.0088733	633
362	*BCAP31*	0.003741	888	362	*TREM1*	0.0088914	NA
363	*SALL4*	0.0037704	343	363	*RNF167*	0.0089248	967
364	*PRX*	0.0037715	587	364	*DPCD*	0.0089763	502
365	*RNF183*	0.0037965	895	365	*C14orf105*	0.008992	519
366	*TTC4*	0.0038243	411	366	*SNAPC1*	0.0090279	NA
367	*EVA1A*	0.0038491	564	367	*SESN1*	0.0090794	372
368	*DDHD1*	0.0038625	354	368	*MFGE8*	0.0091051	736
369	*VCX3B*	0.0038767	385	369	*GPX4*	0.009131	822
370	*NGFRAP1*	0.0039035	390	370	*ZNF853*	0.0091589	NA
371	*MTMR1*	0.0039142	875	371	*FOXD4L1*	0.0091825	1069
372	*APOBEC4*	0.0039156	226	372	*FAM122B*	0.0091949	257
373	*SORT1*	0.0039477	211	373	*TTC13*	0.009261	928
374	*NT5C*	0.0039567	938	374	*RNF5*	0.009267	237
375	*TLL2*	0.0039649	1044	375	*KCNA4*	0.009279	480
376	*KLHDC8A*	0.003966	1009	376	*CCL2*	0.0092911	NA
377	*HOXC10*	0.003966	842	377	*VASN*	0.0093635	288

378	*RFC1*	0.003976	1002	378	*KCNJ12*	0.0093665	444
379	*ATG3*	0.0039921	633	379	*SUN5*	0.0093886	941
380	*FGFBP1*	0.003996	484	380	*GRM4*	0.0094401	NA
381	*DNAJC15*	0.0039981	682	381	*RNF7*	0.0094544	173
382	*PRH2*	0.0040372	90	382	*NDNL2*	0.0094666	NA
383	*BIRC6*	0.0040608	844	383	*ANGPTL5*	0.0095214	837
384	*TMEM261*	0.0040716	28	384	*LOC100862671*	0.0095824	NA
385	*SYNGR4*	0.0040735	694	385	*PON2*	0.0095947	1087
386	*ITCH*	0.0040858	444	386	*JMJD4*	0.0096977	271
387	*ENTPD6*	0.0041186	942	387	*SIGLEC10*	0.0097379	266
388	*XAGE2*	0.0041212	606	388	*EMR3*	0.0097492	162
389	*CALD1*	0.0041398	880	389	*SERBP1*	0.0098007	357
390	*PAAF1*	0.0041633	499	390	*C19orf82*	0.0098474	989
391	*RIN2*	0.0041764	948	391	*NUP62*	0.0098522	NA
392	*NDUFB4*	0.0041801	4	392	*REG3G*	0.0098531	NA
393	*JMJD8*	0.0041851	686	393	*COX6A1*	0.0099037	637
394	*COL17A1*	0.0041888	245	394	*CD6*	0.0099404	NA
395	*SENP8*	0.0041967	233	395	*MAGEC1*	0.0099552	563
396	*IRAK4*	0.0042147	353	396	*CCDC30*	0.0099711	624
397	*TMEM45A*	0.004222	53	397	*SLC39A9*	0.010015	96
398	*ZBTB14*	0.0042247	287	398	*STEAP2*	0.010021	799
399	*OR6N1*	0.0042261	NA	399	*MMP25*	0.010058	775
400	*STXBP6*	0.0042334	794	400	*STXBP1*	0.010065	NA
401	*DMTN*	0.0042765	900	401	*FLT3LG*	0.01009	370
402	*LEKR1*	0.0043141	NA	402	*SPDL1*	0.01011	591
403	*ALS2*	0.0043245	491	403	*STAT5B*	0.010127	NA
404	*NOSTRIN*	0.0043415	377	404	*KRTAP10-5*	0.010134	NA
405	*ZNF19*	0.0043679	255	405	*MIER3*	0.010146	626
406	*CBLC*	0.004373	1012	406	*LOC100130705*	0.010161	NA
407	*BACE2*	0.0043764	119	407	*DIAPH1*	0.010196	592
408	*TUBA1A*	0.00438	588	408	*TMEM140*	0.010228	673
409	*PUS7L*	0.0043899	533	409	*C18orf63*	0.010264	757
410	*MBD4*	0.0043907	854	410	*TFF2*	0.010278	479
411	*INSR*	0.0043944	162	411	*FGD4*	0.01031	1117
412	*DPY19L2*	0.0044088	849	412	*GSTZ1*	0.010316	923
413	*PDZD9*	0.0044212	117	413	*DPY19L1*	0.010365	234
414	*MTMR9*	0.0044218	266	414	*MSL1*	0.010367	181
415	*SLC33A1*	0.0044293	1080	415	*GOLIM4*	0.0104	368
416	*CCDC137*	0.0044317	1109	416	*CAPN9*	0.010419	263
417	*ZNF683*	0.0044456	244	417	*UBL7*	0.01047	NA
418	*CRB3*	0.0044793	912	418	*SMUG1*	0.010522	710
419	*G3BP2*	0.0044834	441	419	*SOX5*	0.010526	852
420	*SAFB*	0.0044837	504	420	*MKKS*	0.010577	666

421	*TFDP2*	0.0045068	395	421	*TMEM27*	0.010728	77
422	*PIK3R4*	0.0045136	76	422	*IP6K1*	0.01077	NA
423	*PPP1R9A*	0.0045138	865	423	*ZSWIM7*	0.010779	NA
424	*CHDC2*	0.0045148	868	424	*HORMAD2*	0.010783	880
425	*SPC25*	0.0045237	601	425	*SLC7A3*	0.01083	1048
426	*GAGE10*	0.0045299	1095	426	*MFHAS1*	0.010882	654
427	*SIKE1*	0.0045307	227	427	*VAMP8*	0.010886	608
428	*TMIGD1*	0.0045352	685	428	*LEMD2*	0.010902	1002
429	*LAMP5*	0.0045381	239	429	*PTX3*	0.010933	124
430	*SSMEM1*	0.0045437	451	430	*LRCH1*	0.010977	NA
431	*GABRB1*	0.0045765	543	431	*MATN3*	0.010984	NA
432	*C21orf2*	0.0045922	61	432	*SUSD3*	0.010985	801
433	*GTPBP1*	0.0045922	327	433	*MOGAT1*	0.01099	72
434	*CXorf64*	0.0046248	116	434	*ROPN1L*	0.011036	NA
435	*BZW2*	0.0046482	347	435	*ANXA7*	0.011088	702
436	*B3GNTL1*	0.004651	872	436	*PRKCZ*	0.011139	1058
437	*ZNF879*	0.004661	302	437	*CDR1*	0.011191	377
438	*BRCA1*	0.0046659	1106	438	*POLR2H*	0.011242	1080
439	*RAD9B*	0.0046825	96	439	*IGF2BP1*	0.011246	453
440	*ULBP3*	0.0046827	610	440	*TMEM40*	0.011259	514
441	*MCAT*	0.0046833	1068	441	*TM7SF3*	0.011285	886
442	*GPR174*	0.0046869	623	442	*LOC728819*	0.011292	NA
443	*SUMF2*	0.0047258	416	443	*GALK1*	0.011294	537
444	*C5orf28*	0.0047266	387	444	*ELMO3*	0.011345	925
445	*AAAS*	0.0047307	596	445	*ERI2*	0.011371	NA
446	*ACSL1*	0.0047421	993	446	*SIAH1*	0.011448	57
447	*PDZK1*	0.0047513	785	447	*B3GNT7*	0.011457	334
448	*CLEC4F*	0.0047594	837	448	*OR10X1*	0.01147	NA
449	*GPR157*	0.0047785	346	449	*SCLT1*	0.011499	NA
450	*PXDN*	0.0047938	828	450	*TUB*	0.011537	737
451	*RTBDN*	0.0048002	506	451	*TRPV4*	0.011551	515
452	*FBXW7*	0.004812	1142	452	*SLC16A8*	0.01159	779
453	*STAM*	0.0048137	815	453	*SEMA5B*	0.011597	1060
454	*XYLT1*	0.004844	282	454	*RFPL1*	0.011602	NA
455	*PHYKPL*	0.004851	952	455	*CCNK*	0.011705	NA
456	*SLC5A2*	0.0048541	690	456	*POU2AF1*	0.011751	NA
457	*PNMT*	0.0048932	270	457	*VCL*	0.011756	917
458	*C1orf177*	0.0048937	770	458	*ZNF883*	0.011757	NA
459	*VSIG8*	0.004895	135	459	*RPL27*	0.011808	1141
460	*USP10*	0.0048965	990	460	*CLPS*	0.011811	NA
461	*PTCHD4*	0.0048972	577	461	*LGALS13*	0.011909	508
462	*HYKK*	0.0049236	495	462	*INHBE*	0.011911	NA
463	*MYCL1*	0.0049261	NA	463	*SERINC1*	0.011933	319

464	*FKBP9*	0.0049394	219	464	*SIAH3*	0.011962	679
465	*GREB1L*	0.004943	650	465	*CLDN16*	0.011967	172
466	*PKP4*	0.004949	210	466	*PYGO2*	0.012013	617
467	*SENP6*	0.0049526	714	467	*LSG1*	0.012065	NA
468	*SLC22A6*	0.0049818	824	468	*SAPCD2*	0.012089	335
469	*PLEKHA8*	0.0050007	89	469	*ERG*	0.012116	575
470	*C11orf86*	0.005002	797	470	*CAND1*	0.012123	1103
471	*NIM1*	0.0050156	424	471	*MMP19*	0.012168	NA
472	*TMEM135*	0.0050157	520	472	*GM2A*	0.012211	NA
473	*SUMO1*	0.0050158	458	473	*CAPRIN2*	0.012271	76
474	*MAFB*	0.0050382	137	474	*NLGN2*	0.012322	698
475	*RHBDL3*	0.0050668	229	475	*ADRA2A*	0.012348	NA
476	*MAGEA6*	0.0050732	284	476	*XPR1*	0.012397	818
477	*C19orf44*	0.0050913	995	477	*ALOX5AP*	0.012431	869
478	*PRR4*	0.0051275	746	478	*BAIAP2L1*	0.012476	422
479	*GRB2*	0.005129	174	479	*KLRG1*	0.012527	494
480	*APOL1*	0.0051525	326	480	*DEPDC7*	0.012562	1092
481	*COQ7*	0.0051656	86	481	*SPECC1L*	0.012579	NA
482	*COL6A5*	0.0051727	NA	482	*NFX1*	0.012597	662
483	*LIF*	0.0051747	101	483	*TMEM9*	0.01263	NA
484	*TMEM41B*	0.0051782	836	484	*MAN1C1*	0.012687	NA
485	*ALG3*	0.0051967	235	485	*HVCN1*	0.012733	NA
486	*BTG1*	0.0051976	409	486	*TGM7*	0.012784	205
487	*LEMD1*	0.0052013	498	487	*MCC*	0.012834	355
488	*TCAP*	0.0052013	637	488	*TECPR2*	0.012836	NA
489	*OR52B6*	0.0052013	NA	489	*CKMT1B*	0.012868	NA
490	*GGA1*	0.0052096	412	490	*ATP13A5*	0.012876	NA
491	*MTERF*	0.0052153	54	491	*ACCS*	0.012911	214
492	*G2E3*	0.005216	762	492	*GOT1*	0.012939	338
493	*SLC25A36*	0.0052459	330	493	*TMEM194B*	0.013041	302
494	*CLEC1A*	0.0052478	645	494	*SPON2*	0.013065	NA
495	*CACHD1*	0.0052592	396	495	*E2F6*	0.013093	NA
496	*USP34*	0.005263	981	496	*RFPL4B*	0.013093	226
497	*MORN4*	0.0052642	207	497	*PLN*	0.0131	571
498	*KCTD9*	0.0052918	471	498	*PTPN5*	0.013129	415
499	*IGSF6*	0.0053054	580	499	*CAPN12*	0.013144	362
500	*EML4*	0.0053109	118	500	*ACSS1*	0.013195	245
501	*PXK*	0.0053334	487	501	*DMPK*	0.013206	790
502	*WHSC1*	0.0053626	652	502	*PAEP*	0.013249	NA
503	*ASCL5*	0.0053738	172	503	*RNF14*	0.013298	119
504	*ANKS6*	0.005388	905	504	*GBX2*	0.01332	1104
505	*ARPP21*	0.0053964	440	505	*CSNK2B*	0.013327	1133
506	*USP26*	0.0054067	286	506	*SIGIRR*	0.013334	639

507	*TBCEL*	0.0054164	115	507	*DDT*	0.013345	NA
508	*ZNF292*	0.0054325	300	508	*LAPTM5*	0.013349	481
509	*ATRNL1*	0.0054526	648	509	*NTN5*	0.013401	NA
510	*MTMR2*	0.005466	741	510	*OGFOD1*	0.013441	594
511	*PTGIS*	0.0055001	1014	511	*SOWAHB*	0.013452	NA
512	*USP31*	0.0055412	565	512	*FAM110D*	0.013503	579
513	*DCAF8L2*	0.0055596	667	513	*ESPN*	0.013555	360
514	*STAG3*	0.0055694	1087	514	*RRP1*	0.013556	1081
515	*IFNA4*	0.0055994	816	515	*SCARB1*	0.013591	NA
516	*SYTL2*	0.0056168	920	516	*PPP1R37*	0.01362	NA
517	*PTMA*	0.0056211	1101	517	*LYRM1*	0.013627	NA
518	*OGN*	0.005625	134	518	*ZNF587B*	0.013657	NA
519	*NDUFA11*	0.0056499	22	519	*EIF3F*	0.013706	1075
520	*C1QTNF5*	0.0056519	695	520	*ZNF148*	0.013709	NA
521	*STX3*	0.0056567	529	521	*LIF*	0.01376	81
522	*TMEM132D*	0.0056567	208	522	*USP29*	0.013811	NA
523	*CTNNA2*	0.0056615	847	523	*OXTR*	0.013844	746
524	*MTNR1A*	0.0056776	329	524	*SMAD6*	0.01396	723
525	*NBPF9*	0.0056811	NA	525	*C3orf36*	0.013965	1052
526	*GRAMD1C*	0.005695	350	526	*PARP6*	0.014007	73
527	*MPP5*	0.005719	295	527	*SYN1*	0.014011	762
528	*ANKRD1*	0.0057244	389	528	*NKD2*	0.014068	NA
529	*C8orf46*	0.0057371	480	529	*ONECUT1*	0.014119	NA
530	*VN1R2*	0.0057623	337	530	*MYOM3*	0.014134	NA
531	*ZYG11A*	0.0057665	1116	531	*NARR*	0.014149	NA
532	*TRIML1*	0.0057914	418	532	*OR4K5*	0.014171	NA
533	*FANCD2*	0.005797	1129	533	*COG3*	0.014171	1
534	*ARPC1A*	0.0058197	1036	534	*OR6C76*	0.014193	NA
535	*HMOX1*	0.0058275	514	535	*NFIX*	0.0142	469
536	*AVL9*	0.0058278	730	536	*HIST1H2BF*	0.014222	NA
537	*C6orf62*	0.0058278	99	537	*HYAL2*	0.014222	NA
538	*CLDN11*	0.0058378	319	538	*PRR5*	0.014238	NA
539	*DACT3*	0.0058674	139	539	*STX8*	0.014376	NA
540	*BRK1*	0.0058795	969	540	*TC2N*	0.014376	NA
541	*OR2T2*	0.0058833	NA	541	*BRSK1*	0.014524	381
542	*SLC25A52*	0.0058912	1093	542	*RAB1B*	0.01453	NA
543	*BCKDK*	0.0058939	997	543	*DAZL*	0.014568	NA
544	*RAB15*	0.0059115	744	544	*CSDC2*	0.014581	NA
545	*MPPE1*	0.0059208	733	545	*PXDNL*	0.014606	NA
546	*PLA2G4E*	0.0059272	712	546	*POMK*	0.014616	NA
547	*ALDH1A1*	0.0059311	644	547	*GPR75*	0.014633	581
548	*PPIL3*	0.0059354	242	548	*CNOT6*	0.014665	NA
549	*MDH1B*	0.0059488	548	549	*MAGEB4*	0.014684	NA

550	*POC5*	0.0059554	1016	550	*PDLIM3*	0.014732	NA
551	*KIAA2018*	0.0059564	531	551	*CDH19*	0.014735	NA
552	*PSMG2*	0.0059859	1020	552	*RSF1*	0.014762	NA
553	*SOD3*	0.0060259	398	553	*PACS2*	0.014791	93
554	*SNX17*	0.0060301	1077	554	*IMMT*	0.014806	652
555	*PRELID1*	0.0060345	1136	555	*TDP1*	0.014821	1124
556	*CD177*	0.006036	NA	556	*AQP4*	0.014838	NA
557	*KLHL1*	0.0060401	1041	557	*VPS36*	0.014851	NA
558	*SECTM1*	0.0060706	922	558	*ROCK2*	0.014918	347
559	*ACHE*	0.006081	277	559	*CEP85L*	0.01494	NA
560	*RELA*	0.0060825	897	560	*CYP4F8*	0.014948	NA
561	*ACADS*	0.0060861	1089	561	*CNOT7*	0.014992	111
562	*JAM2*	0.0060867	950	562	*FSCB*	0.014993	NA
563	*AES*	0.0060894	546	563	*PLP1*	0.015031	625
564	*CLEC12B*	0.0061054	41	564	*OR8B12*	0.015043	NA
565	*L1TD1*	0.0061076	678	565	*TAX1BP3*	0.015053	473
566	*FOXD4*	0.0061106	892	566	*PPAPDC3*	0.015094	NA
567	*TTC12*	0.0061124	36	567	*PRELID1*	0.015197	1140
568	*ACTL6B*	0.0061191	393	568	*ZNF580*	0.015248	NA
569	*GRIN2A*	0.006127	538	569	*NDRG1*	0.015257	860
570	*WBSCR27*	0.0061378	612	570	*COG7*	0.015272	9
571	*LOC100862671*	0.0061435	NA	571	*BMP2K*	0.015299	NA
572	*COL19A1*	0.0061564	819	572	*OR3A2*	0.015333	NA
573	*FLI1*	0.0061678	198	573	*B3GNTL1*	0.015363	774
574	*TAS2R39*	0.0061702	534	574	*ZFYVE26*	0.015386	933
575	*DEFB125*	0.0061882	128	575	*PSMA3*	0.015402	NA
576	*ANKZF1*	0.0061895	224	576	*LRRC26*	0.015453	NA
577	*BYSL*	0.0062037	692	577	*ASAH2*	0.015504	NA
578	*EPSTI1*	0.0062411	786	578	*DDX25*	0.015523	170
579	*SYT17*	0.0062424	846	579	*FCHO2*	0.015607	16
580	*FAM78B*	0.0062637	42	580	*NBEA*	0.015637	NA
581	*TGM7*	0.0062776	1061	581	*MAS1*	0.015691	538
582	*DNAJC17*	0.0062805	256	582	*MB21D2*	0.015806	970
583	*PRICKLE3*	0.0062928	923	583	*SLCO4C1*	0.015812	416
584	*LOC643669*	0.0062938	940	584	*HOXB1*	0.015829	466
585	*MUC16*	0.0063294	1075	585	*TTYH1*	0.015863	NA
586	*OR10G3*	0.0063294	NA	586	*SEMA4B*	0.015883	NA
587	*DDB2*	0.0063538	777	587	*CCDC129*	0.01591	NA
588	*HEPACAM2*	0.0063623	167	588	*KLHL41*	0.015966	NA
589	*GRIA3*	0.0063723	196	589	*BOD1L1*	0.015975	640
590	*CCL26*	0.0063827	864	590	*GALK2*	0.016017	NA
591	*ZNF764*	0.0063945	1069	591	*TRMT1L*	0.016068	NA
592	*ABCA3*	0.0063961	628	592	*C9orf170*	0.016119	282

593	*HGS*	0.006402	363	593	*RMI2*	0.016134	NA
594	*SGPP2*	0.0064357	728	594	*SEMA3F*	0.016161	999
595	*MCL1*	0.0064457	1085	595	*ZNF77*	0.01617	NA
596	*TMEM155*	0.0064477	662	596	*DYNC1I1*	0.016207	NA
597	*FAM53A*	0.0064532	69	597	*LOC100505841*	0.016219	NA
598	*DCUN1D2*	0.0064691	551	598	*NEURL2*	0.016222	NA
599	*GSX1*	0.006475	683	599	*KLK15*	0.016273	NA
600	*SNAP29*	0.0064816	257	600	*TMEM235*	0.016277	425
601	*C6orf136*	0.0064994	103	601	*SDK2*	0.016316	460
602	*TESPA1*	0.0065014	443	602	*C5orf15*	0.016324	703
603	*HDHD1*	0.0065174	132	603	*GLUD1*	0.016375	693
604	*CD2*	0.00656	1013	604	*PRDX2*	0.016394	834
605	*PADI6*	0.0065783	NA	605	*TMEM184C*	0.01641	NA
606	*PSEN1*	0.0065853	213	606	*TIPARP*	0.016427	NA
607	*TBCE*	0.0065929	1112	607	*DDX3Y*	0.016473	655
608	*AAED1*	0.0066027	192	608	*RC3H2*	0.016478	577
609	*CLPTM1L*	0.0066184	967	609	*PRSS35*	0.016504	NA
610	*PPIC*	0.006643	65	610	*FAM200B*	0.016551	NA
611	*FCER1A*	0.0066431	276	611	*RPS3A*	0.016575	NA
612	*NUSAP1*	0.0066543	216	612	*GLIPR1*	0.01658	244
613	*PELI1*	0.0066728	522	613	*GLB1L*	0.016582	520
614	*DNAJB2*	0.0067009	166	614	*RBM24*	0.016606	215
615	*IZUMO4*	0.006718	998	615	*CCDC90B*	0.016631	NA
616	*ENG*	0.0067216	550	616	*SLIT1*	0.016661	NA
617	*ARHGEF19*	0.0067348	218	617	*TMPRSS5*	0.016677	NA

EXPERIMENTAL PROCEDURES

Generation of GLUT reporter cell lines

HeLa cells, 293T cells, and mouse preadipocytes (derived from inguinal white adipocyte tissues, a gift from Dr. Shingo Kajimura) were maintained in Dulbecco's Modified Eagle Medium (DMEM) supplemented with 10% FBS and penicillin/streptomycin. To differentiate into adipocytes, preadipocytes were cultured to ~95% confluence before a differentiation cocktail was added to the following concentrations: 5 µg/mL insulin (Sigma, #I0516), 1 nM T3 (Sigma, #T2877), 125 mM indomethacin (Sigma, #I-7378), 5 µM dexamethasone (Sigma, #D1756), and 0.5 mM IBMX (Sigma, #I5879). After two days, the cells were switched to DMEM supplemented with 10% FBS, 5 µg/mL insulin, and 1 nM T3. After another two days, fresh media of the same composition were supplied. Differentiated adipocytes were usually analyzed six days after addition of the differentiation cocktail.

To generate cell lines expressing the GFP-GLUT4-HA reporter, lentiviruses were produced by transfecting 293T cells with a mixture of plasmids including GFP-GLUT4-HA (Muretta et al., 2008) pAdVAntage (Promega, #E1711), pCMV-VSVG, and psPax2. Lentiviral particles were collected 40 hours after transfection and every 24 hours thereafter for a total of four collections. Lentiviruses were pooled and concentrated by centrifugation in a Beckman SW28 rotor at 25,000 RPM for 1.5 hours. The viral pellets were resuspended in PBS and used to transduce HeLa cells and preadipocytes. HeLa cells expressing the reporter were enriched for the strongest responses to insulin using fluorescence activated cell sorting (FACS) on a MoFlo cell sorter (Beckman

Coulter). A clonal cell line with the strongest insulin response was used in the genetic screens. Mouse preadipocytes expressing the reporter were similarly generated except that pooled cell populations were used.

Flow cytometry analysis of insulin-triggered GLUT translocation

HeLa cells or adipocytes were washed three times with KRH buffer (121 mM NaCl, 4.9 mM KCl, 1.2 mM $MgSO_4$, 0.33 mM $CaCl_2$, and 12 mM HEPES [pH7.0]). After incubation in the KRH buffer for two hours, the cells were treated with 100 nM insulin for 30 minutes. When applicable, 100 nM wortmannin (Sigma, #W1628) was added 10 minutes prior to insulin treatment. After insulin stimulation, the cells were rapidly chilled on an ice bath and their surface reporters were stained using anti-HA antibodies (BioLegend, #901501) and allophycocyanin (APC)-conjugated secondary antibodies (eBioscience, #17-4014). The cells were dissociated from the plates using Accutase (Innovative Cell Technologies, #AT 104) and their APC and GFP fluorescence was measured on a CyAN ADP analyzer. Data from populations of >5,000 cells were analyzed using the FlowJo software. Statistical significance was calculated based on experiments run in triplicate.

Genome-wide CRISPR mutagenesis of HeLa reporter cells

HeLa cells expressing the GFP-GLUT4-HA reporter were mutagenized using the GeCKO V2 CRISPR Knockout Pooled Library (Addgene, #1000000048), following previously described procedures with minor modifications (Marceau et al., 2016; Parnas et al., 2015; Sanjana et al.,

2014; Shalem et al., 2014; Sidik et al., 2016; Zhang et al., 2016). When delivered into targeted cells, Cas9 and sgRNAs encoded by the library introduced loss-of-function indel mutations through non-homologous end joining (Cong et al., 2013; Doudna and Charpentier, 2014; Fu et al., 2014; Hart et al., 2015; Mali et al., 2013; Marceau et al., 2016; Xiong et al., 2016). Lentiviruses were produced by transfecting the GeCKO V2 library plasmids (Parts A and B) into 293T cells using procedures similar to the generation of GFP-GLUT4-HA reporter cell lines. Starting at 48 hours after transfection, media containing lentiviruses were collected every 24 hours for a total of four collections. Lentiviral particles were pelleted in a Beckman SW28 ultracentrifuge rotor at 25,000 RPM for 1.5 hours. The lentiviral pellets were resuspended in PBS and stored at -70 ^{o}C.

To test viral titers, one million HeLa cells were seeded into each well of a 12-well plate. The cells were spin infected by lentiviruses produced from the Part A or B of the CRISPR library at 2,000 RPM for two hours. The plate was subsequently transferred to a 37 ^{o}C incubator. On the following day, the cells were dissociated and seeded in replicate wells of a 24-well plate. Fresh media were supplied on the following day and 1 μg/ml puromycin (Sigma, #P8833) was added to half of the duplicate wells. After 24 hours, attached cells were washed once with PBS and counted using CountBright beads (Thermo, #C36950) on a CyAN ADP analyzer. Numbers of cells in puromycin-treated wells were divided by those in the parallel untreated wells to calculate multiplicity of infection (MOI). Viral concentrations that yielded an MOI of ~0.4 were chosen for large-scale preparations.

In large-scale preparations, 45 million HeLa reporter cells were seeded for each part of the library. Small-scale replicates of these mutagenized populations were separately treated with puromycin and counted to verify the MOI. After puromycin treatment, the large-scale mutant populations were combined at a 1:1 ratio and frozen on the sixth day after viral transduction.

Genome-wide CRISPR screens

In each screen, 40 million mutagenized HeLa reporter cells were seeded at 1.2 million cells per 10-cm dish. On the following day, the cells were incubated in KRH buffer for two hours. In the translocation defective screen, the cells were treated with 100 nM insulin for 30 minutes. In the constitutive translocation screen, the cells were left untreated. The dishes were subsequently chilled on an ice bath and the cells were stained with anti-HA antibodies and APC-conjugated secondary antibodies. After dissociation from the plates by Accutase, the cells were concentrated by centrifugation and sorted by FACS. The cells in the bottom 3% of the APC channel were collected in the translocation defective screen while the top 1.2% of the cells were sorted in the constitutive translocation screen. The collected cells were expanded and sorted for another two rounds using the same fluorescence gating.

Illumina deep sequencing

Genomic DNA was isolated using a genomic DNA isolation kit (Thermo, #K0721). The unsorted control population contained 50 million cells whereas each of the sorted populations contained five million cells. The isolated genomic DNA was used as template to amplify guide

sequences. In the first round of PCR, each reaction was performed in a total volume of 100 µL containing 10 µg genomic DNA and the following primers:

Forward: AATGGACTATCATATGCTTACCGTAACTTGAAAGTATTTCG

Reverse: AATGGACTATCATATGCTTACCGTAACTTGAAAGTATTTCG

The second round of PCR reactions was performed in a total volume of 50 µL, using 5 µL of the PCR products from the first round as template. Of the 12 forward barcoded primers, six were used for the sorted populations and six were used for the unsorted control population. The barcoded forward primers (F01-12) and the reverse primer (R01) are listed below with barcodes highlighted in bold. Stagger sequences are shown to the 5' of the barcode in lower case, while the priming sites are shown to the 3' of the barcode in lower case (Table 1.2).

PCR products were pooled, purified using a gel purification kit (Clontech, #740609), and sequenced on an Illumina HiSeq2000 using 1x125 v4 Chemistry. Sequencing reads were demultiplexed and processed to contain only the 20-bp unique guide sequences using the FASTX-toolkit (http://hannonlab.cshl.edu/fastx_toolkit/). Readcount tables and gene enrichment analysis were performed using the MAGeCK algorithm (http://sourceforge.net/projects/mageck/).

Table 1.2: Illumina sequencing primers

F01	AATGATACGGCGACCACCGAGATCTACACTCTTTCCCTACACGACGCTCTTCCGATCTt**AAGTAGAG**tcttgtggaaaggacgaaacaccg
F02	AATGATACGGCGACCACCGAGATCTACACTCTTTCCCTACACGACGCTCTTCCGATCTat**ACACGATC**tcttgtggaaaggacgaaacaccg
F03	AATGATACGGCGACCACCGAGATCTACACTCTTTCCCTACACGACGCTCTTCCGATCTgat**CGCGCGGT**tcttgtggaaaggacgaaacaccg
F04	AATGATACGGCGACCACCGAGATCTACACTCTTTCCCTACACGACGCTCTTCCGATCTcgat**CATGATCG**tcttgtggaaaggacgaaacaccg
F05	AATGATACGGCGACCACCGAGATCTACACTCTTTCCCTACACGACGCTCTTCCGATCTtcgat**CGTTACCA**tcttgtggaaaggacgaaacaccg
F06	AATGATACGGCGACCACCGAGATCTACACTCTTTCCCTACACGACGCTCTTCCGATCTatcgat**TCCTTGGT**tcttgtggaaaggacgaaacaccg
F07	AATGATACGGCGACCACCGAGATCTACACTCTTTCCCTACACGACGCTCTTCCGATCTgatcgat**AACGCATT**tcttgtggaaaggacgaaacaccg
F08	AATGATACGGCGACCACCGAGATCTACACTCTTTCCCTACACGACGCTCTTCCGATCTcgatcgat**ACAGGTAT**tcttgtggaaaggacgaaacaccg
F09	AATGATACGGCGACCACCGAGATCTACACTCTTTCCCTACACGACGCTCTTCCGATCTacgatcgat**AGGTAAGG**tcttgtggaaaggacgaaacaccg
F10	AATGATACGGCGACCACCGAGATCTACACTCTTTCCCTACACGACGCTCTTCCGATCTt**AACAATGG**tcttgtggaaaggacgaaacaccg
F11	AATGATACGGCGACCACCGAGATCTACACTCTTTCCCTACACGACGCTCTTCCGATCTat**ACTGTATC**tcttgtggaaaggacgaaacaccg
F12	AATGATACGGCGACCACCGAGATCTACACTCTTTCCCTACACGACGCTCTTCCGATCTgat**AGGTCGCA**tcttgtggaaaggacgaaacaccg
R01	CAAGCAGAAGACGGCATACGAGATAAGTAGAGGTGACTGGAGTTCAGACGTGTGCTCTTCCGATCTtTCTACTATTCTTTCCCCTGCACTGT

Pooled secondary CRISPR screens

We constructed a pooled secondary CRISPR library based on the guide sequences of an activity-optimized library (Wang et al., 2015). Ten sgRNAs were selected for each of the top 1,170 genes from the genome-wide genetic screens (598 genes from the translocation defective screen and 572 genes from the constitutive translocation screen). The secondary library also contained 1,000 non-targeting control sgRNAs. Oligonucleotides containing the guide sequences were synthesized by CustomArray and amplified by PCR using the following primers:

ArrayF: TAACTTGAAAGTATTTCGATTTCTTGGCTTTATATATCTTGTGGAAAGGACGAAACACCG

ArrayR: ACTTTTTCAAGTTGATAACGGACTAGCCTTATTTTAACTTGCTATTTCTAGCTCTAAAAC

PCR products were ligated into the pLenti-CRISPR vector (addgene, #49535) using a Gibson assembly kit (Synthetic Genomics, #GA1200). pLenti-CRISPR vector was digested using BsmBI followed by alkaline phosphatase treatment and gel purification. Each Gibson assembly reaction contained 100 ng vector and 40 ng PCR products in triplicate. The reactions were subsequently dialyzed against deionized water and transformed into electrocompetent *E. coli* cells (Lucigen, #60242). *E. coli* colonies were counted to ensure >20x coverage of the library. HeLa cells expressing the GLUT reporter were mutagenized by the secondary CRISPR library and sorted as described in the primary screens.

CRISPR-Cas9 genome editing of candidate genes

To edit a candidate gene, two independent guide sequences were selected within the early constitutive exons of the gene (Table 1.3). Oligonucleotides containing one guide sequence were cloned into the pLenti-CRISPR-V2 vector (Addgene, #52961) as we previously described (Davis et al., 2015). Oligonucleotides containing the other guide sequence were cloned in a modified version of the CRISPR vector in which the puromycin selection marker was replaced with a hygromycin selection marker (pLenti-CRISPR-Hygro). Lentiviruses produced from the CRISPR plasmids were used to infect target cells. The infected cells were consecutively selected using 1 μg/mL puromycin and 500 μg/mL hygromycin B (Thermo, #10687010). Supplementary Table 7 lists the gRNAs used to edit individual genes.

Table 1.3 gRNAs used in individual CRISPR KO experiments

Species	Gene	Target 1	Target 2
mouse	*Exoc7*	GGCACTGACGCAGTGAATGT	ATGGCGGATGATGGCTTTCC
mouse	*Rabif*	GAACGAGCTCGTGTCAGCCG	CATGAGAAAGAAGCCAGATC
mouse	*Rab10*	CCACTCCCGAGTCCCCGATC	GTTCTCAAAGCTTTTACCGT
mouse	*Vps35*	AAAGTTTTTCCTGCTCATCC	TTACCAGGCATCTTTTCATC
mouse	*Ankrd13d*	GTGGCTCTCTTTGCCCACGT	CCCTCTGGAAGTCCCGATAC
mouse	*Osbpl8*	TCTCCCAAAGGTTTTGAAAG	GGAAAGATGAGTCAGCGCCA
mouse	*Osbpl10*	CCAGGACCTGCTTCTCCTGA	CCGCCAGTGCCAACATAACA
mouse	*Tbc1d4*	AGCCGGAAGCGCTTGTCGCC	ATCTGTGACTCGGGGTCGTC
mouse	*Ap2s1*	CCGGGCAGGCAAGACGCGCC	GGATGTCAACGACAACAATC
mouse	*Aagab*	GCTAGCTGAGGTGATGATCC	CAACTTCCAGCGATGCTGTG
human	*AP2S1*	GCGTCTTGCCTGCCCGGTTC	GGTCCAGTTCACAGACATTG
human	*AAGAB*	CAGCTGGTCTCCTGAGAAGA	GCAGTAACAAGAAATTTGTT
human	*RABIF*	GCACCCGGGAGCCGCAACGC	TCCTGGAGGAGATCGCCGTC
human	*RAB10*	CCTGATCGGGGATTCCGGAG	ATCAAAACAGTTGAATTACA
human	*TBC1D4*	AAGTCAGCCAGGTCCTCTCC	CTGGGTCATCCTCCCCAGAC

Chapter 2

AAGAB regulates Adapter protein 2 complex formation on the plasma membrane

Introduction

In the constitutive translocation screen we sought to generate a list of all proteins whose loss resulted in constitutive translocation of the GLUT reporter to the cell surface. One prominent class of genes identified in this screen were those predicted to be involved in the endocytosis of GLUT4. There are four main forms of endocytosis: clathrin-mediated endocytosis, caveolae, macropinocytosis, and phagocytosis. In our screen, we recovered genes involved in clathrin-mediated endocytosis, which is consistent with previous reports indicating GLUT4 internalization is dependent on clathrin-mediated endocytosis. Among the genes identified were the adapter protein complex 2 constitutes, AP2S1 and AP2M1 and a known binding partner AAGAB.

Clathrin mediated endocytosis

Clathrin-mediated endocytosis occurs through five steps: nucleation, cargo selection, clathrin coat assembly, vesicle scission, uncoating and recycling (McMahon and Boucrot, 2011). Initially, during nucleation, there is a slight membrane invagination concurrent with the assembly of the nucleation module which includes FCH domain only (FCHO) proteins, EGFR pathway

substrate protein (EPS15) and intersectins (McMahon and Boucrot, 2011). Subsequently, during cargo selection, adaptor protein 2 (AP2) is recruited to the site of endocytosis. AP2 can bind directly to the membrane through a phosphatidylinositol-4,5-bisphosphate (PIP2) binding domain, and interacts directly with cargo through its μ-subunit (Bonifacino and Glick, 2004). Next, the clathrin coat assembles into a lattice that helps to stabilize the membrane's curvature. It is thought that some accessory proteins such as EPS15 move to the periphery where the curvature is most dramatic, thus stabilizing the expanding invaginated membrane bud (Tebar et al., 1996). BAR domain-containing proteins then bind to the severe curvature at the neck of the developing vesicle where they recruit dynamin (Ferguson et al., 2009). It is thought that GTP hydrolysis of dynamin causes a conformational change, which results in the scission of the vesicle (Stowell et al., 1999). Once scission has occurred, the clathrin coat is disassembled by ATPase heat shock cognate 70 (HSC70) (Böcking et al., 2011). This allows the uncoated vesicle to be competent for fusion with the endosome and the clathrin coat and accessory proteins to be recycled for another round of endocytosis.

AAGAB mutation in human disease

AAGAB was first identified in a yeast-2-hybrid experiment that used the γ-adaptin subunit of AP1 as bait (Page et al., 1999b). Although AAGAB was shown to bind both AP1 and AP2 complex no further progress was made on the function of AAGAB (Page et al., 1999b). Later, the disease-causing locus of a collection of families with autosomal dominant palmoplantar keratoderma (PPK) was mapped to *AAGAB* (Pohler et al., 2012). PPK is hereditary skin disorder resulting in thickening of the epidermis on the palms and the soles of the feet. Onset occurs in

the first twenty years of life and is first noticeable with the development of small growths on the palms and soles. As the disease progresses these growths converge resulting in larger lesions (Pohler et al., 2012) (Fig 2.1).

Figure 2.1 Phenotype observed in patients with loss of function mutation in AAGAB. (Pohler et al., 2012)

AAGAB KO results in trafficking defect and acts downstream of insulin signaling

Given that AAGAB was among the highest scoring genes we identified, its known association with human disease, and its unknown function, we decided to investigate the molecular mechanism of AAGAB. KO of *AAGAB* using CRISPR-Cas9 strongly increased the basal surface levels of GLUT reporter in both HeLa cells and adipocytes (Figs. 2.2a, 2.3a,b). Insulin-induced AKT phosphorylation was intact in *AAGAB* KO cells (Fig 2.2b), suggesting that AAGAB acts downstream of insulin signaling.

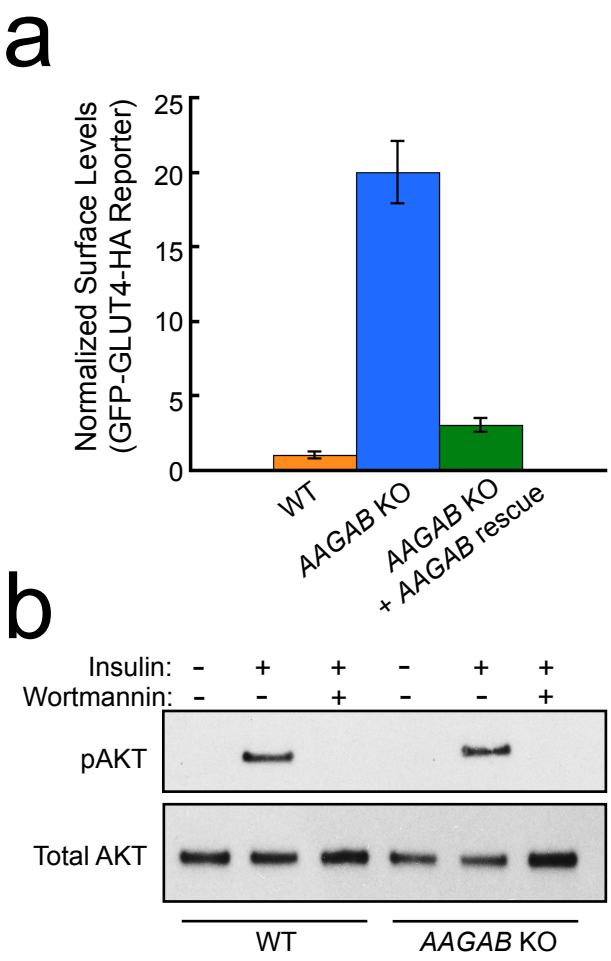

Figure 2.2 *AAGAB* knockout results in a trafficking defect and acts downstream of insulin signaling.
a, Normalized surface levels of the GLUT reporter in WT or mutant HeLa cells (in the absence of insulin). All error bars in this figure indicate standard deviation**. b,** Immunoblots showing total AKT and insulin-stimulated AKT phosphorylation in WT or mutant HeLa cells.

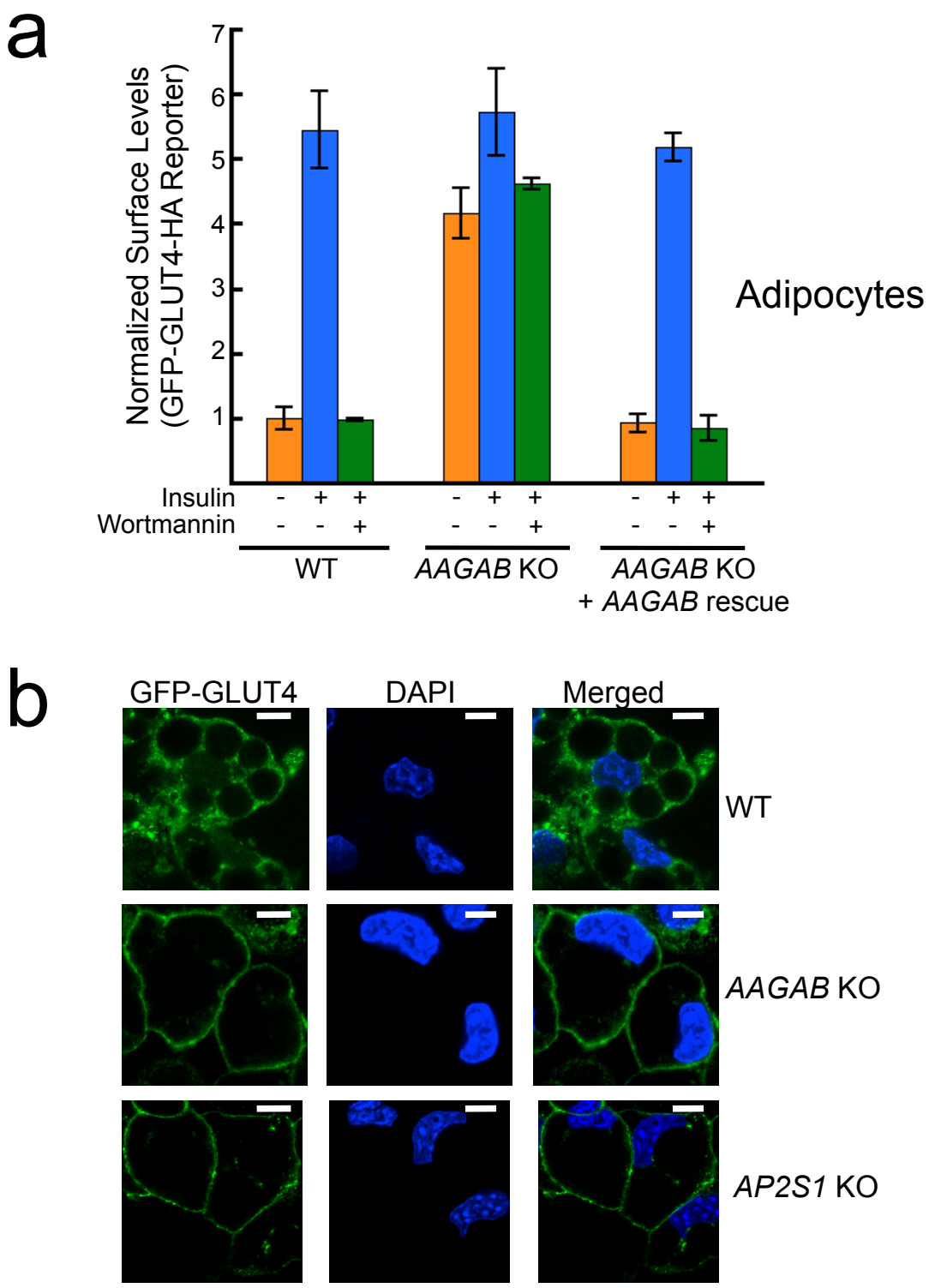

Figure 2.3: *AAGAB* KO results in GLUT4 plasma membrane localization.
a. Normalized surface levels of the GLUT reporter in WT or mutant adipocytes were measured by flow cytometry. Error bars indicate standard deviation. **b**, Confocal images showing the surface or intracellular localization of GFP-GLUT4 in WT or mutant adipocytes. Bar: 10 μm. Imaging was performed by Jingshi Shen.

AAGAB KO results in an endocytosis defect

We hypothesized that AAGAB mutation disrupts the retrieval of cargo proteins through clathrin-mediated endocytosis (CME). Indeed, using a fluorescent antibody-based endocytosis assay, we observed that the endocytosis of the GLUT reporter was abolished in *AAGAB* KO cells or in cells deficient in *AP2S1* (Fig. 2.4), which encodes the σ subunit of the AP2 adaptor. Thus, AAGAB is crucial to the endocytic retrieval of the GLUT reporter.

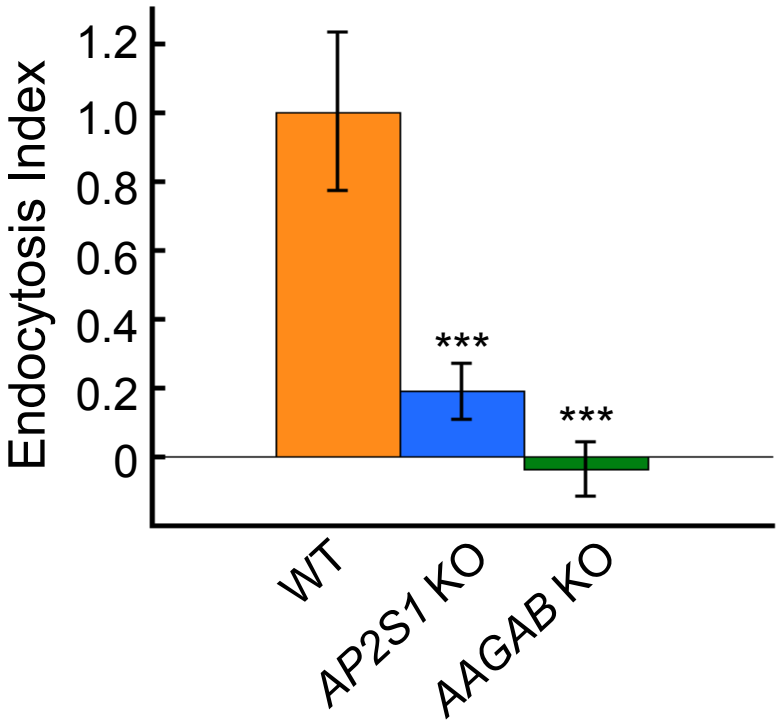

Figure 2.4: *AAKAB* KO disrupts endocytosis.
Relative endocytosis was measured by flow cytometry using fluorescent antibodies against GLUT4 and measuring increased fluorescence over time.

AAGAB regulates AP2 adaptor formation on the plasma membrane

To further determine the molecular mechanism of AAGAB, we examined whether AAGAB may regulate AP2 adaptor complex formation on the plasma membrane, a key step in CME (Brodsky, 2012; Martens and McMahon, 2008; Traub and Bonifacino, 2013). Confocal imaging of wild-type (WT) cells using anti-α-adaptin antibodies revealed abundant AP2 puncta on the cell surface (Fig. 2.5a). Strikingly, AP2 puncta disappeared in *AAGAB* deficient cells (Fig. 2.5a). Total internal reflection fluorescence microscopy (TIRFM), which selectively visualizes events near the plasma membrane, confirmed that AP2 puncta were eliminated in *AAGAB* KO cells (Fig. 2.5b). These data suggest that AAGAB is essential to the formation of AP2 adaptor complex on the plasma membrane. Furthermore, the total cell levels of α-adaptin was decreased in *AAGAB* KO cells (Fig. 2.6). Overexpression of α-adaptin was able to rescue GLUT4 internalization (Fig. 2.7) demonstrating that AAGAB is not directly required for CME. Although AAGAB interacts with α-adaptin, they did not show significant co-localization in the cell (Fig. 2.8), suggesting that AAGAB regulates AP2 adaptor formation via transient interactions. AAGAB also binds to γ-adaptin, a subunit of the AP1 adaptor required for clathrin-mediated transport from the *trans*-Golgi to the lysosome (Page et al., 1999a). However, lysosomal morphology (based on LAMP1 staining) was not impaired in *AAGAB* KO cells (Fig. 2.9), suggesting that the function of AAGAB is dispensable for AP1-dependent cargo transfer.

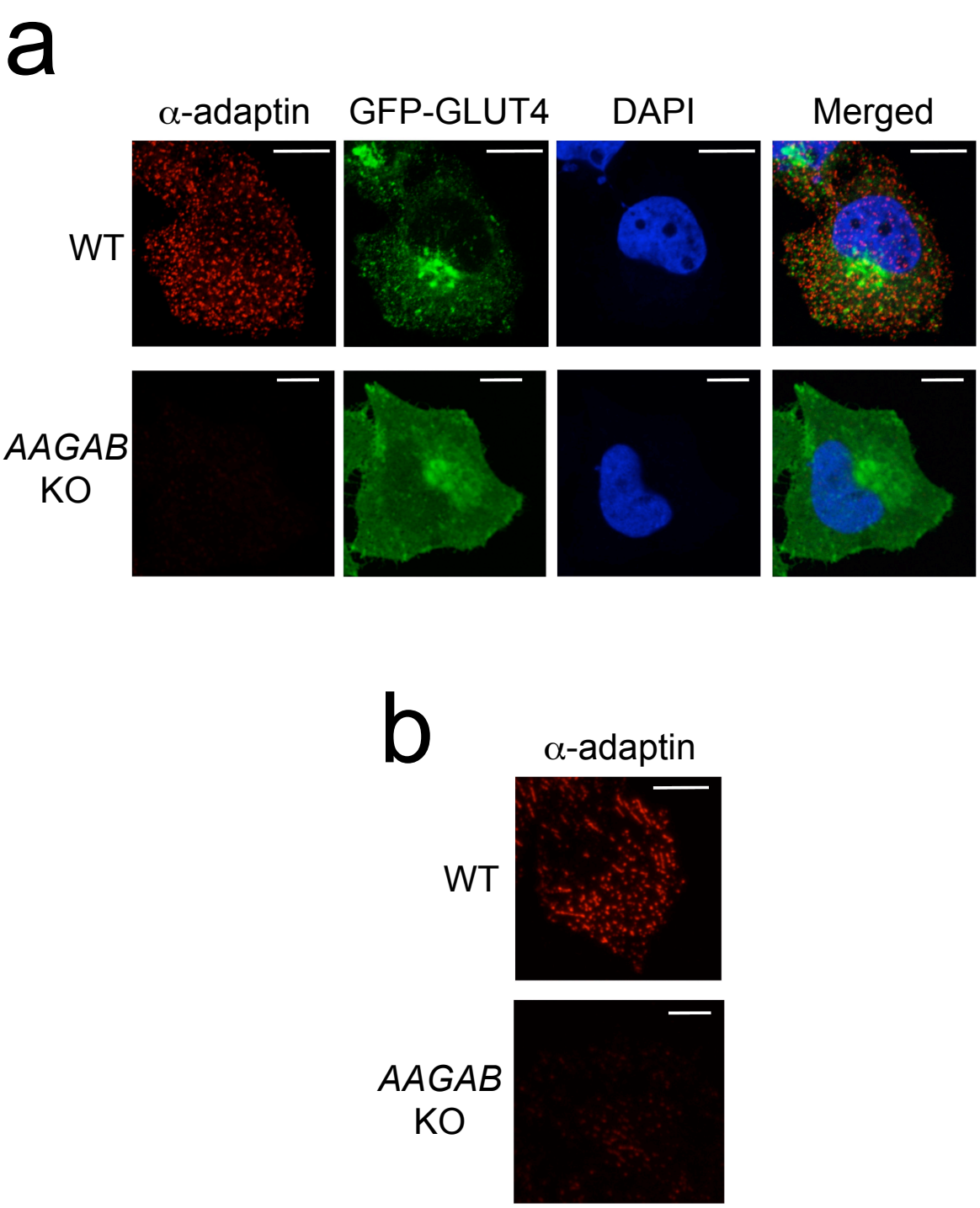

Figure 2.5: AAGAB regulates AP2 formation on the plasma membrane.
a. Representative confocal images showing the localization of α-adaptin and GLUT reporter in WT or mutant HeLa cells. Bar: 10 µm. **b.** Representative TIRFM images showing the localization of α-adaptin in WT or mutant HeLa cells. Bar: 10 µm. Imaging was performed by Jingshi Shen.

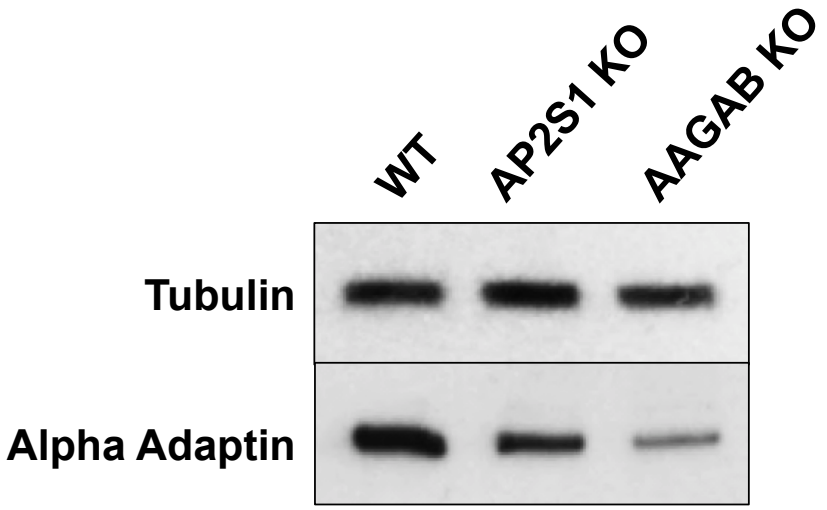

Figure 2.6: AAGAB regulates total α-adaptin levels.
Immunoblots showing total cell α-adaptin levels in WT, *AP2S1* KO and *AAGAB* KO cells.

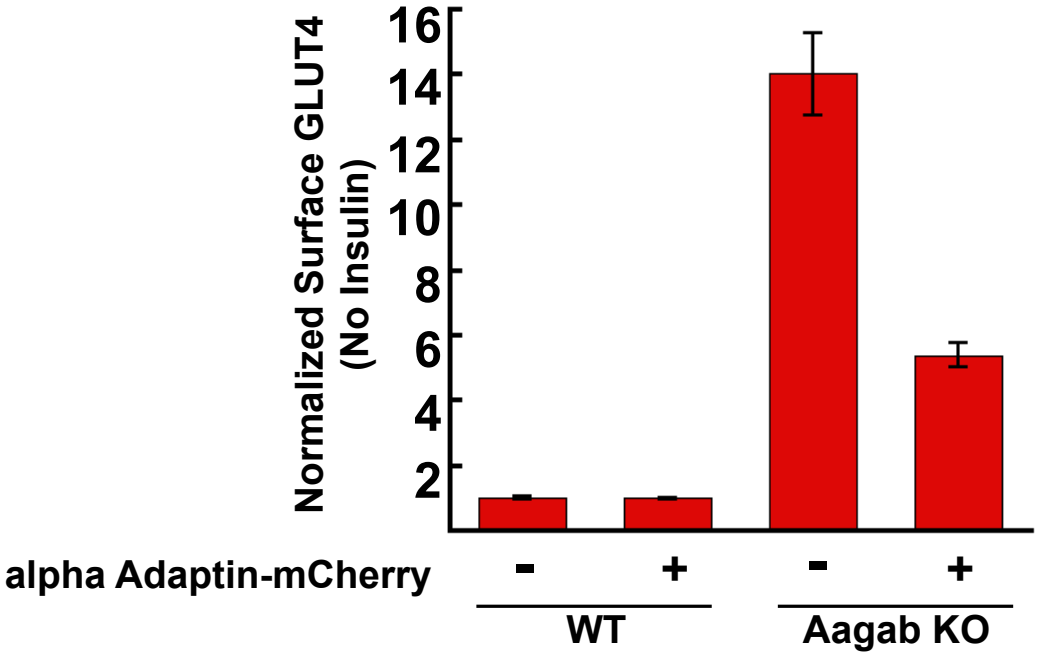

Figure 2.7: α-adaptin overexpression partially rescues AAGAB KO.
Normalized surface levels of the GLUT reporter in WT or mutant adipocytes with or without α-adaptin were measured by flow cytometry. Error bars indicate standard deviation.

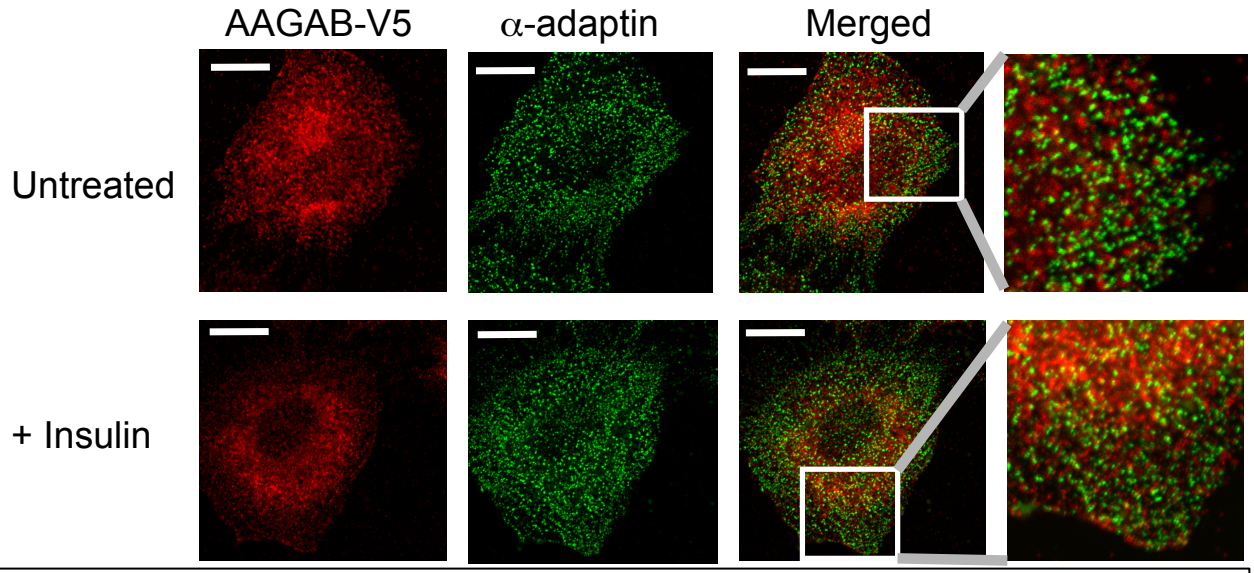

Figure 2.8: AAGAB does not colocalize with α-adaptin.
AAGAB-V5 was transiently expressed in HeLa cells. The cells were either untreated or treated with 100 nM insulin for 30 minutes before AAGAB-V5 and α-adaptin were stained and visualized by confocal microscopy. Bar: 10 μm. Imaging was performed by Jingshi Shen.

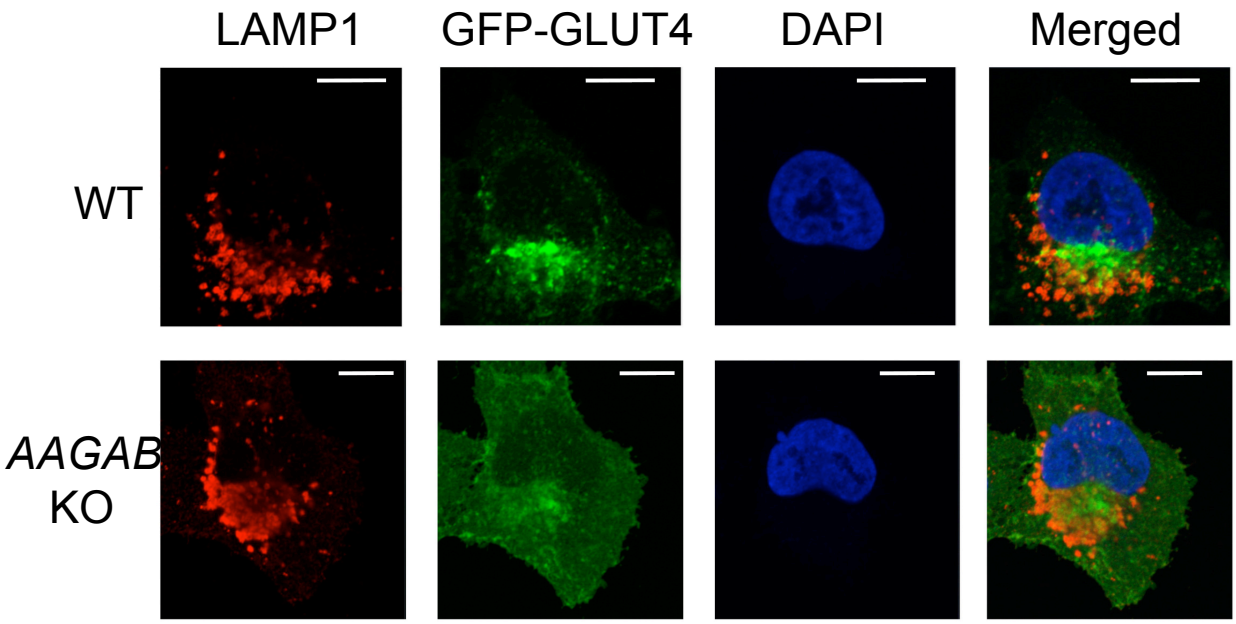

Figure 2.9: LAMP1 trafficking is intact in *AAGAB* KO cells.
Representative confocal images showing the localization of LAMP1 and GLUT reporter in WT or mutant HeLa cells. Bar: 10 μm. Imaging was performed by Jingshi Shen.

Surface proteomics identifies many cargo similarly regulated by *AAGAB* or *AP2S1* KO

Finally, we used mass spectrometry (MS)-based proteomics to identify cargo proteins regulated by AAGAB. Cell surface proteins were biotinylated, purified and analyzed by MS. Surface levels of many proteins such as TFRC (transferrin receptor), a known CME cargo (Conner and Schmid, 2003; Page et al., 1999a), were markedly elevated in *AAGAB* KO cells (Fig. 2.10a, Table 2.1). Other surface proteins such as FAS and PVR were not significantly affected in *AAGAB* KO cells (Fig. 2.10a, Table 2.1). Using flow cytometry, we confirmed that the surface levels of TFRC were strongly elevated in *AAGAB* KO cells, whereas FAS and PVR remained unchanged (Fig. 2.10b). The ability of AAGAB to regulate a large number of cargo proteins is in agreement with its crucial role in AP2-dependent CME. To further validate that AAGAB functions by regulating AP2 complex subunits we compared the surface proteomics of *AAGAB* KO cells to *AP2S1* KO cells. Overall, many of the quantified proteins were similarly affected by either *AAGAB* or *AP2S1* knockout (Table 2.1). Together, these data demonstrate that AAGAB plays an essential role in CME by regulating AP2 adaptor formation on the plasma membrane. Thus, our unbiased CRISPR screens allowed us to uncover a new component even in the extensively investigated CME pathway.

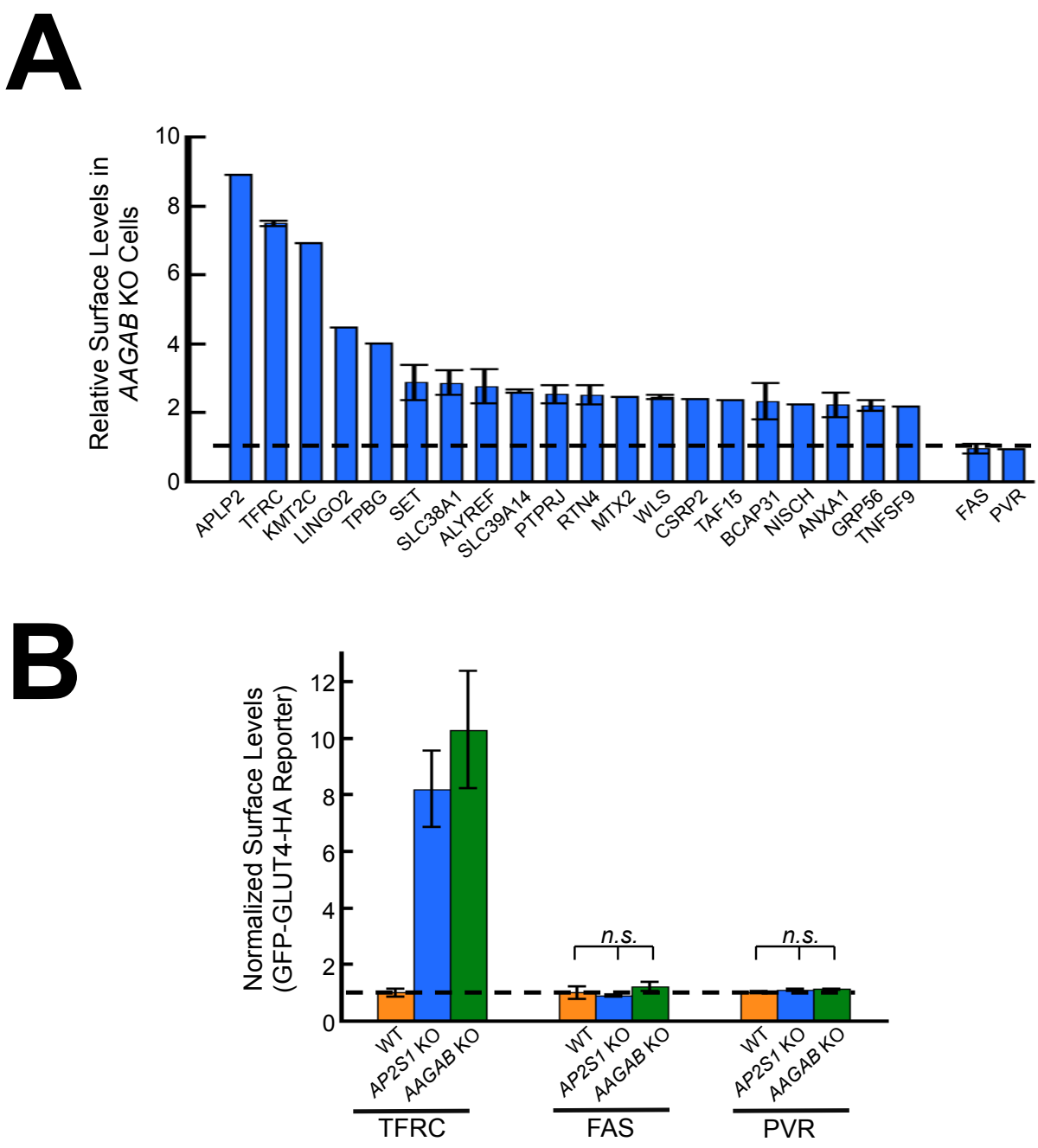

Figure 2.10 *AAGAB* KO effects the cellular localization of endogenous CME cargo.
a. Proteomic analysis of surface proteins in *AAGAB* KO cells. Top 20 proteins with greatest increases in surface levels are shown. FAS and PVR are included as representative cargo proteins not affected in *AAGAB* KO cells. Average values of two technical replicates are shown. For proteins quantified only in one replicate, the values are shown without error bars. Dashed line indicates the basal levels in WT cells. **b.** Normalized surface levels of the indicated molecules in WT or mutant HeLa cells (FAS and PVR) or adipocytes (TFRC) were measured by flow cytometry. Error bars indicate standard deviation. *n.s.*: not significant.

Discussion

AAGAB was one of the strongest scoring genes observed in our constitutive translocation screen. Validation in both HeLa cells and adipocytes confirmed that AAGAB knockout was one of the most severe phenotypes of all genes we have tested to date. AAGAB loss of function causes type I punctate palmoplantar keratoderma (PPKP1) through an unknown mechanism. Together, this made AAGAB a strong candidate for mechanistic study. In this work we have demonstrated that AAGAB functions by regulating the surface localization of the AP2 complex, thereby regulating CME.

Further work is needed to clarify which CME cargos contribute to the development of PPKP1. In the *Nature Genetics* paper (and in later work from other labs), Pohler *et al.* provide strong evidence that AAGAB is the causal mutation; however, to date the mis-regulated cargo causing the disease is still unresolved (Pohler et al., 2012). Pohler *et al*. suggested that AAGAB mutation drives constitutive surface localization of EGFR, which leads to constitutive EGFR signaling. Our proteomics analysis in either *AAGAB* KO or *AP2S1* KO did not reveal an EGFR trafficking defect in HeLa cells, though this does not exclude a defect in other cell types such as keratinocytes. Additionally, our assay may not have captured all changes in surface localization.

In our surface proteomics experiments we set out to identify all endogenous CME cargo. Surprisingly, although surface expression was changed for a large number of proteins, only a small subset of those proteins showed a dramatic change. This could be due to technical limitations of our experiment, redundancy of endocytic pathways for the majority of CME cargo,

or the relative rate of recycling amongst the CME cargo. Among the proteins whose surface localization was dramatically increased in the absence of either *AP2S1* or *AAGAB* was TFRC, which is known to have a very high recycling rate between the plasma membrane and the endosome. Another protein with a high surface expression change with the loss of AP2S1 was amlyoid beta precursor protein like 2 (APLP2). APLP2 has heparin, copper, and zinc binding domains, but its recycling rate and molecular role remains unclear. It would be interesting to test if APLP2 has a rapid recycling rate similar to TFRC. Another surprising result from our surface proteomics experiments were the large number of proteins not previously predicted to be CME cargo. Many of the proteins localize to a wide array of cellular organelles. Further work is needed to validate these candidates as bona fide CME cargo, but if confirmed this would underline the vast dynamics of the secretary pathway in regulating cellular localization.

Table 2.1: Surface proteomics for either *AP2S1* or *AAGAB* KO

Gene	Expression level AP2S1:WT	Rank	Expression level AAGAB:WT	Rank
APLP2	NA	NA	8.8855	1
TFRC	3.1995	1	7.4854	2
KMT2C	NA	NA	6.8903	3
LINGO2	NA	NA	4.4446	4
TPBG	NA	NA	4.0023	5
SET	NA	NA	2.8679	6
SLC38A1	2.0594	10	2.85935	7
ALYREF	2.352	3	2.74365	8
SLC39A14	2.4664	2	2.6114	9
PTPRJ	2.0932	7	2.5247	10
RTN4	NA	NA	2.51865	11
MTX2	NA	NA	2.4608	12
WLS	NA	NA	2.45445	13
CSRP2	NA	NA	2.3802	14
TAF15	1.168	186	2.3656	15
BCAP31	NA	NA	2.32595	16
NISCH	NA	NA	2.2193	17
ANXA1	NA	NA	2.2177	18
GPR56	NA	NA	2.1898	19
TNFSF9	1.3933	56	2.1816	20
FH	NA	NA	2.1688	21
ANXA4	NA	NA	2.1563	22
LMAN1	NA	NA	2.1533	23
FLOT1	NA	NA	2.1392	24
SLC2A4	1.2517	111	2.12695	25
CD97	1.451	39	2.11725	26
GNAS;GNAL	NA	NA	2.1168	27
PSME3	1.3661	65	2.1003	28
NPR3	NA	NA	2.1	29
CPOX	NA	NA	2.0844	30
P4HB	1.6468	19	2.0827	31
HSPE1;HSPE1-MOB4	NA	NA	2.079	32
PRDX4	1.2176	142	2.0665	33
DDR2	NA	NA	2.0645	34

MCM4	NA	NA	2.0477	35
HDGF	NA	NA	2.0265	36
LGALS3BP	1.7202	15	2.0225	37
PODXL	1.155	217	2.0018	38
HSD17B4	NA	NA	1.9972	39
MCM2	0.88049	752	1.9918	40
CLU	NA	NA	1.9561	41
CKMT1B;CKMT1A	NA	NA	1.9556	42
PDIA3	1.757	13	1.9531	43
PHB	1.4148	49	1.9346	44
COLGALT1	NA	NA	1.9251	45
CPS1	1.2422	120	1.92395	46
PHB2	1.3242	76	1.92	47
AIFM1	NA	NA	1.9195	48
PCDH1	NA	NA	1.9193	49
NRP1	NA	NA	1.8896	50
YES1;FYN	NA	NA	1.8886	51
PRKCSH	NA	NA	1.88165	52
LONP2	NA	NA	1.8813	53
COX4I1	NA	NA	1.8753	54
ACTN4	NA	NA	1.8724	55
NCSTN	1.4684	35	1.8555	56
YTHDC2	NA	NA	1.8423	57
AP2M1	0.54299	908	1.8353	58
PSG11	NA	NA	1.8352	59
LDLR	NA	NA	1.8233	60
NCL	1.362	66	1.82225	61
PDIA4	NA	NA	1.8198	62
EBP	NA	NA	1.8164	63
GANAB	1.6908	16	1.81255	64
HNRNPA1;HNRNPA1L2	1.5029	29	1.8087	65
FLOT2	NA	NA	1.802	66
SPTBN1	NA	NA	1.789	67
HSP90B1	1.4508	40	1.78845	68
CALR	NA	NA	1.7807	69
TPM4;TPM2	NA	NA	1.7748	70
TKT	1.1688	183	1.768	71
SSB	NA	NA	1.76095	72
CYB5R3	NA	NA	1.7596	73
SLC1A1	NA	NA	1.7586	74

SAMM50	1.3172	81	1.7558	75
GNAI3;GNAI1;GNAO1;GNAI2	NA	NA	1.7503	76
TNFRSF10A	NA	NA	1.7468	77
PDIA6	1.3854	60	1.74675	78
AK2	2.2591	4	1.74465	79
MDH2	NA	NA	1.733	80
ERP29	NA	NA	1.7219	81
HNRNPR	0.78117	853	1.7216	82
NCLN	NA	NA	1.7204	83
HNRNPAB	NA	NA	1.7131	84
UQCRC1	NA	NA	1.7048	85
RCN1	1.3945	55	1.6962	86
HDAC2;HDAC1	NA	NA	1.69	87
ATAD3A;ATAD3B	1.1393	242	1.68515	88
HSPD1	1.2599	106	1.68215	89
ANXA6	1.9326	12	1.676	90
ACLY	NA	NA	1.676	91
PTGES2	NA	NA	1.6743	92
FUBP1	NA	NA	1.66805	93
PDCD6	NA	NA	1.6667	94
PTPN1	NA	NA	1.6653	95
GEMIN5	0.98055	577	1.6638	96
SFXN1	1.267	101	1.65985	97
RAB7A	NA	NA	1.6575	98
ULBP2;RAET1G;RAET1L	NA	NA	1.6532	99
PHGDH	0.99869	533	1.6498	100
CAV1	NA	NA	1.6449	101
SLC25A4	NA	NA	1.6424	102
GART	NA	NA	1.6365	103
HNRNPA1	NA	NA	1.6318	104
HNRNPUL1	1.2718	98	1.626	105
PCNA	1.094	317	1.6255	106
CLPTM1L	NA	NA	1.6221	107
ANXA6	1.9326	12	1.619	108
GPR89B;GPR89A;GPR89C	NA	NA	1.6182	109
VCP	1.4419	42	1.6175	110
UGGT1	NA	NA	1.6114	111
RPN2	1.4585	37	1.6107	112
ZC3HAV1	1.0626	386	1.60595	113

MYBBP1A	0.95174	646	1.6046	114
CHCHD3	1.3198	79	1.6014	115
CBX3	1.0319	453	1.59985	116
HMMR	1.1412	238	1.5994	117
GOT2	NA	NA	1.5966	118
MTCH2	1.2277	133	1.5905	119
PDIA3	1.757	13	1.58695	120
NENF	NA	NA	1.5796	121
SURF4	1.0608	390	1.57685	122
PABPC4	1.3403	73	1.5742	123
UBA1	0.75625	862	1.5715	124
NOP9	NA	NA	1.5707	125
DDB1	NA	NA	1.567	126
BAG2	1.1034	302	1.56535	127
SPTAN1	1.3853	61	1.5637	128
STT3A	NA	NA	1.5636	129
CANX	2.0793	8	1.5587	130
CD81	1.1597	208	1.5557	131
PRPF19	1.2127	146	1.5515	132
HLA-B	0.44627	917	1.5448	133
MATR3	1.1228	266	1.54305	134
PSMD13	NA	NA	1.543	135
ACTN4;ACTN1	NA	NA	1.5427	136
S100A4	NA	NA	1.54	137
SIGMAR1	1.2569	107	1.5362	138
CD320	NA	NA	1.534	139
CAD	1.0312	456	1.527	140
ASNS	NA	NA	1.5263	141
VDAC2	1.3466	69	1.52625	142
HSD17B11	NA	NA	1.5259	143
SLC31A1	NA	NA	1.5218	144
POR	0.68754	888	1.5194	145
NUP155	1.2897	94	1.5192	146
PFDN2	NA	NA	1.5103	147
SERPINH1	1.1509	226	1.50725	148
IMMT	1.1945	161	1.5069	149
HNRNPA0	1.0288	463	1.5068	150
ATP5B	1.0315	454	1.5052	151
ESYT2	NA	NA	1.5019	152
PUM1	NA	NA	1.5005	153
MBOAT7	NA	NA	1.5002	154

EXPERIMENTAL PROCEDURES

Endocytosis assay

HeLa cells were incubated with the KRH buffer for two hours prior to treatment with 100 nM insulin for 30 minutes. The plates were then transferred to a 37 ^{o}C water bath and, where appropriate, treated with 200 μM Dynasore (Sigma, #D7693) for five minutes. After addition of 5 μg/mL anti-HA antibodies, the cells were incubated at 37 ^{o}C for another five minutes. The cells were then washed with a wash buffer (KRH buffer supplemented with 5% FBS) and dissociated from the plate using Accutase. The cells were then fixed by 2% paraformaldehyde (PFA) for 15 minutes at room temperature. After washing with wash buffer, the cells were incubated with APC-conjugated anti-mouse antibodies at room temperature for one hour in the KRH buffer supplemented with 2% FBS and 0.2 % saponin (Sigma, #47036). Subsequently the cells were washed and analyzed on a Cyan ADP Analyzer. Endocytosis Index was calculated using the following formula: $(\alpha - \delta)/\delta$, where α is the mean fluorescence of the wells without dynasore treatment whereas δ is the mean fluorescence of the dynasore-treated wells.

Immunoblotting

Cells grown in 24-well plates were lysed in 1x SDS protein sample buffer and the cell lysates were resolved on 8% Bis-Tris SDS-PAGE. Proteins were detected using primary antibodies and

horseradish peroxidase-conjugated secondary antibodies. Primary antibodies used in immunoblotting were: anti-AKT antibodies (Cell Signaling Technology, #9272), anti-phospho-AKT antibodies (Cell Signaling Technology, #5473), anti-α-adaptin antibodies (BD Biosciences, #610502), anti-α-tubulin antibodies (eBioscience, #14-4502-82),

Immunostaining and imaging

HeLa cells were seeded on coverslips coated with fibronectin (Sigma, #F1144). The cells were fixed using 2% PFA and permeabilized in PBS supplemented with 5% FBS and 0.2% saponin. Antigens were stained using the following primary antibodies: anti-α-adaptin antibodies (Thermo, #MAL-064), anti-LAMP1 antibodies (SCBT, clone H5G11), anti-Myc antibodies (SCBT, clone#9E10), anti-FLAG antibodies (Sigma, #F7425), anti-V5 antibodies, anti-CD47 antibodies (eBioscience, #14-0479-82), anti-CD95 antibodies (eBioscience, #14-0959-80), and anti-PVR antibodies (BioLegend, #337602). The cells were subsequently incubated with Alexa Fluor 488- or Alexa Fluor 568-conjugated secondary antibodies. After mounting on glass slides using the ProLong Antifade mountant with DAPI (Thermo, #P36931), the cells were visualized on a Carl Zeiss LSM780 confocal microscope. Cell images were captured and processed using the Carl Zeiss Zen 2 and Adobe Photoshop software. To visualize the GFP-GLUT4-HA reporter in adipocytes, the cells were fixed and permeabilized similarly to HeLa cells.

In TIRF imaging, cells grown on Delta T dishes (Bioptechs, #04200417B) were fixed and stained in a similar way as in confocal imaging. The cells were submerged in the PBS-based Citifluor AF3 anti-fade solution (EMS, #17972-25) and visualized on a Carl Zeiss Observer Z1

microscope equipped with a Stable Z heating system (Bioptechs) for maintenance at 37°C. The TIRF angle was set at 66° for Alexa Fluor 488 fluorescence and 68° for Alexa Fluor 568 fluorescence.

Surface proteomics

Quantitative proteomic analysis of protein levels was performed using stable isotope labeling with amino acids in cell culture (SILAC) and mass spectrometry (MS). Cells were grow in SILAC media (Thermo, #88423) supplemented with 10% dialyzed FBE (Seradigm, #3100). WT HeLa cells were grown in the presence of light lysine and arginine (Sigma, #L1262 and A5131), whereas AAGAB or AP2S1 KO cells were grown in the presence of heavy lysine and arginine (Cambridge Isotope Laboratories, #CNLM-291 and CNLM-539). After five days, surface proteins were biotinylated prior to the cells being harvested at ~60% confluence in a lysis buffer (4% SDS and 50 mM Tris-HCl [pH 6.8]). Surface proteins were biotinylated by incubation with 1mg/mL Sulfo-NHS-biotin (Thermo, #21217) for 20 minutes at 4 °C prior to quenching with 100mM glycine and subsequent lysis in IP buffer (25 mM Tris-HCl [pH 7.4], 150 mM NaCl, 1 mM EDTA, 1% NP-40, 5% glycerol, and a protease inhibitor cocktail). Protein content from WT and AAGAB or AP2S1 KO cell lysates were quantified by Bradford assay and combined in equal proportion prior to immunoprecipitation with streptavidin-paramagnetic beads (Promega, Z5482). Streptavidin-biotin binding was carried out overnight at 4 °C. Beads were washed twice with IP buffer, twice with IP buffer with NaCl level adjusted to 500mM, and twice with TE buffer. Beads were boiled in lysis buffer (4% SDS and 50mM Tris-HCl [pH 6.8]) prior to mass spectrometry analysis.

The cell lysates were processed for MS analysis following the filter-aided sample preparation (FASP) protocol (Erde et al., 2014; Wisniewski et al., 2009). Briefly, after addition of 20 mM DTT, equal amounts of whole-cell lysates were mixed and loaded onto a spin filter with a molecular weight cutoff of 30 kDa. The sample was then washed with the UA solution (8 M Urea and 0.1 M Tris-HCl [pH 7.9]) and alkylated using 0.1 M iodoacetamide. The sample was further washed with the UA solution and equilibrated with 0.1 M ammonium bicarbonate and 0.01% deoxycholic acid. The sample was then digested using 1% (w/w) trypsin at 37 ^{o}C for 16 hours. The resulting tryptic peptides were eluded by centrifugation, and acidified using formic acid. Deoxycholic acid was removed using phase transfer with ethyl acetate. The tryptic peptides were fractionated by a Pierce high pH reversed-phase spin column using 18 step gradients (4% acetonitrile for the first fraction, 1% increment for each fraction to the 17th fraction, and 50% acetonitrile for the 18th fraction). The fractions were dried using vacuum centrifugation.

One third of each fraction (5 µL) from high pH fractionation was analyzed by UPLC-MS/MS. The tryptic peptides were loaded onto a Waters nanoACQUITY UPLC BEH C18 column (130 Å, 1.7 µm × 75 µm × 250 mm) equilibrated with 0.1% formic acid/3% acetonitrile/water. Mobile phase A was 0.1% formic acid/water, while B was 0.1% formic acid/acetonitrile. The peptides were eluted at 0.3 mL/min using a gradient of 3-8% B (0-5 minutes) and 8-35% B (5-123 minutes).

Precursor ions between 300-1800 m/z (1x10^{6} ions, 60,000 resolution) were scanned on a LTQ Orbitrap Velos mass spectrometer. The 10 most intense ions for MS/MS were selected with 180-second dynamic exclusion, 10 ppm exclusion width, with a repeat count=1, and a 30-second

repeat duration. Ions with unassigned charge state and MH+1 were excluded from MS/MS. Maximal ion injection times were 500 milliseconds for FT (one microscan) and 250 milliseconds for LTQ, and the AGC was $1x10^4$. The normalized collision energy was 35% with activation Q 0.25 for 10 milliseconds.

Raw data files from MS were searched against the Uniprot human proteome database (Consortium, 2015) (total 88,479 entries), using the MaxQuant/Andromeda search engine (version 1.5.2.8) (Cox et al., 2011). Searches allowed trypsin specificity with two missed cleavages, and included fixed Cys carbamidomethylation, and variable acetylation (protein N-terminus) and methionine oxidation. Mass tolerances were set to 20 ppm (first search) and 4.5 ppm (main search) for precursor ions, and 0.5 Da for ITMS MS/MS ions. MaxQuant/Andromeda used the top 8 MS/MS peaks per 100 Da and seven amino acid minimum peptide length, with 0.01 false discovery rate for both protein and peptide identification. For SILAC ratio measurements, minimum two independent peptide ratios were used to calculate a protein ratio.

Chapter 3

RABIF regulates RAB10 expression

Introduction

In the translocation defective screens we sought to generate a list of all genes whose protein products positively regulate insulin stimulated GLUT4 exocytosis. In this screen we identified nearly all known positive regulators including members of the insulin signaling pathway, the exocyst complex, and RAB10, which is thought to be the main RAB regulating insulin stimulated GLUT4 exocytosis. Since RAB10 could be considered an inflection point in the pathway, where the insulin signaling pathway converges to initiate vesicle trafficking, we expected to recover regulators of RAB10. We did not recover the Rab10 GEF, Dennd4c, which is consistent with the current model which suggests that there is redundancy among the Dennd4 family. One protein we did recover that is known to interact with RAB10 was RABIF.

RABIF KO results in defective insulin response

RABIF/MSS4 (not the lipid kinase MSS4) is a 14 kDa soluble protein that has been predicted to act as a Rab GEF, but its biological function and molecular mechanism remain unknown (Wixler et al., 2011; Zhu et al., 2001). KO of *RABIF* strongly reduced insulin-triggered GLUT4 translocation in both adipocytes and HeLa cells (Figs. 3.1, 3.2). Insulin signaling was intact (Fig.

3.3a) suggesting that RABIF acts downstream of insulin signaling. Furthermore, surface levels of insulin receptor were not affected, suggesting that insulin receptor moves to the plasma membrane via a distinct route (Fig. 3.4b).

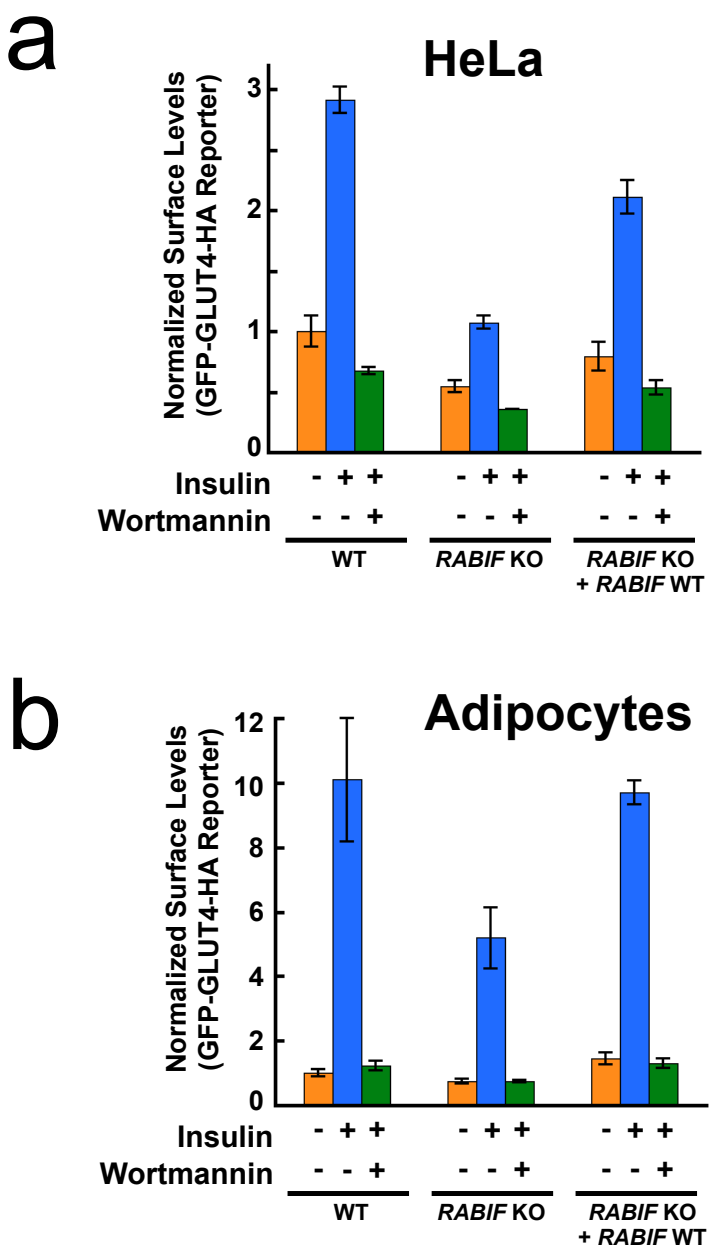

Figure 3.1: *RABIF* KO results in decreased insulin response.
WT or mutant adipocytes were untreated or treated with 100 nM insulin for 30 minutes before surface levels of GLUT reporter were measured by flow cytometry. When applicable, 100 nM wortmannin was added prior to insulin treatment. Error bars indicate standard deviation. **a,** HeLa cells. **b,** Adipocytes.

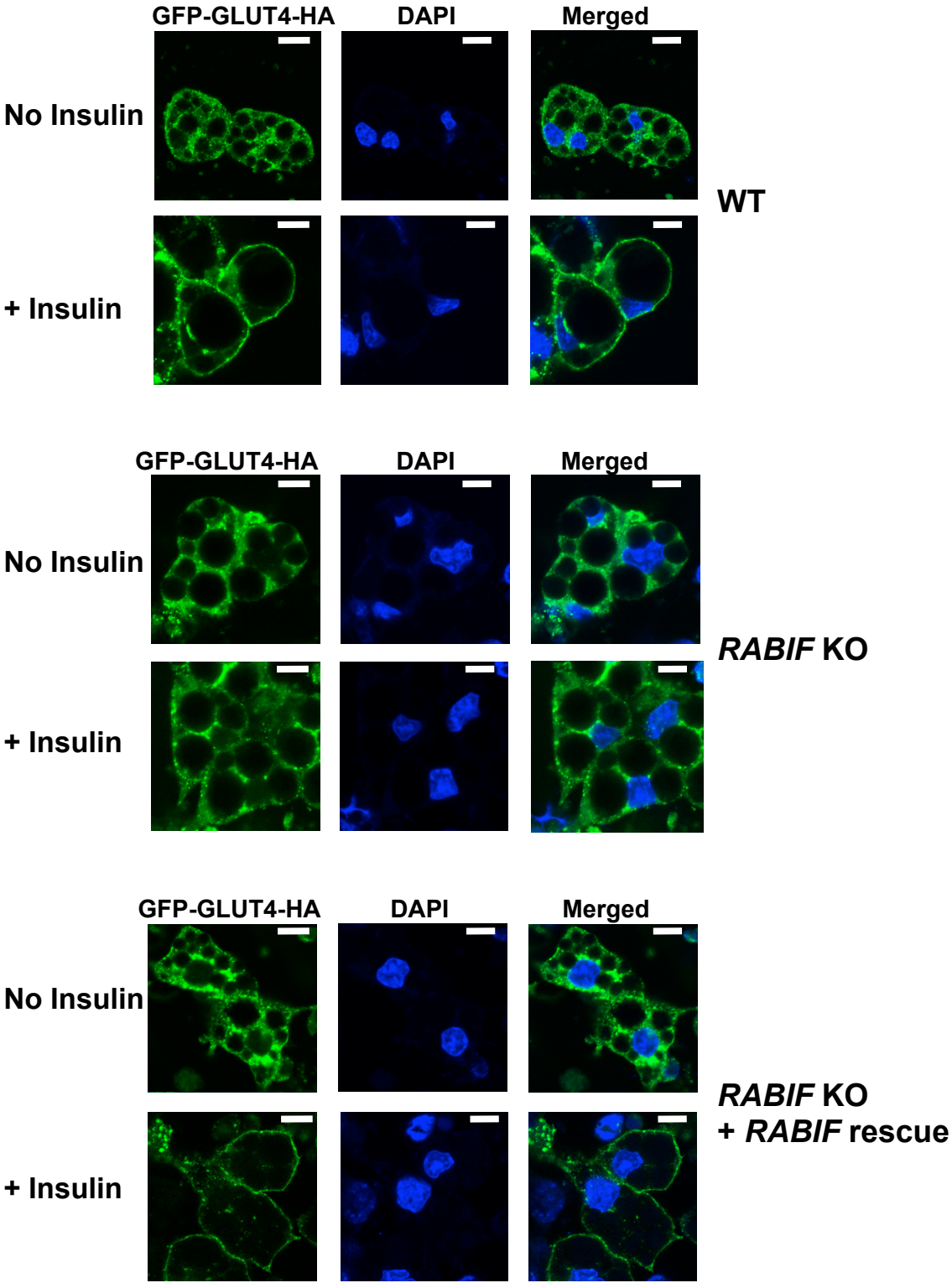

Figure 3.2: *RABIF* KO results in decreased insulin response.
WT or *RAFIF*-deficient adipocytes were either untreated or treated with 100 nM insulin for 30 minutes before the localization of the GLUT reporter was visualized by confocal microscopy. Bar: 10 µm. Data generated by Jingshi Shen.

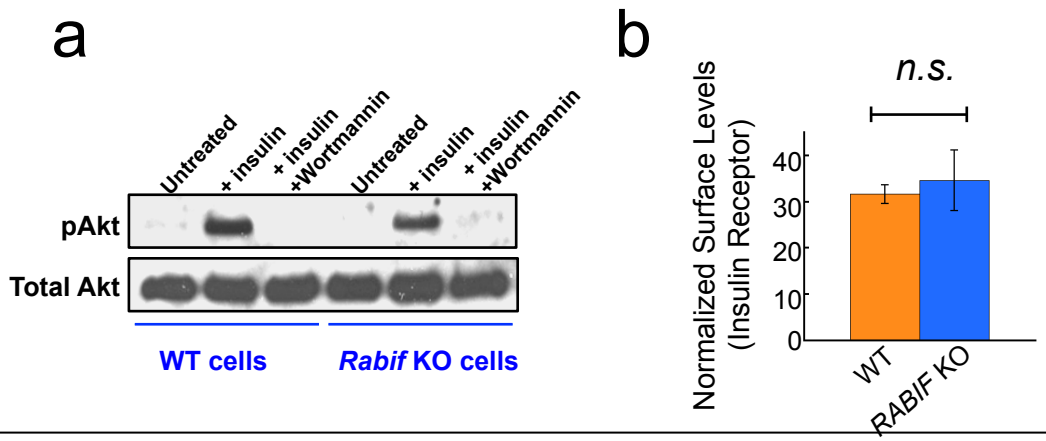

Figure 3.3: Rabif acts downstream of insulin signaling to regulate GLUT4 exocytosis. **A.** Immunoblots showing total AKT and insulin-stimulated AKT phosphorylation in WT or mutant HeLa cells. **B.** Normalized surface levels of insulin receptor in WT or mutant adipocytes. Error bars indicate standard deviation.

RABIF interacts with RAB10 and prevents RAB10 degradation

RABIF was identified in the same screen as RAB10 (Figs. 1.7, 1.12), an established mediator of exocytic vesicle fusion in GLUT translocation (Figs. 1.2, 1.10a) (Sano et al., 2007). We observed that RABIF interacted with RAB10 both on membranes and in solution (Fig. 3.4 a,b). Furthermore, RABIF and RAB10 exhibited partial co-localization in the cell (Fig. 3.4c). These data raise the possibility that RABIF directly regulates RAB10 in GLUT translocation. Interestingly, RAB10 protein levels were strongly reduced in *RABIF* KO cells (Fig. 3.5). Treatment with proteasomal inhibitors restored RAB10 expression in *RABIF* KO cells (Fig. 3.5), indicating that RAB10 is subject to proteasomal degradation in the absence of RABIF. This is an unexpected finding because no GEF was previously shown to regulate the stability of cognate Rab GTPases.

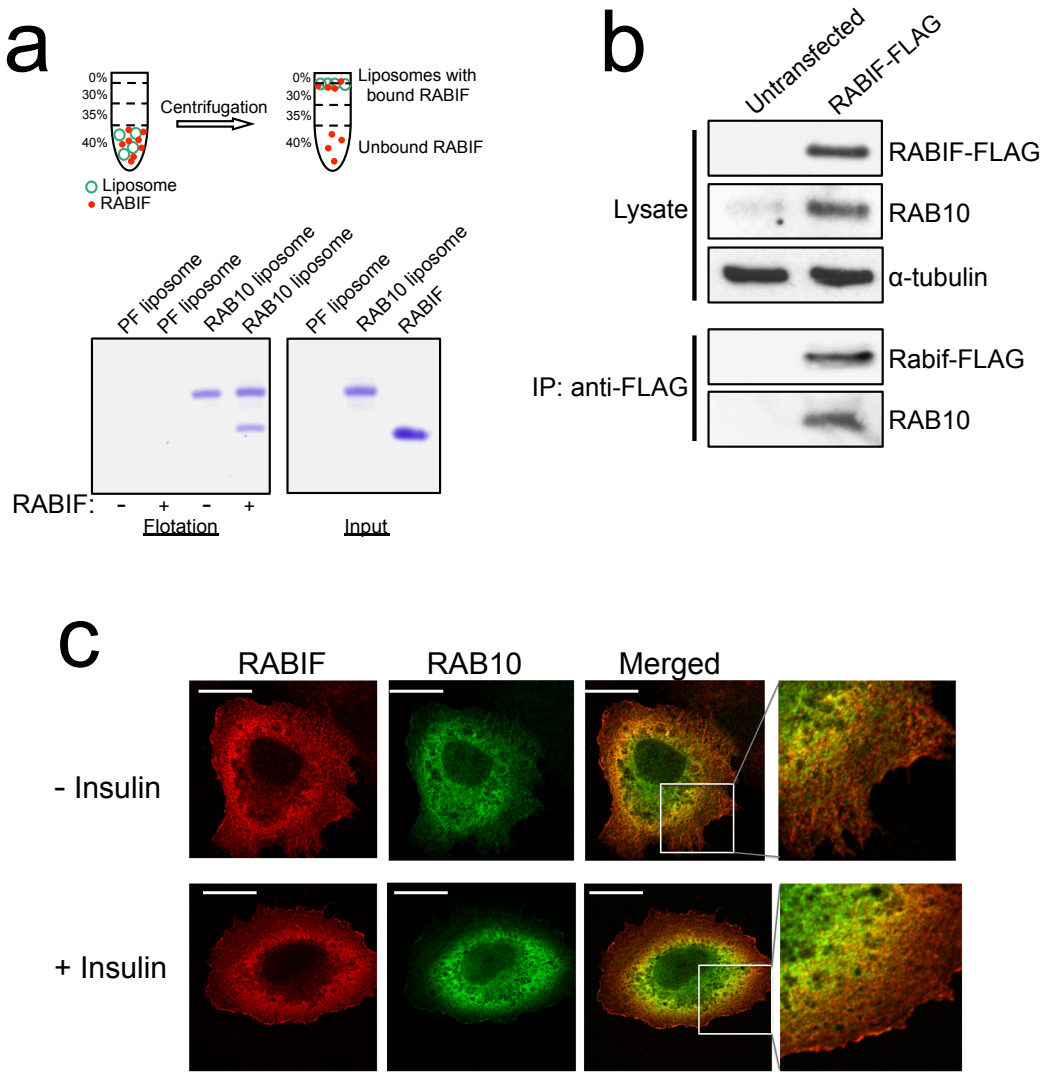

Figure 3.4: RABIF interacts with RAB10.
A. Top: diagram of the liposome co-flotation assay. Bottom: coomassie blue-stained denaturing gels showing the interaction between RABIF and RAB10 in the liposome co-flotation assay. PF: protein free. **B.** RABIF-FLAG was transiently expressed in *RABIF* KO HeLa cells. RABIF-FLAG was immunoprecipitated using anti-FLAG antibodies and the presence of RABIF-FLAG and RAB10 in the precipitates were detected by immunoblotting. **C.** Representative confocal images showing the localization of RAB10-Myc and RABIF-FLAG in HeLa cells with or without 30 min of insulin treatment (100 nM). Bar: 10 μm. Imaging data was generated by Jingshi Shen. Flotation assay was performed by Haijia Yu.

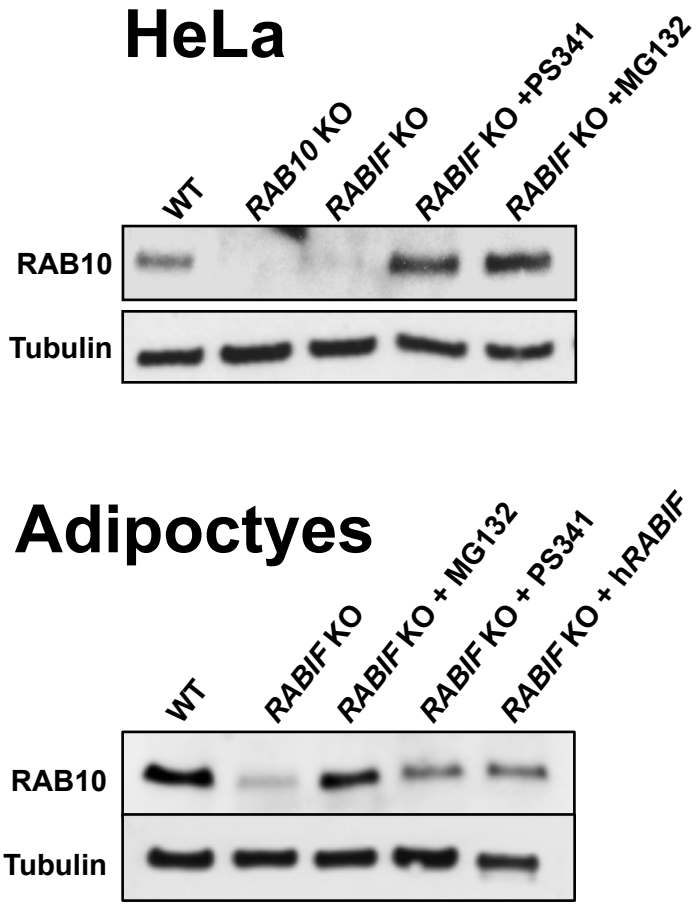

Figure 3.5: *RABIF* KO results in RAB10 degradation via proteasome. *RABIF* KO cells (HeLa or Adipocytes) were either untreated or treated with the indicated proteasome inhibitors for 16 hours. The expression levels of RAB10 and α-tubulin were probed by immunoblotting.

RABIF's role in GLUT4 trafficking is independent of its putative GEF domain

We next examined whether the GEF catalytic activity of RABIF is required for GLUT4 translocation. Structural studies suggested that the conserved residues D73, M74 and F75 are likely required for the GEF catalytic activity of RABIF (3.6a) (Zhu et al., 2001). Indeed, in an *in vitro* nucleotide release assay, the GEF activity of RABIF was largely abolished by a single F75A substitution (M1) or the triple D73A/M74A/F75A mutations (M2) (Fig. 3.6 b,d). Strikingly, these GEF-defective mutants rescued GLUT translocation to similar levels as WT RABIF (Fig. 3.7 b,c). RAB10 expression was also restored by the expression of these RABIF GEF mutants (Fig. 3.7a). Finally, overexpression of RAB10 could rescue GLUT4 exocytosis in RABIF KO cells (Fig. 3.8). By contrast, overexpression of DENND4C, a known GEF for RAB10 (Sano et al., 2011) failed to rescue GLUT4 translocation or RAB10 expression in *RABIF* KO cells (Fig. 3.9), further suggesting that the stability of RAB10 is regulated by RABIF independent of its GEF catalytic activity. Thus, RAB10 exploits RABIF itself, rather than its GEF catalytic activity, to regulate GLUT4 translocation.

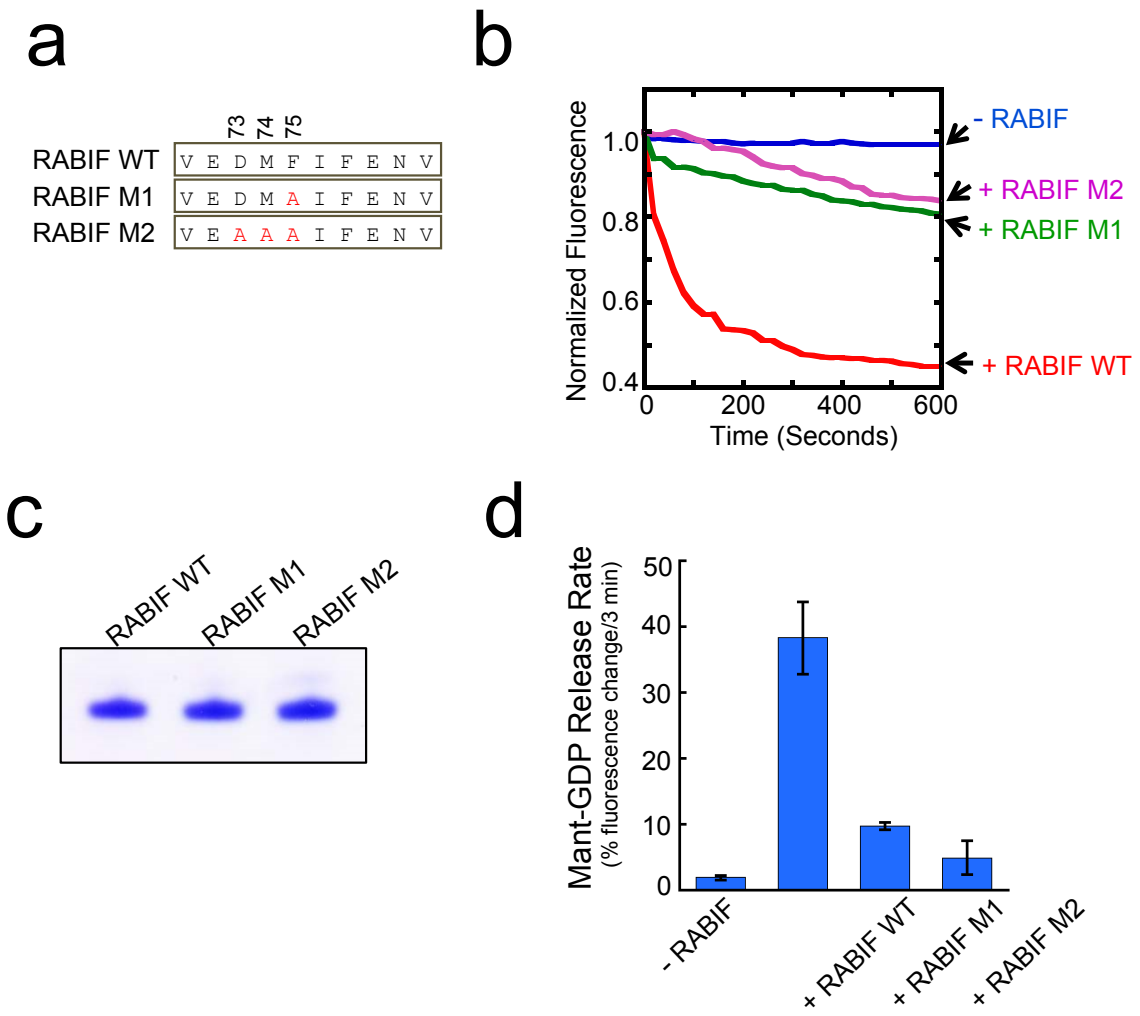

Figure 3.6: Catalytic domain mutants disrupt RABIF GEF activity.
A. Diagram showing RABIF point mutations predicted to impair GEF activity. **B.** Kinetics of fluorescence changes resulting from RABIF-catalyzed mant-GDP release. The reactions were carried out in the presence of WT or mutant RABIF, using RAB10 as the substrate. **C.** Coomassie blue-stained gel showing purified WT and mutant RABIF proteins. **D.** Initial rates of the reactions in h. Data are shown as percentage of fluorescence change within the first three minutes of the reactions. This data was generated by Haijia Yu.

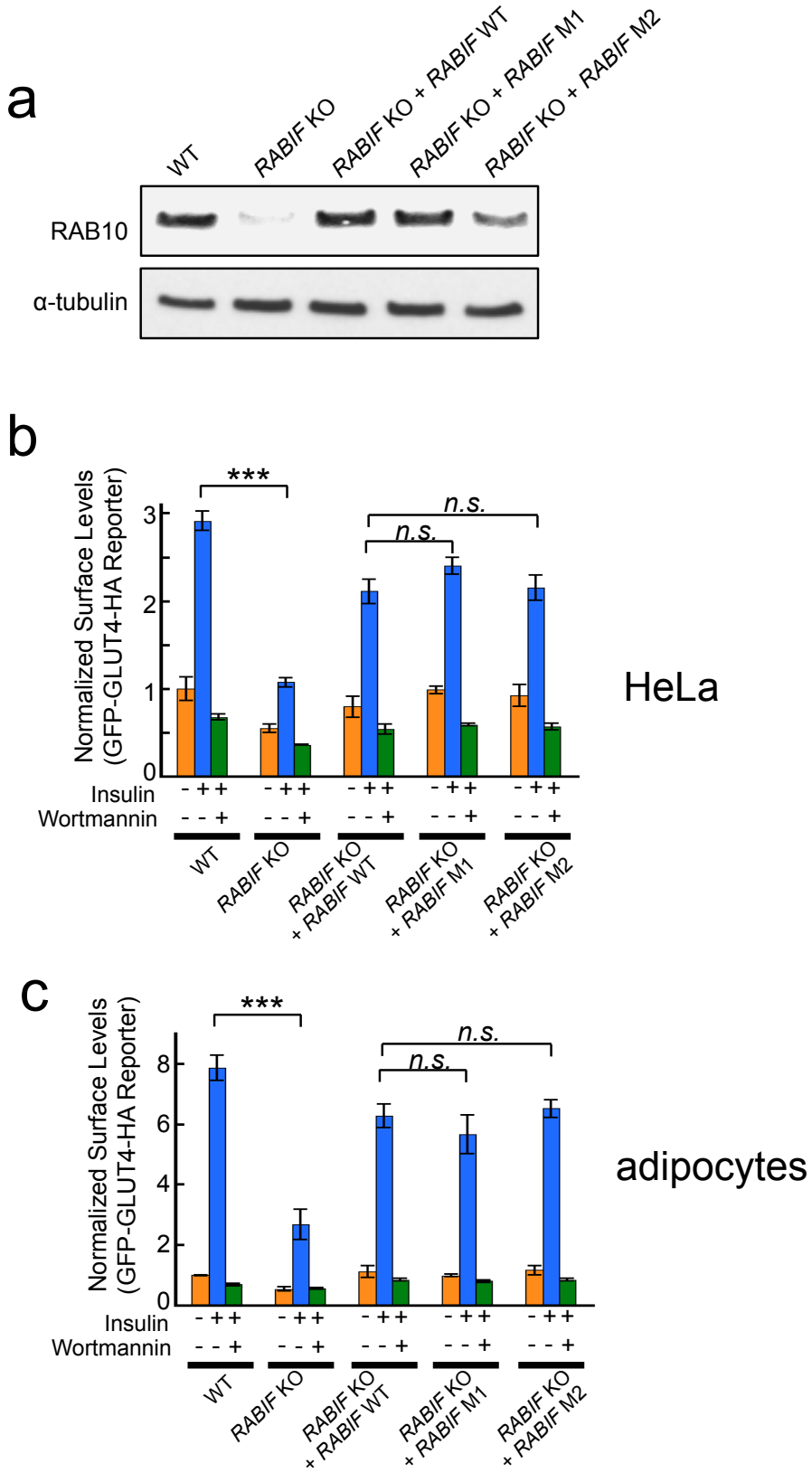

Figure 3.7: GEF catalytic domain mutation does not disrupt GLUT4 exocytosis activity. **A.** Immunoblots showing the expression levels of endogenous RAB10 and α-tubulin in the indicated HeLa cells. **B.** Normalized surface levels of the GLUT reporter in the indicated HeLa cells. ***P<0.001. **C.** Normalized surface levels of the GLUT reporter in the indicated adipocytes cells. ***P<0.001.

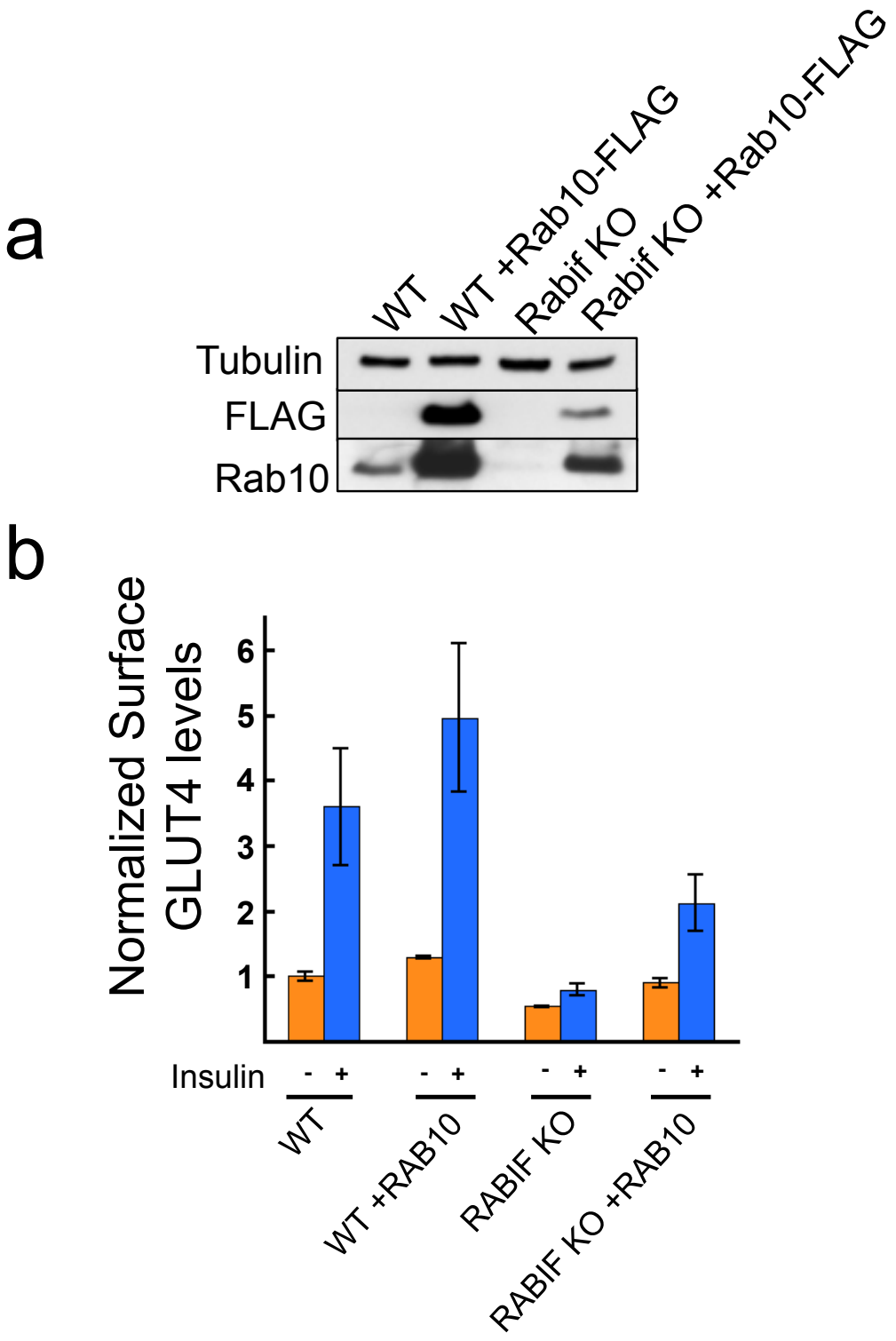

Figure 3.8: *RAB10* overexpression rescues *RABIF* KO GLUT4 exocytosis.
A. Immunoblots showing the expression levels of FLAG-tagged RAB10, total RAB10 and α-tubulin in the indicated HeLa cells. **B.** Normalized surface levels of the GLUT reporter in the indicated HeLa cells. ***P<0.001.

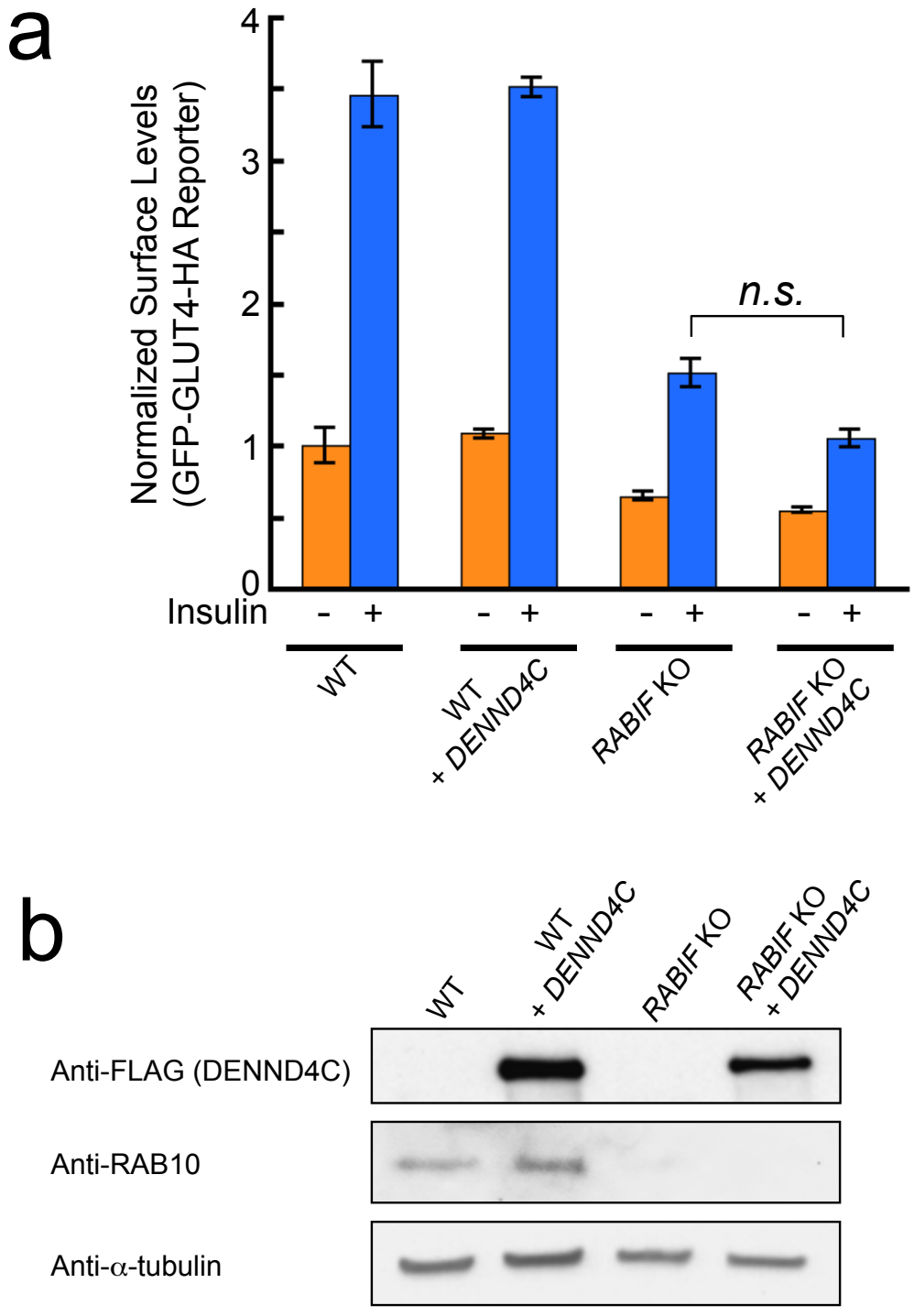

Figure 3.9: Overexpression of *DENND4C* does not rescue GLUT translocation defects in *RABIF* KO cells. A, *DENND4C* was overexpressed in WT or *RABIF*- deficient HeLa cells. Effects of *DENND4C* overexpression on GLUT reporter translocation were measured by flow cytometry. Error bars indicate standard deviation. **B**, Immunoblots showing the expression of DENND4C, RAB10 and α-tubulin in the indicated cells.

Whole cell proteomics show that RABIF regulates a small subset of RABs

Finally, we determined whether RABIF regulates other Rabs in addition to RAB10. To this end, we performed mass spectrometry-based quantitative proteomic analysis of WT and *RABIF* deficient cells. Among the 19 Rab GTPases detected by mass spectrometry, RAB10 level was reduced by over 10-fold in *RABIF* null cells (Fig. 3.10), consistent with the immunoblotting results (Fig. 3.5, 3.7a). Besides RAB10, RAB8A expression was also diminished in *RABIF* deficient cells. Using overexpression of a panel of fluorescently labeled RAB proteins we confirmed that RAB8a expression was also effected by *RABIF* KO (Fig 3.11a) while endogenous expression of RAB5a, RAB6 and RAB7 were not effected (Fig 3.11b). Therefore, the protein stabilizing function of RABIF is restricted to a subset of Rab GTPases. RAB8A was not recovered in our screens (Extended Data Fig. 2), confirming that RAB10 is the molecular target of RABIF in the GLUT translocation pathway. Together, these data demonstrate that, although predicted as a GEF, RABIF regulates RAB10 through a new function independent of its GEF catalytic activity (Fig. 3.12).

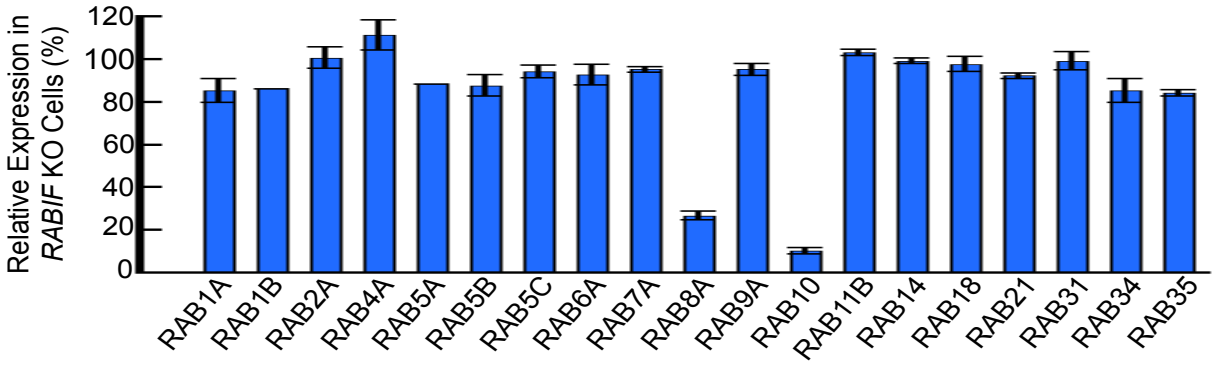

Figure 3.10: RABIF regulates a small subset of RAB proteins.
Proteomic analysis of Rab GTPase expression in *RABIF* KO cells. Data are presented as percentage of expression levels in WT cells. Average values of two technical replicates are shown (RAB1B levels were identical in the replicates, while RAB5A was only quantified in one replicate).

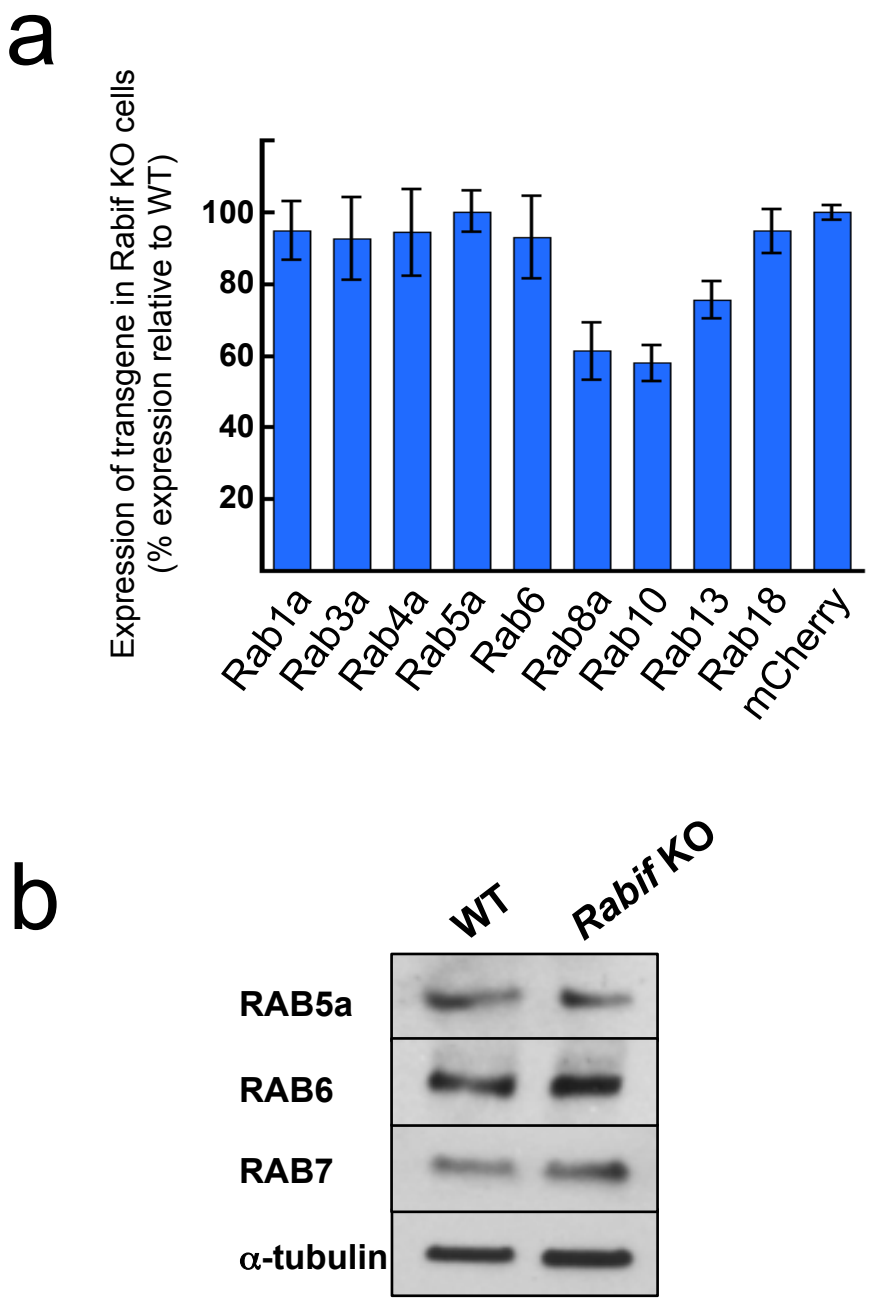

Figure 3.11: RABIF regulates a subset of RAB proteins.
A. Cerulean tagged RABS were transiently transfected in indicated HeLa cells. Fluorescence was quantified by flow cytometry. Error bars indicate standard deviation.
B. Imunoblots showing the endogenous expression of the indicated RAB proteins.

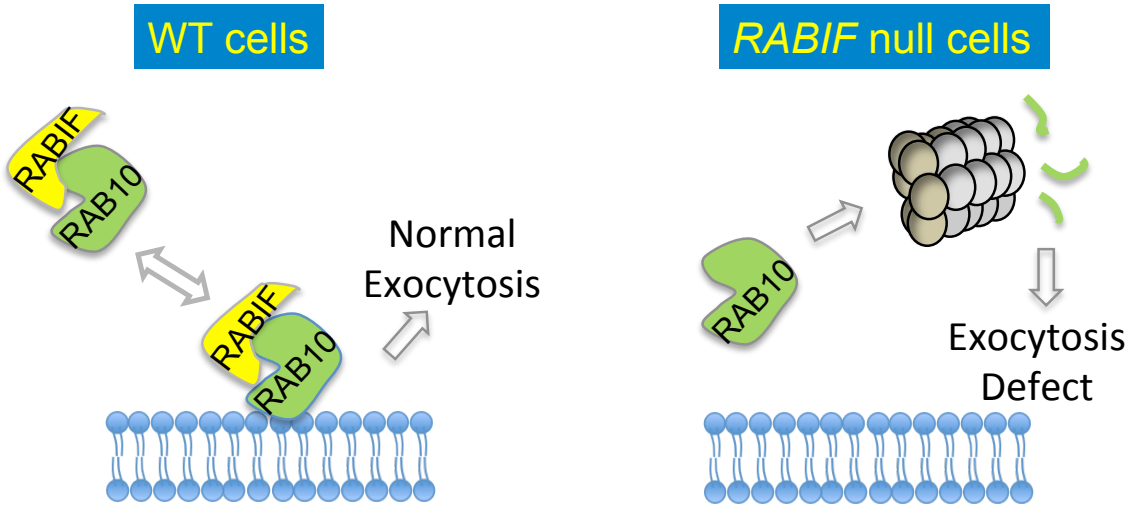

Figure 3.12: RABIF regulates the expression of RAB10

Discussion

In this work we demonstrated that RABIF regulates RAB10 expression independent of its canonical GEF domain. Further work is needed to distinguish whether RABIF protects the mature form of RAB10 from degradation or if it is required for maturation of RAB10. Furthermore, the precise role of RAB10 in the cell remains unresolved. While RAB10 is clearly required for a large insulin response in both adipocytes and HeLa cells, it remains unclear if it is playing a direct role in vesicle trafficking and fusion or if it is required for a more upstream step such as sorting GLUT4 into the insulin responsive vesicles.

The whole cell proteomics revealed that RABIF is regulating a small subset of RABs. Other proteins with a more mild reduction may be secondary in nature, for example down regulated in response to Rab10 reduction rather than Rabif. Among the mildly down-regulated proteins (~25% reduction) were a large number of mitochondrial-localized proteins. This is a very

interesting finding because it would link the cells ability to import glucose to its ability to metabolize glucose. This is potentially related to the large number of genes whose protein products localize to the mitochondria, which were recovered in the GLUT4 exocytosis defective screen. These two findings could represent opposite sides of a feedback loop. Further work is needed to validate this feedback mechanism, and identify the specific mechanism of feedback inhibition.

Table 3.1. Proteomic analysis of WT and *Rabif* KO cells

Protein name	Gene name	Average	Standard Deviation
Ras-related protein Rab-10	RAB10	0.1	0.014
Ras-related protein Rab-8A	RAB8A	0.265	0.021
Abhydrolase domain-containing protein 16A	ABHD16A	0.39	NA
Proteolipid protein 2	PLP2	0.41	NA
Lysosomal-associated transmembrane protein 4A	LAPTM4A	0.495	0.049
Syndecan-1	SDC1	0.53	NA
Monocarboxylate transporter 7	SLC16A6	0.53	NA
Folate receptor alpha	FOLR1	0.59	0.014
Disco-interacting protein 2 homolog B	DIP2B	0.595	0.615
ATP synthase mitochondrial F1 complex assembly factor 1	ATPAF1	0.6	0.255
Microtubule-associated proteins 1A/1B light chain 3B	MAP1LC3B	0.605	0.035
Glucocorticoid modulatory element-binding protein 1	GMEB1	0.61	NA
Sin3 histone deacetylase corepressor complex component SDS3	SUDS3	0.63	NA
CD81 antigen	CD81	0.64	0.028
NEDD4 family-interacting protein 1	NDFIP1	0.645	0.007
Deoxynucleotidyltransferase terminal-interacting protein 1	DNTTIP1	0.65	NA
Focadhesin	FOCAD	0.65	NA
Type 1 phosphatidylinositol 4,5-bisphosphate 4-phosphatase	TMEM55B	0.65	NA
Glutathione peroxidase	GPX4	0.655	0.078
Cytochrome c oxidase subunit 1	MT-CO1	0.655	0.007

Serine/threonine-protein phosphatase 1 regulatory subunit 10	PPP1R10	0.665	0.078
G antigen 12F	GAGE12F	0.67	0.085
2-oxoisovalerate dehydrogenase subunit beta, mitochondrial	BCKDHB	0.67	NA
Ephrin type-A receptor 2	EPHA2	0.67	NA
Ferritin light chain	FTL	0.67	0.014
Glutathione peroxidase 1	GPX1	0.675	0.021
Neurogenic locus notch homolog protein 2	NOTCH2	0.675	0.007
G antigen 2D	GAGE2D	0.685	0.035
Ferritin	FTH1	0.69	0.014
Integrin alpha-5	ITGA5	0.69	NA
Protein PML	PML	0.69	NA
E3 ubiquitin-protein ligase RNF149	RNF149	0.695	0.021
Alpha-adducin	ADD1	0.7	NA
Nuclear factor 1	NFIA	0.7	NA
Transmembrane protein 205	TMEM205	0.7	NA
CD70 antigen	CD70	0.705	0.064
Endothelial protein C receptor	PROCR	0.705	0.092
Alanine aminotransferase 2	GPT2	0.71	0.113
MARCKS-related protein	MARCKSL1	0.71	NA
28S ribosomal protein S25, mitochondrial	MRPS25	0.72	0.085
Protein MTO1 homolog, mitochondrial	MTO1	0.72	NA
Lipid phosphate phosphohydrolase 2	PPAP2C	0.72	NA
Prostaglandin F2 receptor negative regulator	PTGFRN	0.72	0.028
Folate transporter 1	SLC19A1	0.72	NA
Tumor necrosis factor ligand superfamily member 9	TNFSF9	0.725	0.035
Acyl-CoA synthetase family member 3, mitochondrial	ACSF3	0.73	0.085
CD63 antigen	CD63	0.73	0.071
Bifunctional ATP-dependent dihydroxyacetone kinase/FAD-AMP lyase (cyclizing)	DAK	0.73	NA
NADPH:adrenodoxin oxidoreductase, mitochondrial	FDXR	0.73	NA
Transmembrane protein 209	TMEM209	0.73	NA
Neural cell adhesion molecule L1	L1CAM	0.735	0.021
Leukemia inhibitory factor receptor	LIFR	0.735	0.035
Receptor expression-enhancing protein 6	REEP6	0.74	NA
Splicing factor, arginine/serine-rich 15	SCAF4	0.74	NA
Leucine-rich repeat and WD repeat-containing protein 1	LRWD1	0.745	0.191
39S ribosomal protein L45, mitochondrial	MRPL45	0.745	0.007
Solute carrier family 35 member F2	SLC35F2	0.745	0.049
Disintegrin and metalloproteinase domain-containing protein 9	ADAM9	0.75	NA

Quinone oxidoreductase-like protein 1	CRYZL1	0.75	NA
Protein FAM115A	FAM115A	0.75	NA
HIG1 domain family member 2A, mitochondrial	HIGD2A	0.75	NA
Interferon-induced transmembrane protein 1	IFITM2	0.75	NA
39S ribosomal protein L3, mitochondrial	MRPL3	0.75	NA
Brain acid soluble protein 1	BASP1	0.755	0.049
DNA-directed RNA polymerase I subunit RPA34	CD3EAP	0.755	0.021
28S ribosomal protein S18b, mitochondrial	MRPS18B	0.755	0.021
ATP synthase subunit f, mitochondrial	ATP5J2	0.76	NA
1,4-alpha-glucan-branching enzyme	GBE1	0.76	NA
Glutaryl-CoA dehydrogenase, mitochondrial	GCDH	0.76	NA
General transcription factor IIH subunit 2-like protein	GTF2H2C	0.76	NA
Haloacid dehalogenase-like hydrolase domain-containing protein 3	HDHD3	0.76	NA
Homeodomain-interacting protein kinase 4	HIPK4	0.76	NA
HLA class I histocompatibility antigen, B-42 alpha chain	HLA-B	0.76	NA
28S ribosomal protein S30, mitochondrial	MRPS30	0.76	0.170
NADH dehydrogenase [ubiquinone] 1 beta subcomplex subunit 11, mitochondrial	NDUFB11	0.76	NA
Pituitary tumor-transforming gene 1 protein-interacting protein	PTTG1IP	0.76	NA
Zinc transporter ZIP10	SLC39A10	0.76	NA
Zinc transporter ZIP14	SLC39A14	0.76	NA
Activating transcription factor 7-interacting protein 1	ATF7IP	0.765	0.078
Cdc42 effector protein 1	CDC42EP1	0.77	NA
Epsin-1	EPN1	0.77	NA
HCLS1-associated protein X-1	HAX1	0.77	0.028
Myristoylated alanine-rich C-kinase substrate	MARCKS	0.77	0.085
NADH-ubiquinone oxidoreductase chain 5	MT-ND5	0.77	0.071
Putative nascent polypeptide-associated complex subunit alpha-like protein	NACAP1	0.77	NA
Polypyrimidine tract-binding protein 2	PTBP2	0.77	0.014
Parathymosin	PTMS	0.77	0.283
All-trans-retinol 13,14-reductase	RETSAT	0.77	NA
Shugoshin-like 2	SGOL2	0.77	NA
Sequestosome-1	SQSTM1	0.77	0.000
28S ribosomal protein S35, mitochondrial	MRPS35	0.775	0.078
Creatine kinase U-type, mitochondrial	CKMT1A	0.775	0.021
Acylpyruvase FAHD1, mitochondrial	FAHD1	0.775	0.134
ATPase family AAA domain-containing protein 3B	ATAD3B	0.78	NA
Interferon-induced transmembrane protein 3	IFITM3	0.78	NA
NADH dehydrogenase [ubiquinone] 1 beta subcomplex subunit 3	NDUFB3	0.78	NA

NAD-dependent protein deacylase sirtuin-5, mitochondrial	SIRT5	0.78	NA
Synaptophysin-like protein 1	SYPL1	0.78	0.042
Mitochondrial import receptor subunit TOM6 homolog	TOMM6	0.78	0.014
Tetraspanin-3	TSPAN3	0.78	NA
UBX domain-containing protein 8	UBXN8	0.78	NA
Lysosomal alpha-glucosidase	GAA	0.785	0.092
High mobility group protein HMG-I/HMG-Y	HMGA1	0.785	0.049
Heterogeneous nuclear ribonucleoproteins C1/C2	HNRNPC	0.785	0.049
Scavenger receptor class B member 1	SCARB1	0.785	0.092
Zinc finger CCCH domain-containing protein 18	ZC3H18	0.785	0.064
Neutral amino acid transporter B(0)	SLC1A5	0.785	0.007
A-kinase anchor protein 13	AKAP13	0.79	NA
HMG box transcription factor BBX	BBX	0.79	NA
2-methoxy-6-polyprenyl-1,4-benzoquinol methylase, mitochondrial	COQ5	0.79	NA
Protein SGT1	ECD	0.79	0.057
Integrin alpha-2	ITGA2	0.79	0.057
Microtubule-associated protein 2	MAP2	0.79	NA
39S ribosomal protein L4, mitochondrial	MRPL4	0.79	0.042
39S ribosomal protein L54, mitochondrial	MRPL54	0.79	NA
Phosphoenolpyruvate carboxykinase [GTP], mitochondrial	PCK2	0.79	0.057
[Pyruvate dehydrogenase (acetyl-transferring)] kinase isozyme 3, mitochondrial	PDK3	0.79	NA
Membralin	TMEM259	0.79	0.028
Dystroglycan	DAG1	0.795	0.106
ATP-binding cassette sub-family G member 2	ABCG2	0.795	0.021
Mitochondrial inner membrane protein OXA1L	OXA1L	0.795	0.163

EXPERIMENTAL PROCEDURES

Recombinant protein expression and purification

Recombinant RAB10 proteins were produced in *Sf9* insect cells using baculovirus infection. The full-length mouse *Rab10* gene was cloned into the baculovirus transfer vector pFastBac to generate a construct encoding a His_6-tagged RAB10 protein with a tobacco etch virus (TEV) protease cleavage site. His_6-Rab10 was expressed in *Sf9* cells as we previously described for other proteins(Yu et al., 2016; Yu et al., 2013b). The cells were harvested in a lysis buffer (25 mM HEPES [pH 7.4], 400 mM KCl, 10% glycerol, 20 mM imidazole, 5 mM $MgCl_2$, 1% Triton, 2 mM β-mercaptoethanol, and a protease inhibitor cocktail). RAB10 proteins were purified by nickel affinity chromatography and the His_6 tag was removed by TEV protease digestion.

Recombinant RABIF proteins were expressed and purified from *E. coli* as we previously described for other soluble proteins (Rathore et al., 2010; Yu et al., 2013a; Yu et al., 2013c). The human *RABIF* gene was cloned into a pET28a-based SUMO vector. Purified His_6-SUMO-RABIF fusion proteins were digested by SUMO proteases to obtain untagged RABIF proteins. RABIF mutants were generated by site-directed mutagenesis and expressed using the same procedure as the WT protein.

Liposome co-flotation assay

Protein-free or RAB10 liposomes were prepared using POPC (1-palmitoyl-2-oleoyl-sn-glycero-3-phosphocholine), following a liposome reconstitution protocol previously established in our group (Rathore et al., 2011; Shen et al., 2010; Yu et al., 2013c). Soluble RABIF proteins were incubated with liposomes at 4 ^{o}C with gentle agitation. After one hour, an equal volume of 80% nycodenz (w/v) in reconstitution buffer was added and transferred to 5 mm by 41 mm centrifuge tubes. The liposomes were overlaid with 200 µl each of 35% and 30% Nycodenz, and then with 20 µl reconstitution buffer on the top. The gradients were centrifuged for 4 hours at 52,000 RPM in a Beckman SW55 rotor. Samples were collected from the 0/30% Nycodenz interface (2 x 20 µl) and analyzed by SDS-PAGE.

Guanine nucleotide release assay

Recombinant RAB10 proteins were incubated with the fluorescent GDP analogue 2'-(or-3')-*O*-(*N*-Methylanthraniloyl) Guanosine 5'-Diphosphate (mant-GDP, Molecular Probes, #M12414) at room temperature for one hour in a loading buffer (20 mM HEPES [pH 7.4], 50 mM NaCl, 5 mM EDTA, and a 25-fold molar excess of mant-GDP). The loading reaction was terminated by addition of 10 mM $MgCl_2$. Free mant-GDP was removed using desalting columns (GE Healthcare, #17-0853-02). Mant-GDP-bound RAB10 was diluted to 0.2 µM using the exchange buffer (20 mM HEPES [pH 7.4], 50 mM NaCl, and 5 mM $MgCl_2$) in the absence or presence of 10 µM RABIF and 100 µM unlabeled GDP. Fluorescence changes associated with mant-GDP

release were measured on a SpectraMax M5 microplate reader (Molecular Devices) at the excitation wavelength of 365 nm and emission wavelength of 440 nm.

Immunoblotting and immunoprecipitation

Cells grown in 24-well plates were lysed in 1x SDS protein sample buffer and the cell lysates were resolved on 8% Bis-Tris SDS-PAGE. Proteins were detected using primary antibodies and horseradish peroxidase-conjugated secondary antibodies. Primary antibodies used in immunoblotting were: anti-AKT antibodies (Cell Signaling Technology, #9272), anti-phospho-AKT antibodies (Cell Signaling Technology, #5473), anti-RAB10 antibodies (Cell Signaling Technology, #8127) anti-α-tubulin antibodies (eBioscience, #14-4502-82), and anti-FLAG antibodies (Sigma, #F1804).

In immunoprecipitation experiments, cells were lysed in a buffer containing 25 mM Tris-HCl [pH 7.4], 150 mM NaCl, 1 mM EDTA, 1% NP-40, 5% glycerol, and a protease inhibitor cocktail. Proteins were precipitated by using anti-FLAG magnetic beads (Sigma, M8823). Proteins in the precipitates were detected by immunoblotting.

Immunostaining and imaging

HeLa cells were seeded on coverslips coated with fibronectin (Sigma, #F1144). The cells were fixed using 2% PFA and permeabilized in PBS supplemented with 5% FBS and 0.2% saponin. Antigens were stained using the following primary antibodies: anti-Myc antibodies (SCBT,

clone#9E10), anti-FLAG antibodies (Sigma, #F7425). The cells were subsequently incubated with Alexa Fluor 488- or Alexa Fluor 568-conjugated secondary antibodies. After mounting on glass slides using the ProLong Antifade mountant with DAPI (Thermo, #P36931), the cells were visualized on a Carl Zeiss LSM780 confocal microscope. Cell images were captured and processed using the Carl Zeiss Zen 2 and Adobe Photoshop software. To visualize the GFP-GLUT4-HA reporter in adipocytes, the cells were fixed and permeabilized similarly as HeLa cells.

Mass spectrometry

Quantitative proteomic analysis of protein levels was performed using stable isotope labeling with amino acids in cell culture (SILAC) and mass spectrometry (MS). Cells were grow in SILAC media (Thermo, #88423) supplemented with 10% dialyzed FBE (Seradigm, #3100). WT HeLa cells were grown in the presence of light lysine and arginine (Sigma, #L1262 and A5131), whereas RABIF null cells were grown in the presence of heavy lysine and arginine (Cambridge Isotope Laboratories, #CNLM-291 and CNLM-539). After five days, the cells were harvested at ~60% confluence in a lysis buffer (4% SDS and 50 mM Tris-HCl [pH 6.8]). The cell lysates were processed for MS analysis following the filter-aided sample preparation (FASP) protocol (Erde et al., 2014; Wisniewski et al., 2009). Briefly, after addition of 20 mM DTT, equal amounts of whole-cell lysates were mixed and loaded onto a spin filter with a molecular weight cutoff of 30 kDa. The sample was then washed with the UA solution (8 M Urea and 0.1 M Tris-HCl [pH 7.9]) and alkylated using 0.1 M iodoacetamide. The sample was further washed with the UA solution and equilibrated with 0.1 M ammonium bicarbonate and 0.01% deoxycholic

acid. The sample was then digested using 1% (w/w) trypsin at 37 ^{o}C for 16 hours. The resulting tryptic peptides were eluded by centrifugation, and acidified using formic acid. Deoxycholic acid was removed using phase transfer with ethyl acetate. The tryptic peptides were fractionated by a Pierce high pH reversed-phase spin column using 18 step gradients (4% acetonitrile for the first fraction, 1% increment for each fraction to the 17th fraction, and 50% acetonitrile for the 18th fraction). The fractions were dried using vacuum centrifugation.

One third of each fraction (5 µL) from high pH fractionation was analyzed by UPLC-MS/MS. The tryptic peptides were loaded onto a Waters nanoACQUITY UPLC BEH C18 column (130 Å, 1.7 µm × 75 µm × 250 mm) equilibrated with 0.1% formic acid/3% acetonitrile/water. Mobile phase A was 0.1% formic acid/water, while B was 0.1% formic acid/acetonitrile. The peptides were eluted at 0.3 mL/min using a gradient of 3-8% B (0-5 minutes) and 8-35% B (5-123 minutes).

Precursor ions between 300-1800 m/z (1x10^{6} ions, 60,000 resolution) were scanned on a LTQ Orbitrap Velos mass spectrometer. The 10 most intense ions for MS/MS were selected with 180-second dynamic exclusion, 10 ppm exclusion width, with a repeat count=1, and a 30-second repeat duration. Ions with unassigned charge state and MH+1 were excluded from MS/MS. Maximal ion injection times were 500 milliseconds for FT (one microscan) and 250 milliseconds for LTQ, and the AGC was 1x10^{4}. The normalized collision energy was 35% with activation Q 0.25 for 10 milliseconds.

Raw data files from MS were searched against the Uniprot human proteome database (Consortium, 2015) (total 88,479 entries), using the MaxQuant/Andromeda search engine (version 1.5.2.8)(Cox et al., 2011). Searches allowed trypsin specificity with two missed cleavages, and included fixed Cys carbamidomethylation, and variable acetylation (protein N-terminus) and methionine oxidation. Mass tolerances were set to 20 ppm (first search) and 4.5 ppm (main search) for precursor ions, and 0.5 Da for ITMS MS/MS ions. MaxQuant/Andromeda used the top 8 MS/MS peaks per 100 Da and seven amino acid minimum peptide length, with 0.01 false discovery rate for both protein and peptide identification. For SILAC ratio measurements, minimum two independent peptide ratios were used to calculate a protein ratio.

REFERENCES

Antonescu, C.N., McGraw, T.E., and Klip, A. (2014). Reciprocal regulation of endocytosis and metabolism. Cold Spring Harbor perspectives in biology *6*, a016964.

Böcking, T., Aguet, F., Harrison, S.C., and Kirchhausen, T. (2011). Single-molecule analysis of a molecular disassemblase reveals the mechanism of Hsc70-driven clathrin uncoating. Nature structural & molecular biology *18*, 295-301.

Bonifacino, J.S., and Glick, B.S. (2004). The mechanisms of vesicle budding and fusion. Cell *116*, 153-166.

Brodsky, F.M. (2012). Diversity of clathrin function: new tricks for an old protein. Annu Rev Cell Dev Biol *28*, 309-336.

Bryant, N.J., Govers, R., and James, D.E. (2002). Regulated transport of the glucose transporter GLUT4. Nat Rev Mol Cell Biol *3*, 267-277.

Cong, L., Ran, F.A., Cox, D., Lin, S., Barretto, R., Habib, N., Hsu, P.D., Wu, X., Jiang, W., Marraffini, L.A.*, et al.* (2013). Multiplex genome engineering using CRISPR/Cas systems. Science (New York, NY) *339*, 819-823.

Conner, S.D., and Schmid, S.L. (2003). Differential requirements for AP-2 in clathrin-mediated endocytosis. The Journal of cell biology *162*, 773-779.

Cox, J., Neuhauser, N., Michalski, A., Scheltema, R.A., Olsen, J.V., and Mann, M. (2011). Andromeda: a peptide search engine integrated into the MaxQuant environment. J Proteome Res *10*, 1794-1805.

Davis, E.M., Kim, J., Menasche, B.L., Sheppard, J., Liu, X., Tan, A.C., and Shen, J. (2015). Comparative Haploid Genetic Screens Reveal Divergent Pathways in the Biogenesis and Trafficking of Glycophosphatidylinositol-Anchored Proteins. Cell Rep *11*, 1727-1736.

Doudna, J.A., and Charpentier, E. (2014). Genome editing. The new frontier of genome engineering with CRISPR-Cas9. Science (New York, NY) *346*, 1258096.

Dummler, B., Tschopp, O., Hynx, D., Yang, Z.Z., Dirnhofer, S., and Hemmings, B.A. (2006). Life with a single isoform of Akt: mice lacking Akt2 and Akt3 are viable but display impaired glucose homeostasis and growth deficiencies. Mol Cell Biol *26*, 8042-8051.

Eguez, L., Lee, A., Chavez, J.A., Miinea, C.P., Kane, S., Lienhard, G.E., and McGraw, T.E. (2005). Full intracellular retention of GLUT4 requires AS160 Rab GTPase activating protein. Cell Metab *2*, 263-272.

Erde, J., Loo, R.R., and Loo, J.A. (2014). Enhanced FASP (eFASP) to increase proteome coverage and sample recovery for quantitative proteomic experiments. J Proteome Res *13*, 1885-1895.

Ferguson, S.M., Raimondi, A., Paradise, S., Shen, H., Mesaki, K., Ferguson, A., Destaing, O., Ko, G., Takasaki, J., Cremona, O.*, et al.* (2009). Coordinated actions of actin and BAR proteins upstream of dynamin at endocytic clathrin-coated pits. Developmental cell *17*, 811-822.

Fu, Y., Sander, J.D., Reyon, D., Cascio, V.M., and Joung, J.K. (2014). Improving CRISPR-Cas nuclease specificity using truncated guide RNAs. Nat Biotechnol *32*, 279-284.

Gilbert, L.A., Horlbeck, M.A., Adamson, B., Villalta, J.E., Chen, Y., Whitehead, E.H., Guimaraes, C., Panning, B., Ploegh, H.L., Bassik, M.C.*, et al.* (2014). Genome-Scale CRISPR-Mediated Control of Gene Repression and Activation. Cell *159*, 647-661.

Hart, T., Chandrashekhar, M., Aregger, M., Steinhart, Z., Brown, K.R., MacLeod, G., Mis, M., Zimmermann, M., Fradet-Turcotte, A., Sun, S.*, et al.* (2015). High-Resolution CRISPR Screens Reveal Fitness Genes and Genotype-Specific Cancer Liabilities. Cell *163*, 1515-1526.

Huang, S., and Czech, M.P. (2007). The GLUT4 glucose transporter. Cell Metab *5*, 237-252.
Koike-Yusa, H., Li, Y., Tan, E.P., Velasco-Herrera Mdel, C., and Yusa, K. (2014). Genome-wide recessive genetic screening in mammalian cells with a lentiviral CRISPR-guide RNA library. Nat Biotechnol *32*, 267-273.

Li, W., Xu, H., Xiao, T., Cong, L., Love, M.I., Zhang, F., Irizarry, R.A., Liu, J.S., Brown, M., and Liu, X.S. (2014). MAGeCK enables robust identification of essential genes from genome-scale CRISPR/Cas9 knockout screens. Genome biology *15*, 554.

Mali, P., Yang, L., Esvelt, K.M., Aach, J., Guell, M., DiCarlo, J.E., Norville, J.E., and Church, G.M. (2013). RNA-guided human genome engineering via Cas9. Science (New York, NY) *339*, 823-826.

Marceau, C.D., Puschnik, A.S., Majzoub, K., Ooi, Y.S., Brewer, S.M., Fuchs, G., Swaminathan, K., Mata, M.A., Elias, J.E., Sarnow, P.*, et al.* (2016). Genetic dissection of Flaviviridae host factors through genome-scale CRISPR screens. Nature *535*, 159-163.

Martens, S., and McMahon, H.T. (2008). Mechanisms of membrane fusion: disparate players and common principles. Nat Rev Mol Cell Biol *9*, 543-556.

McMahon, H.T., and Boucrot, E. (2011). Molecular mechanism and physiological functions of clathrin-mediated endocytosis. Nat Rev Mol Cell Biol *12*, 517-533.

Muretta, J.M., Romenskaia, I., and Mastick, C.C. (2008). Insulin releases Glut4 from static storage compartments into cycling endosomes and increases the rate constant for Glut4 exocytosis. J Biol Chem *283*, 311-323.

Page, L.J., Sowerby, P.J., Lui, W.W., and Robinson, M.S. (1999a). Gamma-synergin: an EH domain-containing protein that interacts with gamma-adaptin. The Journal of cell biology *146*, 993-1004.

Page, L.J., Sowerby, P.J., Lui, W.W.Y., and Robinson, M.S. (1999b). γ-Synergin: An Eh Domain–Containing Protein That Interacts with γ-Adaptin. The Journal of Cell Biology *146*, 993-1004.

Palade, G. (1975). Intracellular aspects of the process of protein synthesis. Science *189*, 347-358.
Parnas, O., Jovanovic, M., Eisenhaure, T.M., Herbst, R.H., Dixit, A., Ye, C.J., Przybylski, D., Platt, R.J., Tirosh, I., Sanjana, N.E.*, et al.* (2015). A Genome-wide CRISPR Screen in Primary Immune Cells to Dissect Regulatory Networks. Cell *162*, 675-686.

Pohler, E., Mamai, O., Hirst, J., Zamiri, M., Horn, H., Nomura, T., Irvine, A.D., Moran, B., Wilson, N.J., Smith, F.J.*, et al.* (2012). Haploinsufficiency for AAGAB causes clinically heterogeneous forms of punctate palmoplantar keratoderma. Nat Genet *44*, 1272-1276.

Rathore, S.S., Bend, E.G., Yu, H., Hammarlund, M., Jorgensen, E.M., and Shen, J. (2010). Syntaxin N-terminal peptide motif is an initiation factor for the assembly of the SNARE-Sec1/Munc18 membrane fusion complex. Proc Natl Acad Sci U S A *107*, 22399-22406.

Rathore, S.S., Ghosh, N., Ouyang, Y., and Shen, J. (2011). Topological arrangement of the intracellular membrane fusion machinery. Molecular biology of the cell *22*, 2612-2619.

Saltiel, A.R., and Kahn, C.R. (2001). Insulin signalling and the regulation of glucose and lipid metabolism. Nature *414*, 799-806.

Sanjana, N.E., Shalem, O., and Zhang, F. (2014). Improved vectors and genome-wide libraries for CRISPR screening. Nature methods *11*, 783-784.

Sano, H., Eguez, L., Teruel, M.N., Fukuda, M., Chuang, T.D., Chavez, J.A., Lienhard, G.E., and McGraw, T.E. (2007). Rab10, a target of the AS160 Rab GAP, is required for insulin-stimulated translocation of GLUT4 to the adipocyte plasma membrane. Cell Metab *5*, 293-303.

Sano, H., Peck, G.R., Kettenbach, A.N., Gerber, S.A., and Lienhard, G.E. (2011). Insulin-stimulated GLUT4 Protein Translocation in Adipocytes Requires the Rab10 Guanine Nucleotide Exchange Factor Dennd4C. J Biol Chem *286*, 16541-16545.

Schekman, R., and Novick, P. (2004). 23 genes, 23 years later. Cell *116*, S13-15, 11 p following S19.

Shalem, O., Sanjana, N.E., Hartenian, E., Shi, X., Scott, D.A., Mikkelsen, T.S., Heckl, D., Ebert, B.L., Root, D.E., Doench, J.G.*, et al.* (2014). Genome-scale CRISPR-Cas9 knockout screening in human cells. Science (New York, NY) *343*, 84-87.

Shen, J., Rathore, S., Khandan, L., and Rothman, J.E. (2010). SNARE bundle and syntaxin N-peptide constitute a minimal complement for Munc18-1 activation of membrane fusion. J Cell Biology *190*, 55-63.

Sidik, S.M., Huet, D., Ganesan, S.M., Huynh, M.H., Wang, T., Nasamu, A.S., Thiru, P., Saeij, J.P., Carruthers, V.B., Niles, J.C.*, et al.* (2016). A Genome-wide CRISPR Screen in Toxoplasma Identifies Essential Apicomplexan Genes. Cell *166*, 1423-1435 e1412.

Simpson, I.A., Dwyer, D., Malide, D., Moley, K.H., Travis, A., and Vannucci, S.J. (2008). The facilitative glucose transporter GLUT3: 20 years of distinction. Am J Physiol Endocrinol Metab *295*, E242-253.

Stowell, M.H.B., Marks, B., Wigge, P., and McMahon, H.T. (1999). Nucleotide-dependent conformational changes in dynamin: evidence for a mechanochemical molecular spring. Nat Cell Biol *1*, 27-32.

Sudhof, T.C., and Rothman, J.E. (2009). Membrane fusion: grappling with SNARE and SM proteins. Science *323*, 474-477.

Tebar, F., Sorkina, T., Sorkin, A., Ericsson, M., and Kirchhausen, T. (1996). Eps15 Is a Component of Clathrin-coated Pits and Vesicles and Is Located at the Rim of Coated Pits. Journal of Biological Chemistry *271*, 28727-28730.

Traub, L.M., and Bonifacino, J.S. (2013). Cargo recognition in clathrin-mediated endocytosis. Cold Spring Harbor perspectives in biology *5*, a016790.

Trefely, S., Khoo, P.S., Krycer, J.R., Chaudhuri, R., Fazakerley, D.J., Parker, B.L., Sultani, G., Lee, J., Stephan, J.P., Torres, E.*, et al.* (2015). Kinome Screen Identifies PFKFB3 and Glucose Metabolism as Important Regulators of the Insulin/Insulin-like Growth Factor (IGF)-1 Signaling Pathway. J Biol Chem *290*, 25834-25846.

Wang, T., Birsoy, K., Hughes, N.W., Krupczak, K.M., Post, Y., Wei, J.J., Lander, E.S., and Sabatini, D.M. (2015). Identification and characterization of essential genes in the human genome. Science (New York, NY) *350*, 1096-1101.

Wang, T., Wei, J.J., Sabatini, D.M., and Lander, E.S. (2014). Genetic screens in human cells using the CRISPR-Cas9 system. Science (New York, NY) *343*, 80-84.

Wisniewski, J.R., Zougman, A., Nagaraj, N., and Mann, M. (2009). Universal sample preparation method for proteome analysis. Nature methods *6*, 359-362.

Wixler, V., Wixler, L., Altenfeld, A., Ludwig, S., Goody, R.S., and Itzen, A. (2011). Identification and characterisation of novel Mss4-binding Rab GTPases. Biol Chem *392*, 239-248.

Xiong, X., Chen, M., Lim, W.A., Zhao, D., and Qi, L.S. (2016). CRISPR/Cas9 for Human Genome Engineering and Disease Research. Annu Rev Genomics Hum Genet *17*, 131-154.

Yu, H., Liu, Y., Gulbranson, D.R., Paine, A., Rathore, S.S., and Shen, J. (2016). Extended synaptotagmins are Ca2+-dependent lipid transfer proteins at membrane contact sites. Proc Natl Acad Sci U S A *113*, 4362-4367.

Yu, H., Rathore, S.S., Davis, E.M., Ouyang, Y., and Shen, J. (2013a). Doc2b promotes GLUT4 exocytosis by activating the SNARE-mediated fusion reaction in a calcium- and membrane bending-dependent manner. Mol Biol Cell *24*, 1176-1184.

Yu, H., Rathore, S.S., Lopez, J.A., Davis, E.M., James, D.E., Martin, J.L., and Shen, J. (2013b). Comparative studies of Munc18c and Munc18-1 reveal conserved and divergent mechanisms of Sec1/Munc18 proteins. Proc Natl Acad Sci U S A *110*, E3271-3280.

Yu, H., Rathore, S.S., and Shen, J. (2013c). Synip arrests soluble N-ethylmaleimide-sensitive factor attachment protein receptor (SNARE)-dependent membrane fusion as a selective target membrane SNARE-binding inhibitor. J Biol Chem *288*, 18885-18893.

Zhang, R., Miner, J.J., Gorman, M.J., Rausch, K., Ramage, H., White, J.P., Zuiani, A., Zhang, P., Fernandez, E., Zhang, Q.*, et al.* (2016). A CRISPR screen defines a signal peptide processing pathway required by flaviviruses. Nature *535*, 164-168.

Zhou, Y., Zhu, S., Cai, C., Yuan, P., Li, C., Huang, Y., and Wei, W. (2014). High-throughput screening of a CRISPR/Cas9 library for functional genomics in human cells. Nature *509*, 487-491.

Zhu, Z., Dumas, J.J., Lietzke, S.E., and Lambright, D.G. (2001). A helical turn motif in Mss4 is a critical determinant of Rab binding and nucleotide release. Biochemistry *40*, 3027-3036.